NASA Contractor Report 3456

A Subsynoptic-Scale Kinetic Energy Study of the Red River Valley Tornado Outbreak (AVE-SESAME I)

Gary J. Jedlovec and Henry E. Fuelberg

CONTRACT NAS8-33370
AUGUST 1981

NASA

NASA Contractor Report 3456

A Subsynoptic-Scale Kinetic Energy Study of the Red River Valley Tornado Outbreak (AVE-SESAME I)

Gary J. Jedlovec and Henry E. Fuelberg
Saint Louis University
Saint Louis, Missouri

Prepared for
Marshall Space Flight Center
under Contract NAS8-33370

NASA
National Aeronautics
and Space Administration

**Scientific and Technical
Information Branch**

1981

A SUBSYNOPTIC-SCALE KINETIC ENERGY STUDY OF THE RED RIVER VALLEY TORNADO OUTBREAK (AVE-SESAME I)

by

Gary J. Jedlovec
Henry E. Fuelberg

Department of Earth and Atmospheric Sciences
Saint Louis University
Saint Louis, Missouri 63103

SUMMARY

The subsynoptic-scale kinetic energy balance during the Red River Valley tornado outbreak is presented in order to diagnose storm-environment interactions. Rawinsonde data from the first AVE-SESAME period, having a station spacing of about 250 km, provide meso-α scale resolution of the storm environment. Several data handling techinques are used which normally are not performed on synoptic-scale data; these include time interpolation to adjust for non-simultaneous sonde release and to partially generate missing data, and adjustments for balloon drift downwind.

Area-time averaged energetics indicate that horizontal flux convergence provides the major energy source to the region while cross-contour flow provides the greatest sink. Maximum energy variability is found in the upper levels in association with jet stream activity. Area averaged energetics at individual observation times show that the energy balance near times of maximum storm activity differs considerably from that of the remaining periods.

The local kinetic energy balance over Oklahoma during the formation of a limited jet streak receives special attention. Cross-contour production of energy is the dominant local source for jet development. Intense convection producing the Red River Valley tornadoes may have contributed to this local development by modifying the surrounding environment.

The energetics associated with areas of convective storms is found to differ greatly from that of areas without storms. Current results using subsynoptic-scale data are compared with those from a concurrent study using only NWS rawinsonde data. A random error analysis is presented to assess confidence limits in the energy parameters.

ACKNOWLEDGMENTS

The authors thank Drs. Yeong-Jer Lin, James T. Moore, and Gandikota V. Rao for reviewing the manuscript and for their helpful suggestions and comments through the course of this research. Thanks also are expressed to Paul Meyer and Matt Printy for their assistance.

This research was sponsored by the National Aeronautics and Space Administration under contract NAS8-33370, under the direction of the Atmospheric Sciences Division, Space Sciences Laboratory, NASA Marshall Space Flight Center, Alabama. NASA personnel who deserve special thanks for their encouragement and assistance in performing this research are our contract monitor, Mr. Kelly Hill, and Drs. William Vaughan, Robert E. Turner, and Gregory S. Wilson.

TABLE OF CONTENTS

TABLE OF CONTENTS (Concl'd)

LIST OF TABLES

LIST OF FIGURES

LIST OF FIGURES (CONTINUED)

LIST OF FIGURES (CONCLUDED)

1. INTRODUCTION

a. Motivation for investigation

In recent years many meteorologists have sought a better understanding of the complex structure of synoptic- and mesoscale weather phenomena. Results of their efforts are beginning to shed light on the role that smaller scale weather events play in the synoptic weather patterns and general circulation of the atmosphere. A lack of data which adequately capture these subsynoptic-scale phenomena has been an obstacle to testing current theories about scale interactions. In most cases the meteorologist has been limited to upper air observations with 12 h time intervals and station spacings near 400 km. This resolution is too coarse in both time and space to capture subsynoptic- and mesoscale phenomena such as short wave troughs, convective complexes, and limited jet streaks. Rawinsonde data from the recent Atmospheric Variability Experments- Severe Environmental Storm and Mesoscale Experiments (AVE-SESAME's) (see Alberty et al., 1979; Hill et al., 1979) provide better resolution than routine observations, thereby making a description of subsynoptic-scale events possible for those limited periods.

Continuous subsynoptic-scale observation of the atmosphere with rawinsondes currently is not feasible because of high operating expense. Indirect atmospheric soundings from the

VISSR Atmospheric Sounder (VAS) geostationary satellites will help alleviate this problem by providing meso-β scale time and space resolution over limited areas. The first VAS satellite was launched on 9 September 1980. During the next several years, the VAS data will be tested against current observational techniques to verify the quality and usefulness of this new mesoscale data source. Until the new system is perfected, meteorologists must rely on the limited amount of special subsynoptic-scale rawinsonde data, such as AVE-SESAME, for their investigations of the smaller-scale features.

Areas of intense convection are subsynoptic-scale phenomena whose formation is influenced by meteorological conditions on both larger and smaller scales of motion. After formation, large areas of storms are thought to modify their synoptic-scale environments through "feedback" mechanisms which, presently are not completely understood. One way of diagnosing interactions between severe storms and their surrounding wind fields is through an examination of the time and space variability of environmental kinematic parameters and the environmental kinetic energy balance. Through such studies, it is hoped that the interplays between intense convection and the synoptic-scale wind field can be better understood.

b. Past studies

It is difficult to determine cause and effect relationships in most diagnostic studies of the atmosphere because of the interaction of the given phenomenon with motions on other scales. This interaction is often non-linear and undetectable with routine atmospheric observations. There is increasing evidence, however, that large areas of intense convection produce effects on their surrounding atmospheric volumes that can be detected using synoptic-scale data.

Aubert (1957) used numerical simulation models to show that latent heat release associated with thunderstorms produced increased large-scale, low-level convergence and enhanced upper-level divergence. The synoptic-scale storm environment experienced low-level height falls and upper-level height rises which were detected in 12 h forecast fields. Ninomiya (1971a and b) used conventional rawinsonde data and satellite pictures to observe mid-tropospheric warming, strong low-level convergence, and strong upper-level divergence near areas of severe storms. He proposed that warming was a result of latent heat release, which then intensified the horizontal temperature gradient thereby producing a jet streak to the northwest of the warm core. Downward convective transport of horizontal momentum was shown to strengthen the low-level jet. Maddox (1980), Fritsch and Maddox (1980), and Maddox et al. (1980) recently investigated large, nearly circular, areas of

intense convection using satellite imagery and conventional rawinsonde data. They concluded that height rises in the upper troposphere, greatly enhanced upper-level divergence, and the formation of jet streaks occurred as a result of mid-tropospheric warming produced by the convection. Maddox (1980) emphasized the difficulty of detecting such influences because of the "chicken and egg" type questions which arise.

Most diagnostic kinetic energy studies have focused on large-scale extratropical cyclones over North America (e.g., Vincent and Chang, 1975; Smith, 1973). The few studies that have examined energetics of the convective environment suggest that large areas of storms can modify the surrounding synoptic-scale kinetic energy balance. Danard (1964, 1966) used numerical methods with and without the inclusion of latent heat to compute the effects of large areas of precipitation on certain kinetic energy budget terms. Horizontal ageostrophic flow near the precipitation region was directed toward decreasing pressure in both the upper and lower levels, resulting in a production of kinetic energy. The induced ageostrophic motion was attributed to the release of latent heat which amplified convergence and divergence within the storm environment.

Fuelberg and Scoggins (1978) investigated the synoptic-scale kinetic energy budget surrounding the mesoscale convective complex described by Maddox (1980). They found the upper-tropospheric storm environment to be characterized by strong generation of kinetic energy due to cross-contour flow,

horizontal flux divergence of kinetic energy, upward transport of kinetic energy, and the transfer of energy from the resolvable to subgrid scales of motion. They suggested that observed systematic changes in certain kinetic energy terms were due in part to the convection. Vincent and Schlatter (1979) proposed that the conversion of potential energy on the cumulus scale to kinetic energy on the synoptic scale could explain regions of mid-tropospheric positive dissipation near tropical storm Candy (1968). Positive dissipation in this sense is a source of energy from the subsynoptic scales of motion. Robertson and Smith (1980) used synoptic-scale data to study storm-environment interactions during the Jumbo (3-5 April 1974) and Palm Sunday (10-12 April 1965) tornado outbreaks. The kinetic energy budgets of the storm environments were different during the two outbreaks, but horizontal flux convergence of energy was dominant during the Palm Sunday outbreak which contrasts with the results from Fuelberg and Scoggins (1978). Although the storm area of the Jumbo outbreak had a source of kinetic energy due to cross-contour flow, the process was small in comparison to horizontal flux convergence of energy. They noted that subgrid-scale sources of kinetic energy often were associated with intense convection.

Very few kinetic energy studies have been conducted on the subsynoptic scale, mainly due to the lack of appropriate data. McInnis and Kung (1972), Kung and Tsui (1975), and

Tsui and Kung (1977) used meso-β scale rawinsonde data (station spacing of 80 km) from the National Severe Storms Laboratory (NSSL) in their studies. The energy transformations on this scale were comparable to those observed in major synoptic-scale cyclones. Areas of intense convection were characterized by large cross-contour generation of kinetic energy and a large dissipational loss in the upper levels, but the import of kinetic energy from the surroundings was rather small. Magnitudes of mesoscale energy transformations were found to vary greatly, depending on the strength of the mesoconvective systems in the area. Time variations in the terms seemed related to the growth and decay of the nearby storms.

Fuelberg et al. (1980) recently completed a synoptic-scale kinetic energy study of the Red River Valley tornado outbreak. They used only the twenty-three National Weather Service (NWS) rawinsonde stations (400 km spacing) although the data were at 3 h intervals. The energetics of the convective environment were found to be distinctively different from that of the non-storm environment. The storm environment was an area of intense generation of kinetic energy by cross-contour flow and of energy losses due to transfers from the resolvable (synoptic) scales to subgrid scales of motion. A detectable feedback mechanism, by which the storms modified their environment, was not readily apparent at the synoptic scale. Theoretically speaking, feedback mechanisms from the convective scale to the larger scales should be present. Such

cooperative effects are believed to be the dominate physical mechanism to promote intense convective outbreaks. Fuelberg et al. (1980) hypothesized that strong synoptic-scale forcing prevented adequate resolution of these interactions. They suggested that subsynoptic-scale data may be necessary to detect these processes when jet intrusion and baroclinic wave intensification occur.

c. Purpose

The purpose of this research is to investigate subsynoptic scale storm-environment interactions of the Red River Valley tornado outbreak (RRVTO). The combination of the NWS and special site soundings that are available from the AVE-SESAME I period are used in the present study. These data, having a station spacing of 250 km and a time interval of 3 h, provide a superior resolution of subsynoptic-scale (meso-α scale) features than was obtained by Fuelberg et al. (1980). As in their study, special attention will be focused on variations in the kinetic energy balance. First, a kinematic analysis will be presented to show that the data handling techniques and computational procedures have produced a superior subsynoptic-scale data set. Second, the area-time averaged energetics will be discussed for the AVE-SESAME I region. The time variability of the area-averaged budget will be demonstrated. Third, spatial maps of energy budget parameters will

be used to relate certain terms to subsynoptic-scale features. Fourth, the energy budgets of limited sub-volumes enclosing features of special interest will be examined. The results of this research will provide additional information on energy transfers between the synoptic- and subsynoptic-scales of motion that hopefully will prove useful for incorporating subsynoptic-scale features in numerical prediction models.

2. THEORETICAL CONSIDERATIONS

The kinetic energy budget equation for a fixed, limited volume in isobaric coordinates is given by Smith (1969) as

$$\frac{\partial K}{\partial t} = \iint -\vec{V}\cdot\vec{\nabla}\phi - \iint \vec{\nabla}\cdot k\vec{V} - \iint \frac{\partial \omega k}{\partial p} + \iint \vec{V}\cdot\vec{F} + \int k_o \frac{\partial p_o}{\partial t} , \qquad (1)$$

where

$\iint = \frac{1}{gA}\iiint dx\, dy\, dp$,

$\vec{V}$ is the horizontal wind velocity,

ω is the vertical motion in isobaric coordinates,

$k = \frac{(u^2+v^2)}{2}$ is the horizontal kinetic energy per unit mass,

$K = \iint k$,

$\phi = gz$ is the geopotential height,

$\vec{F}$ is the frictional force,

A is the computational area, and

$_o$ is a subscript denoting surface values.

Local changes of kinetic energy in the limited volume, $\frac{\partial K}{\partial t}$, are due to five processes. The term $-\vec{V}\cdot\vec{\nabla}\phi$ represents the generation of kinetic energy, or the conversion of potential to kinetic energy, by cross-contour flow. Term $\vec{\nabla}\cdot k\vec{V}$ represents horizontal flux divergence of kinetic energy while $\frac{\partial \omega k}{\partial p}$ is the vertical flux divergence of kinetic energy. Term $k_o \frac{\partial p_o}{\partial t}$ represents variations in kinetic energy due to changes in the mass of the volume being studied. Since it is

several orders of magnitude smaller than the other terms in (1), it will not be considered further.

The term $\vec{V} \cdot \vec{F}$ conceptually represents thermodynamical and mechanical frictional processes, but since it is computed as a residual in order to balance the other terms of the equation, it also represents a transfer of energy between the resolvable and unresolvable scales of motion (Smith and Adhikary, 1974) and possible errors in all of the other terms. It is also called the dissipation term.

3. DATA AND COMPUTATIONAL PROCEDURES

a. Data

The first AVE-SESAME period ran from 1200 GMT 10 April through 1200 GMT 11 April 1979 and included rawinsonde releases at 3 h intervals for twenty-three National Weather Service (NWS) stations plus an additional sixteen special sites (Fig. 1). By including the special site stations an average station spacing of 250 km, instead of the usual 400 km, was achieved. Thus, subsynoptic-scale (meso-α scale) resolution was provided. Further details about the AVE-SESAME program are given by Alberty et al. (1979), Barnes (1979), and Hill et al. (1979). Reduction procedures used to process the rawinsonde data are described by Fuelberg (1974) while the data at 25 mb intervals are given by Gerhard et al. (1979).

b. Data handling procedures

In spite of the care that was taken during the data collection phase of AVE-SESAME, several problems remained in the final tabulated product. First, although the NWS sondes generally were released within 15 minutes of each other, the special sites were much less punctual. In several cases, releases were delayed by as much as one hour. Second, special site soundings were either missing altogether (16 occurrences),

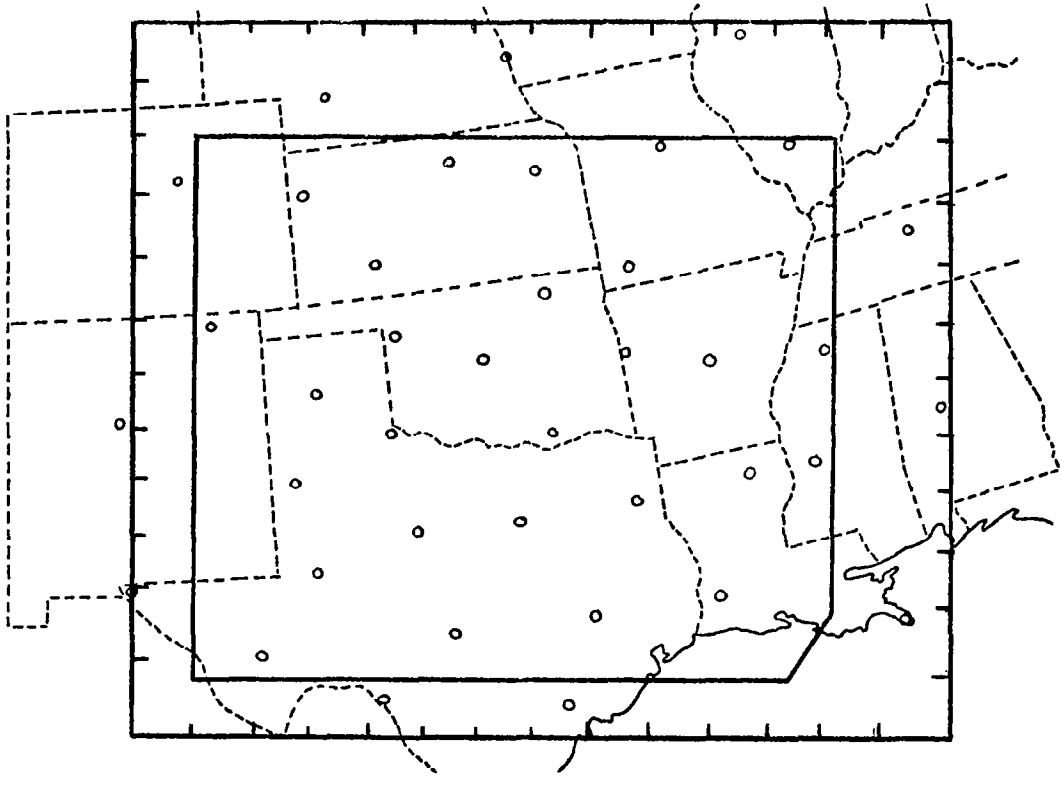

Figure 1. Rawinsonde stations participating in AVE-SESAME I. Outlines indicate the 15 x 13 analysis region (outer) and the energy budget averaging region (inner).

terminated early, or contained data gaps at various levels because of sonde failure or other difficulties. These problem soundings, along with sixteen others that were declared questionable during the data reduction process (Gerhard et al., 1979), created a need for special computational techniques. Furthermore, the use of subsynoptic-scale data may violate several assumptions normally made as part of synoptic-scale computational procedures. Since the uniqueness of the AVE-SESAME I data lies in its subsynoptic-scale time and space resolution, computational procedures must optimize this aspect. The specific problems and their solutions are presented next.

When using data with a temporal spacing of three hours, sondes from the various sites should reach given pressure levels at nearly the same times. This often did not occur during AVE-SESAME I because of the non-simultaneous releases, variations in sonde ascent rate, and the different heights of the stations above sea level. The following scenario illustrates the consequences of these factors. The average time for a sonde to reach 100 mb is 50 minutes after release. By itself this problem would not be critical even with three hour data; however, if a sonde also were released an hour late, the data at 100 mb would be more representative of the later three hour release instead of the one to which it is assigned. Therefore, when sondes are released at many different times, the data must be adjusted so they all describe the atmosphere at a given level at the same time.

The adjustment was accomplished in this study by using a linear scheme similar to that described by Fankhauser (1969). The observation before and after the sounding in question was used to perform the calculations. Sondes generally are released 45 min before the standard observation hour (e.g., 1115 GMT for 1200 GMT), and during AVE-SESAME I the NWS sondes were released as much as 55 min before the hour. The earliest portion of the sounding represents the lower layer of the atmosphere where changes are probably more rapid than in the upper levels. This portion is also more representative of the prior hour than the scheduled hour. Therefore, all data were adjusted to the prior hour although they will be denoted as 1200 GMT, 1500 GMT, etc. soundings. Although it is understood that the atmosphere is non-linear and that a linear scheme will not completely recover the "true" atmospheric values, the linear scheme should be a good approximation to the actual conditions.

As previously mentioned, some of the NWS and special site data were missing. Since the desired subsynoptic-scale resolution depends on having as much data as possible, it would be desirable to generate the missing values. There are at least two methods for producing the data. In several previous synoptic-scale studies, when only 12 h data were available, missing values have been interpolated vertically from available data above and below (Chien and Smith, 1973) and also interpolated in space from surrounding observations (e.g., Chien

and Smith, 1973; Kung, 1977). There are several disadvantages to this approach. First, vertical interpolation over depths of several hundred millibars may not fully capture thin layers containing inversions or jet maxima. Second, while the spatial interpolation uses the surrounding observations, the interpolated value can only represent the gross features of the surroundings.

Because 3 h data were available during the AVE-SESAME I period, it was felt that linear time interpolation at individual stations would produce more consistent and more representative values for missing data. The method is a natural extension of Fankhauser's time adjustment scheme previously mentioned. Several restrictions were placed on the technique. First, the interpolation was limited to 6 h periods; i.e., if data for a given level were missing at two consecutive times, no values were generated. Second, extrapolation was avoided by not using the procedure at the first and last times. Although the scheme takes advantage of the 3 h data interval, it and any other scheme for generating missing values is not without potential problems. Therefore to insure that reasonable time and space continuity were maintained, the adjusted and interpolated data were manually checked using time-series and constant pressure analyses. Any data, whether interpolated or original, which did not appear valid, were removed and not used in further computations.

In atmospheric studies using synoptic-scale rawinsonde

data, the sounding is usually treated as a vertical probe. However, with subsynoptic-scale spatial resolution where the distance between observations is about 250 km, this assumption is questionable. Strong winds during AVE-SESAME I, produced an average downwind sonde drift of 90 km at 100 mb with a maximum drift of 153 km. Because of these large displacements, sonde location at release (station location) was not used as the location at all levels. Instead, sonde location was determined at every level in the vertical, as part of the objective analysis procedure. This procedure is similar to that used by Fankhauser (1969) and McInnis and Kung (1972).

After obtaining the time and space consistent data set using the above techniques, the data were objectively analyzed onto a 15 x 13 grid (see Fig. 1) using the Barnes (1964) scheme. The grid length and scan radius were 127 km and 381 km (3 grid lengths), respectively. Four iterations of the scheme produced the desired accuracy and resolution in the gridded fields of height, temperature, winds, and dew point. Grids were obtained at the surface and at 50 mb intervals between 900 and 100 mb. To reduce the effects of errors, the original wind data at 25 mb increments were averaged over 50 mb layers. Because the Barnes scheme is only mildly sensitive to data errors and because the above mentioned techniques reduce errors by inherent smoothing, only a gentle explicit filter was applied to the gridded fields (Shuman, 1957). This nine point filter changes neither the wavelength nor the phase, but only

the amplitude of each feature. Figure 2 compares current resolutions with those of Fuelberg et al. (1980) who used only NWS data. The subsynoptic-scale gridded fields retain 15-20% more of the original amplitudes than did the synoptic-scale study. Features with wavelengths smaller than 500 km (twice the station spacing) are greatly suppressed. This is desirable since "noise" generated from data errors, although held to a minimum, is contained at these smaller and not fully resolvable wavelengths.

c. Computational procedures

Computation of the kinetic energy budget not only depends on the basic input parameters, but also on divergence and vertical motion. Divergence and all other calculations in this study were made using conventional finite differencing techniques. Kinematic vertical motions were obtained using values of divergence in the integration of the continuity equation in isobaric coordinates. The integration requires a lower boundary condition which, on the synoptic scale, generally is taken to be zero. For this study, the assumed lower boundary condition was the sum of three processes given by

$$\omega_{sfc} = \frac{\partial p_{sfc}}{\partial t} + \vec{V}\cdot\vec{\nabla}p_{sfc} + \rho_{sfc}g(\vec{V}_{sfc}\cdot\vec{\nabla}h), \qquad (2)$$

where h is terrain height (Holton, 1972, p.132). The first term, $\frac{\partial p_{sfc}}{\partial t}$, is the local change of surface pressure. It was

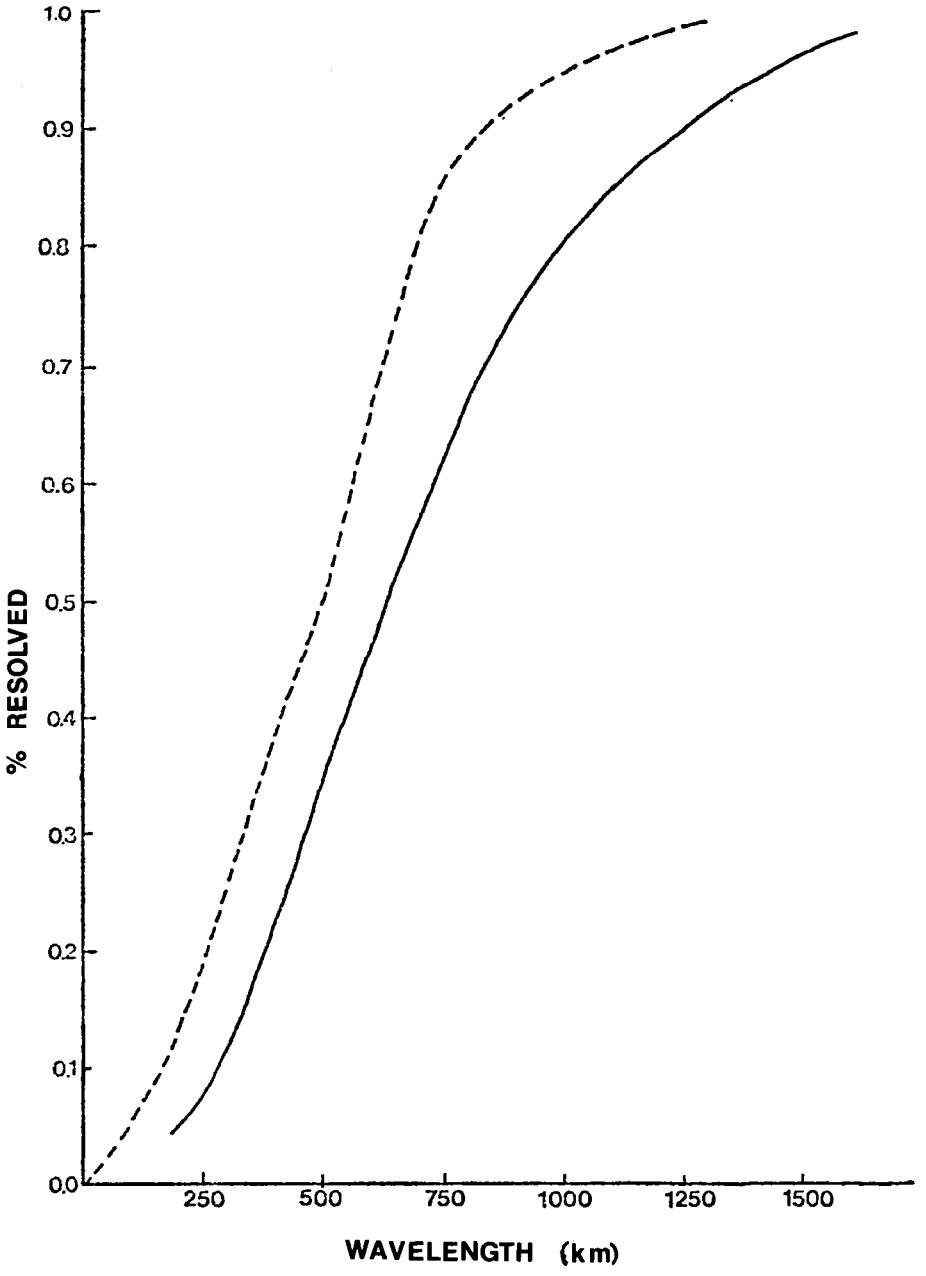

Figure 2. Resolution profiles for synoptic- and subsynoptic-scale studies. The smallest feature resolvable for the synoptic-scale study (solid line) (Fuelberg et al., 1980) and the subsynoptic-scale study (dashed line) is 800 km and 500 km in length, respectively.

computed using 6 h centered differences when possible, but 3 h uncentered differences were used at the first and last times. The largest magnitudes of this term, about 0.3 μb s^{-1}, were somewhat smaller than expected, probably due to the smoothing effect of the 6 h differencing. Although hourly surface data would produce somewhat larger values for this term, they were not incorporated into the AVE-SESAME data set. Therefore consistent surface and upper air resolution was maintained. Term $\vec{V}_{sfc} \cdot \vec{\nabla} p_{sfc}$ represents cross-isobaric flow which may be due to various types of force imbalances. This term was the smallest of the three and contributed little to the surface vertical motions. The third term, $-\rho_{sfc} g \vec{V}_{sfc} \cdot \vec{\nabla} h$, denotes terrain induced vertical motion. This component dominated the surface vertical motion fields over the western half of the region (see Fig. 1) because the low-level flow tended to be perpendicular to the large terrain gradient along the eastern slopes of the Rocky Mountains. Values in the region averaged ± 1 to ± 2 μb s^{-1}.

A disadvantage of the kinematic method is that divergence errors accumulate by the end of the integration process thereby producing unrealistic values of ω near 100 mb. These problems occur in spite of good data and computational procedures. The accurate calculation of divergence is especially difficult in the upper levels where input data errors are largest. To circumvent this problem, the values of ω were modified using the adjustment scheme suggested by O'Brien

(1970). The procedure forces the vertical motion profile to a predetermined value at the top of the model (100 mb), which in this study was taken to be zero. The values of divergence then were adjusted by the amount necessary to achieve $\omega=0$ at 100 mb.

Terms of the kinetic energy budget equation were computed using centered finite differences at 18 levels from the surface to 100 mb. These values were then integrated over 50 mb layers by means of the trapezoidal rule. The dissipation term was calculated as a residual from the other terms in (1).

d. Error analysis

Rawinsonde data contain systematic and random errors which affect energy budget calculations despite the use of objective analysis schemes and horizontal and vertical filtering procedures. In order to obtain quantitative values for confidence limits associated with the derived energy parameters, additional computations were performed using randomly perturbed rawinsonde data. Results of these calculations, described in the Appendix, yield the following conclusions:

1) Area averaged energy parameters are, for the most part, rather insensitive to assumed errors in the input data. Greatest uncertainties are found at the highest altitudes where rawinsonde data are assumed to have the greatest errors. The dissipation term, which is computed as a

residual, generally is the most sensitive term at all levels. Some caution in interpretation should be exercised when original values of any term are near zero.

2) Area averaged budgets obtained for the entire computational area are somewhat more reliable than those describing subsets of the region and consisting of fewer grid points.

3) Spatial fields of energy parameters derived from perturbed data show the major centers of energy conversion and transport despite the presence of assumed data errors. Although space patterns are reliable, values at individual grid points may be altered more significantly.

4) Results of the error analysis, together with qualitative assessments of time and space continuity, suggest that errors in rawinsonde data should not seriously affect the interpretations of results that follow. Discretion should be exercised in assigning significance to minor term fluctuations, especially dissipation, in the upper levels.

4. WEATHER CONDITIONS

a. Introduction

The Red River Valley tornado outbreak (RRVTO) occurred on 10-11 April 1979 in the area separating Texas from Oklahoma. The outbreak began near 2100 GMT 10 April and continued through 0200 GMT 11 April. Major tornadoes at Vernon (Texas), Lawton (Oklahoma), and Wichita Falls (Texas) as well as many less damaging tornadic, hail, and wind storms occurred during the period. The Wichita Falls tornado, which began around 2355 GMT on the outskirts of the city, was the most severe of the outbreak, lasting over 60 min with a path length of nearly 47 miles. By the end of the outbreak, 56 people had been killed, 1916 injured, and damage estimates totalled several hundred million dollars. The following discussion highlights weather conditions leading up to and associated with the RRVTO. More detailed analyses have been given by Moore and Fuelberg (1981), Moller (1980), and Carlson et al. (1980).

b. Pre-outbreak conditions

The RRVTO coincided with the first AVE-SESAME '79 experiment. Synoptic conditions at the beginning of the period (1200 GMT 10 April) are shown in Fig. 3. At the surface, a high pressure area over the Great Lakes carried cool, dry air

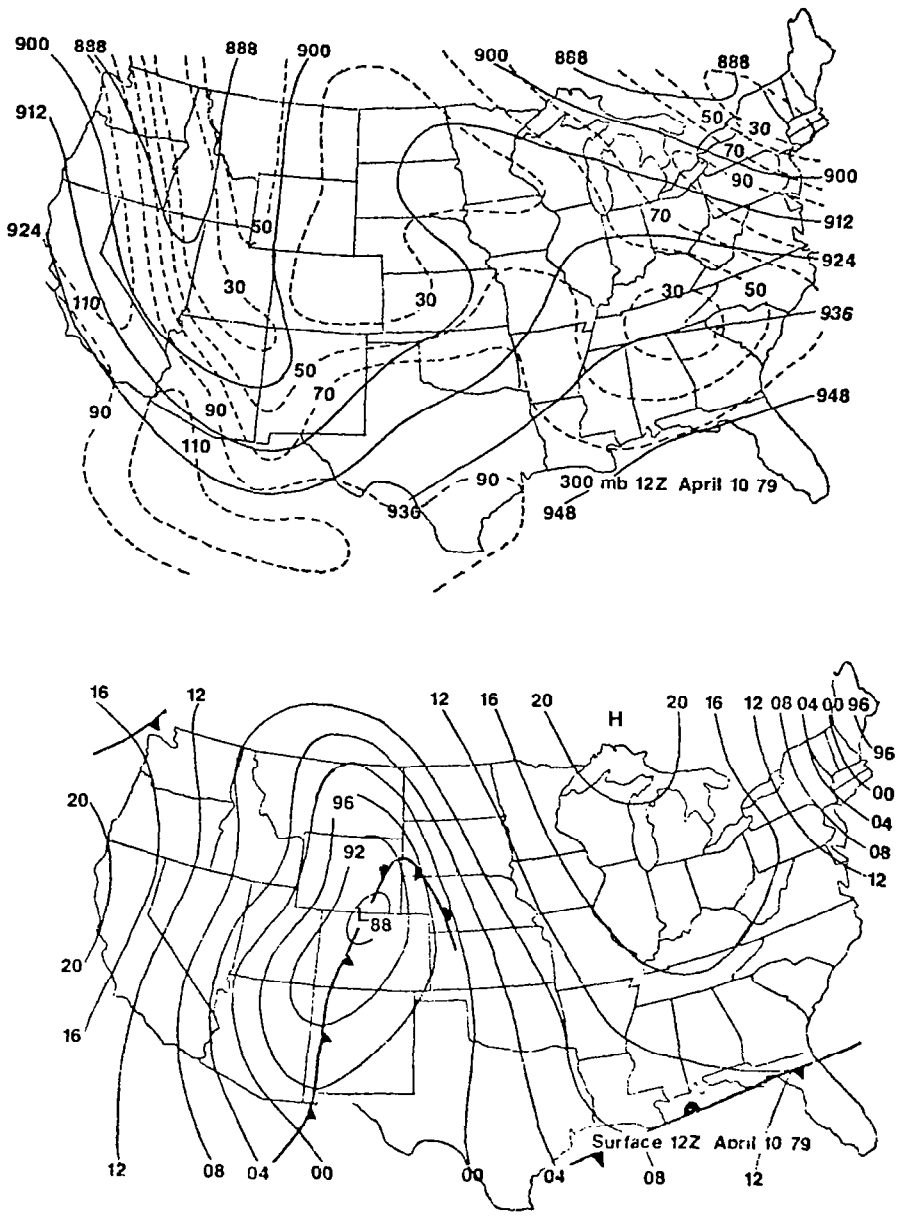

Figure 3. Synoptic conditions at 1200 GMT 10 April 1979. At the surface, presure is in millibars (04 means 1004 mb). At 300 mb, height lines are in tens of meters and isotachs are in knots.

over the eastern half of the country. A deep cyclone (988 mb), located over the Colorado-Wyoming border, was the anchor point for a cold front extending southward into New Mexico and a stationary front extending into Nebraska and Kansas. A stationary front also was positioned along the Gulf Coast.

An amplifying baroclinic wave was the dominant feature in the upper troposphere (Fig. 3). The system exhibited a negative horizontal tilt, stretching from Washington into New Mexico. A weaking short wave extended through the Midwest while a ridge, associated with the surface high pressure area, was located from the middle Mississippi River Valley into the Dakotas. A low-level southerly wind maximum, extending from the middle Texas coast into Kansas contained speeds as great as 20 m s^{-1}, while a middle-level jet stretched from southern New Mexico into Oklahoma with wind speeds up to 30 m s^{-1}. The jet axis at 300 mb was parallel to the mid-tropospheric jet over the AVE-SESAME I region. Within the experiment area, maximum winds at 300 mb were along the Gulf Coast; however, the main jet core was located at the base of the trough over Mexico.

The GOES visible satellite image for 1331 GMT (Fig. 4) reveals the cloud cover near the beginning of the AVE-SESAME I period. Scattered showers and thunderstorms were occurring in Arkansas, southwestern Missouri, and parts of Kansas, but no severe activity or well organized convection was present.

During the next 6 h weather conditions gradually became

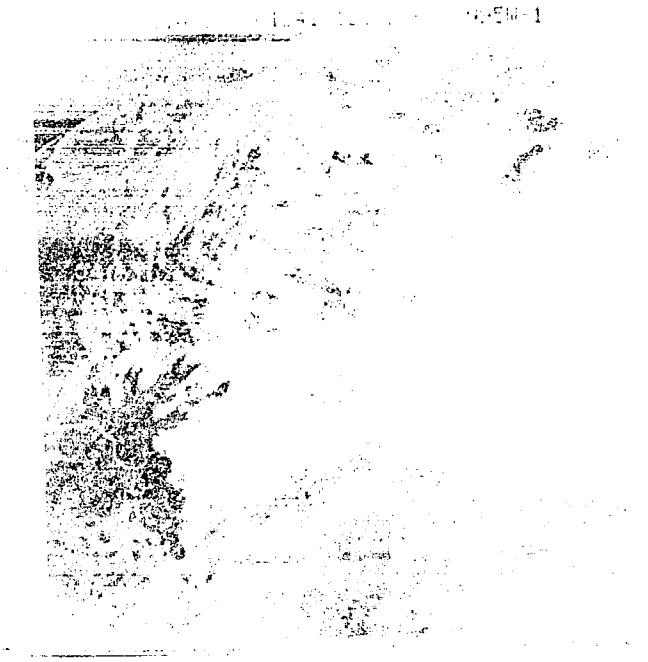

Figure 4. GOES visible satellite image at 1331 GMT 10 April 1979.

more conducive to severe storms. Surface and 300 mb subsynoptic-scale charts for 1800 GMT 10 April are shown in Fig. 5. The surface low over Colorado deepened 3 mb to 985 mb but remained relatively stationary. An occluded front extended southward from the low to the triple point over northern New Mexico. From this point, a cold front stretched through eastern New Mexico and extreme west Texas while a warm front extended from the triple point into northcentral Texas and Louisiana. A dry line had formed in western Texas separating dew points of 19°F at Morton and 10°F at Marfa from values in the sixties over central Texas. The combination of warm, moist air in the low levels with cool, dry air aloft created potential instability in an area from Victoria, Texas to Oklahoma City and westward into New Mexico. Values of the Total Totals index were greater than 50 in this region.

In the upper levels at 1800 GMT (Fig. 5), the major trough had intensified over the mountains, tightening the 300 mb height gradient. A small perturbation in the height field appeared over Amarillo, Morton, and Midland, Texas and is best seen in the 3 h height change fields (not shown). Another major feature at 300 mb was jet intrusion into the southwest portion of the AVE-SESAME I region. Winds in excess of 50 m s^{-1} now extended into west Texas. The continued intrusion of this jet and the propagation of the height perturbation into northcentral Texas helped release the instability and produce the severe storm outbreak.

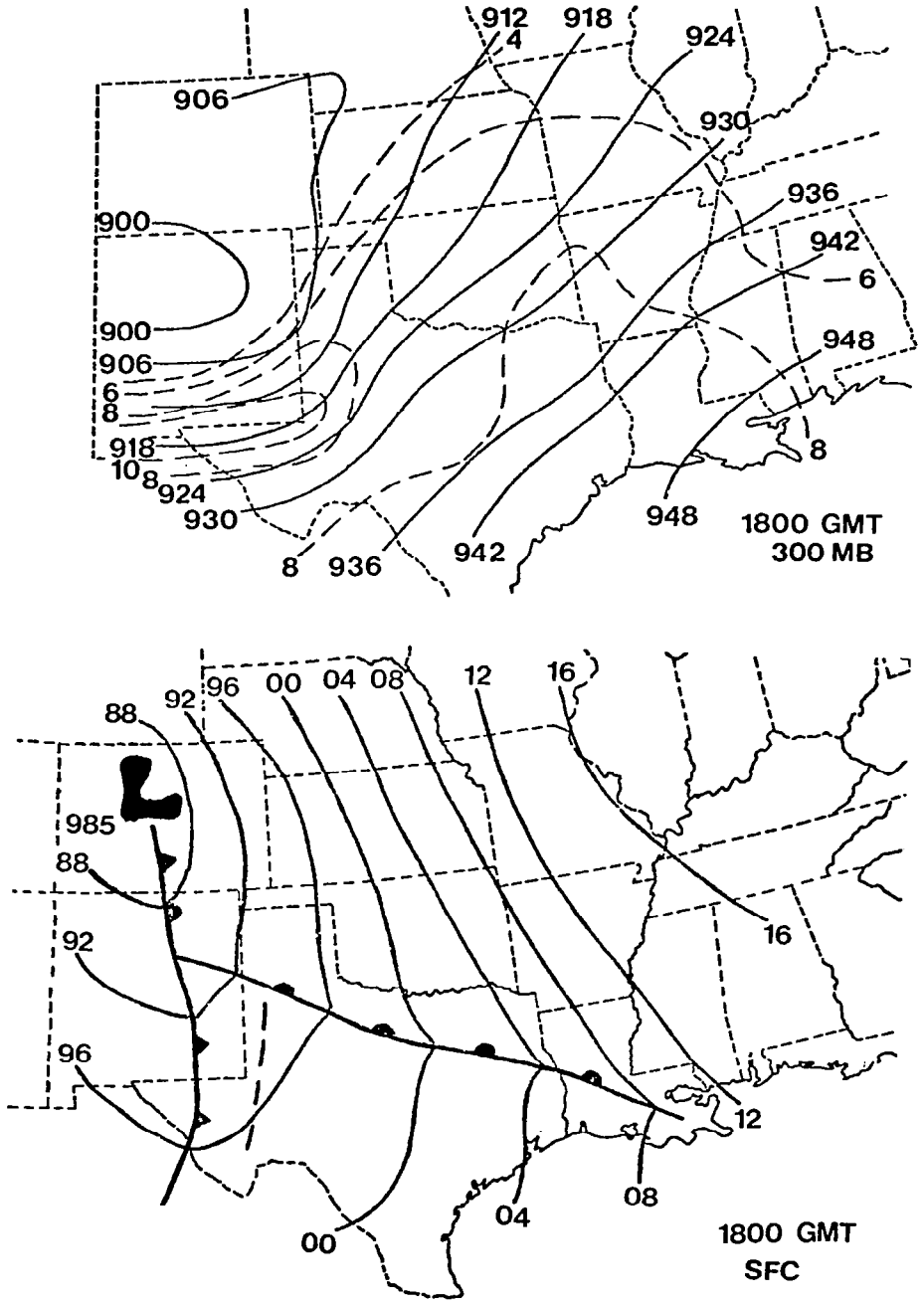

Figure 5. Surface and 300 mb charts at 1800 GMT 10 April 1979. Surface contours are in millibars. Height lines at 300 mb are in tens of meters and isotachs are in tens of knots.

Convection at 1800 GMT (3 h before the first major tornado occurrence) was confined to two regions. The radar summary (Fig. 6) indicates a relatively small storm area over north-central Texas with echo tops reaching 50,000 ft (15.3 km). The second area of developing storms was over eastern New Mexico where echo tops were 33,000 ft (10.1 km). This latter area, although not yet intense or well organized, was located near the upper-level height perturbation and underwent major development as it moved eastward.

c. Outbreak conditions

Shortly after 2100 GMT 10 April the first major tornado was reported near the Red River, 70 km west of Wichita Falls. Surface and 300 mb maps for this time are shown in Fig. 7. At the surface, only minor changes occurred during the last 3 h. The warm front advanced to a position just south of the Red River Valley, bringing warm, moist air further northward. The cold front moved to a position near the Texas-New Mexico border with strong westerly winds behind it. The dry line moved eastward, remaining several hundred kilometers ahead of the cold front. The low pressure center (985 mb) remained stationary over Colorado; however, the horizontal pressure gradient tightened considerably over Oklahoma and Kansas due to strengthening of the high pressure center over the Great Lakes. A low-level jet centered near 850 mb had developed over northcentral Texas

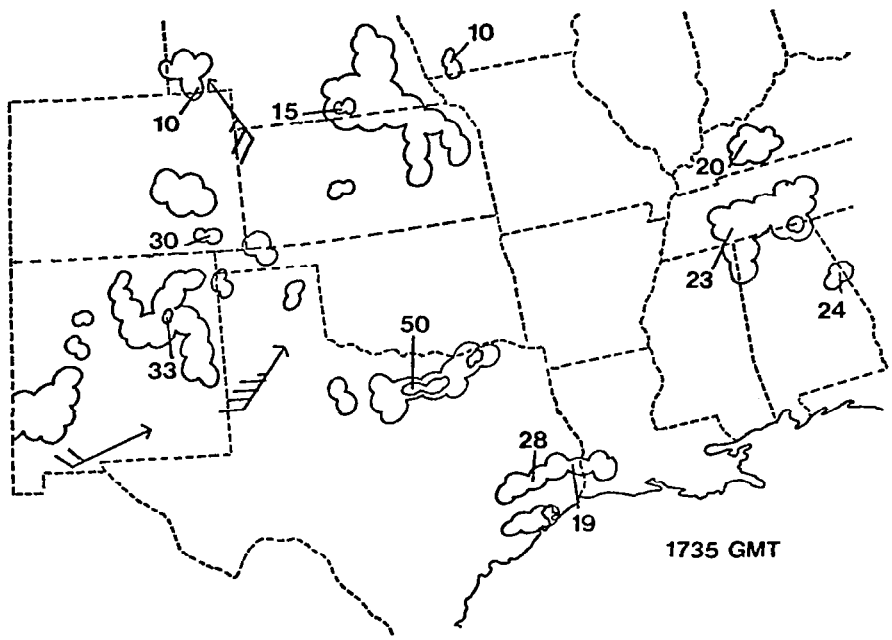

Figure 6. Radar summary at 1735 GMT 10 April 1979. Echo tops are in thousands of feet.

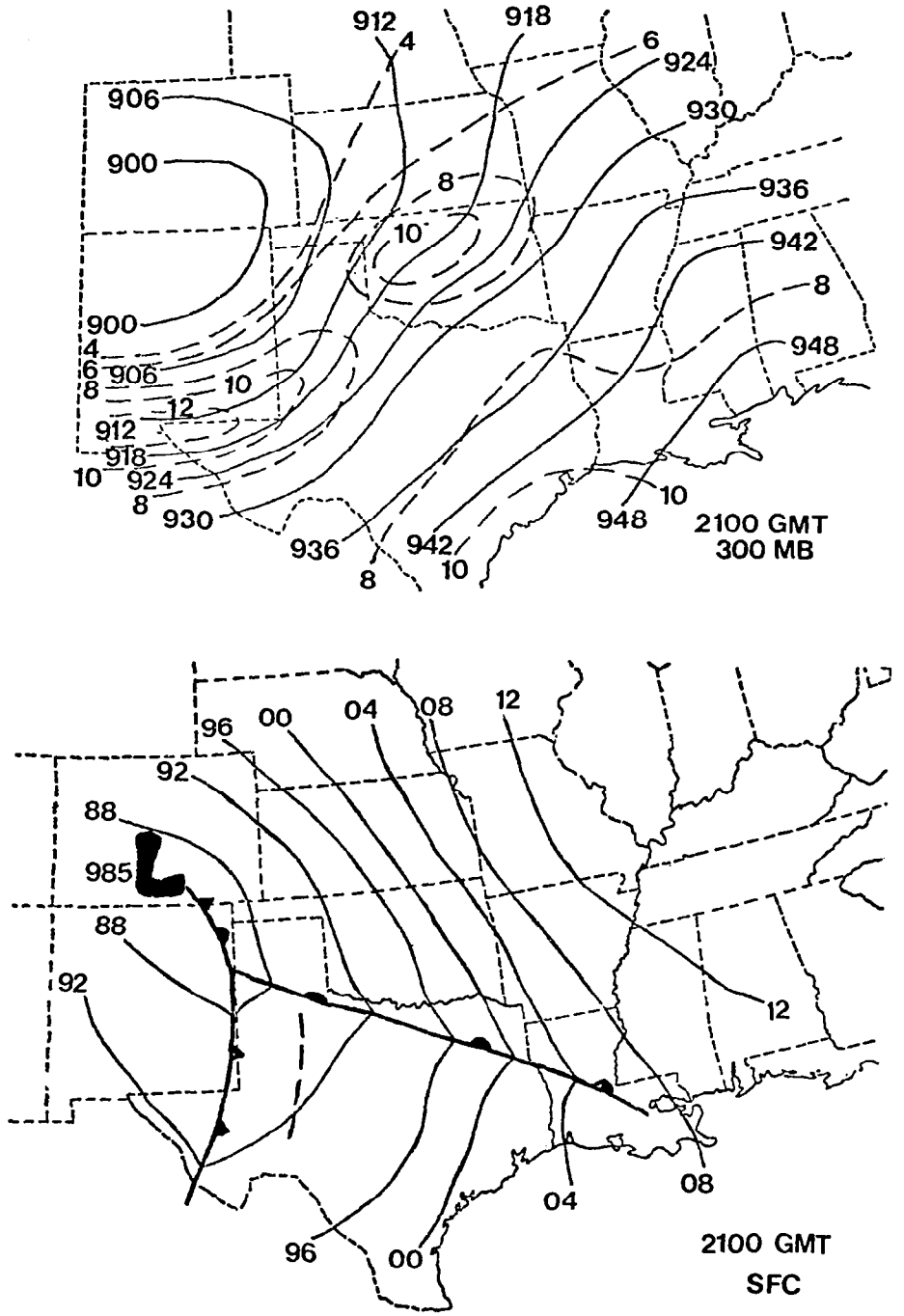

Figure 7. Surface and 300 mb charts at 2100 GMT 10 April 1979. Surface contours are in millibars. Height lines at 300 mb are tens of meters and isotachs are in tens of knots.

during the afternoon with speeds in excess of 20 m s^{-1} (not shown). This feature was an efficient transporter of heat and moisture into the Red River Valley. This low-level jet was located in the exit region of the upper-level jet advancing from the southwest. The development of low-level jets has been linked to mass and momentum adjustments within the exit region of upper-tropospheric jet streaks (Uccellini and Johnson, 1979).

At 300 mb (Fig. 7), the height perturbation was not as apparent as 3 h earlier. However, at 500 mb (not shown) there were 30 m height falls at Oklahoma City, Childress, and Morton and 50 m falls at Amarillo. A major change occurred in the wind field at 300 mb as the jet streak advanced into west Texas and a new isotach maximum formed over Oklahoma and southern Kansas. Winds at Oklahoma City increased from 37 m s^{-1} to 63 m s^{-1} in 3 h while slightly smaller increases occurred at Gage and Bartlesville, Oklahoma. The appearance of this secondary jet streak is quite intriguing. Horizontal maps alone do not suggest its advection from the major streak located to the southwest.

Convection at 2100 GMT (Fig. 8) was more widespread than 3 h earlier (Fig. 6). The storm area in northcentral Texas moved rapidly northward into Oklahoma in advance of the warm front located south of the Red River Valley. The convection along the Texas-New Mexico border at 1800 GMT had moved into the eastern portion of the Texas panhandle with echo tops reach-

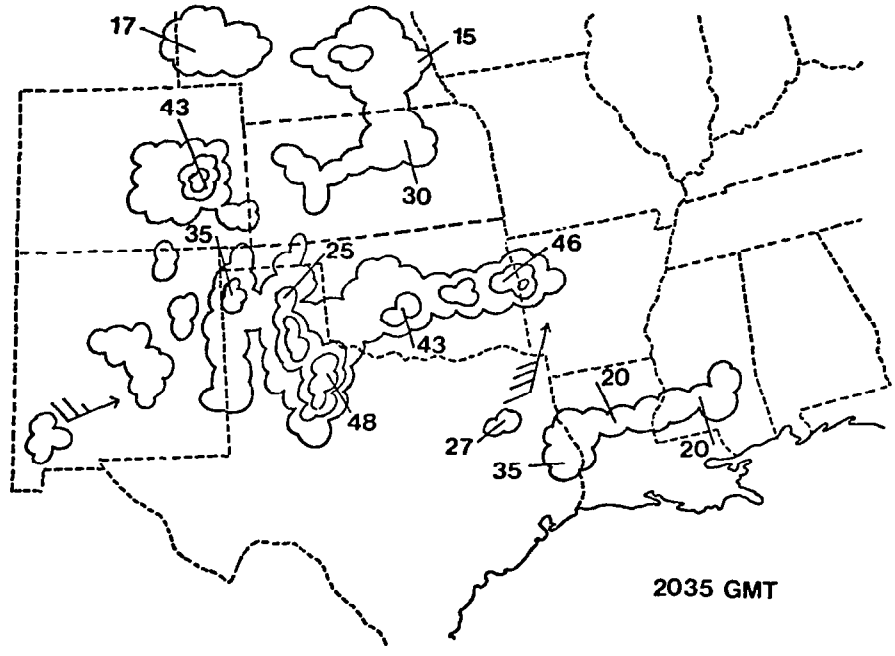

Figure 8. Radar summary at 2035 GMT 10 April 1979. Echo tops are in thousands of feet.

ing 48,000 ft (14.6 km). The cold front which was moving through western Texas undoubtedly provided a lifting mechanism through which potential instability was released producing the convection. The satellite photo for 2300 GMT and the radar summary for 2335 GMT (Fig. 9) show the convective areas near the height of the outbreak. A large area of storms covered extreme northcentral Texas, Oklahoma, Kansas, southwestern Missouri, and eastern Colorado. Flow over the warm front and terrain effects were contributing factors producing this area. A small but intense area of convection continued over the Red River Valley with echo tops reaching 58,000 ft (17.7 km). This area spawned tornadoes at Wichita Falls and other nearby locations.

Figure 10 shows the surface and 300 mb subsynoptic-scale maps for 0000 GMT 11 April, five minutes after the sighting of the Wichita Falls tornado. Changes in surface conditions were small during the 3 h period. One notable feature was a northeastward bulge in the dry line toward the Red River Valley. The low-level jet, now positioned over Oklahoma, had increased in size and strength with speeds greater than 25 m s^{-1} (not shown). Uccellini and Johnson (1979) have shown that the intensification of the low-level jet and its angle to the upper-level jet are related to the isallobaric wind. At 300 mb, a perturbation in the height field was apparent again, this time over the Red River Valley. The 3 h height tendencies (not shown) indicate falls of 50 m over Amarillo and Childress, Texas

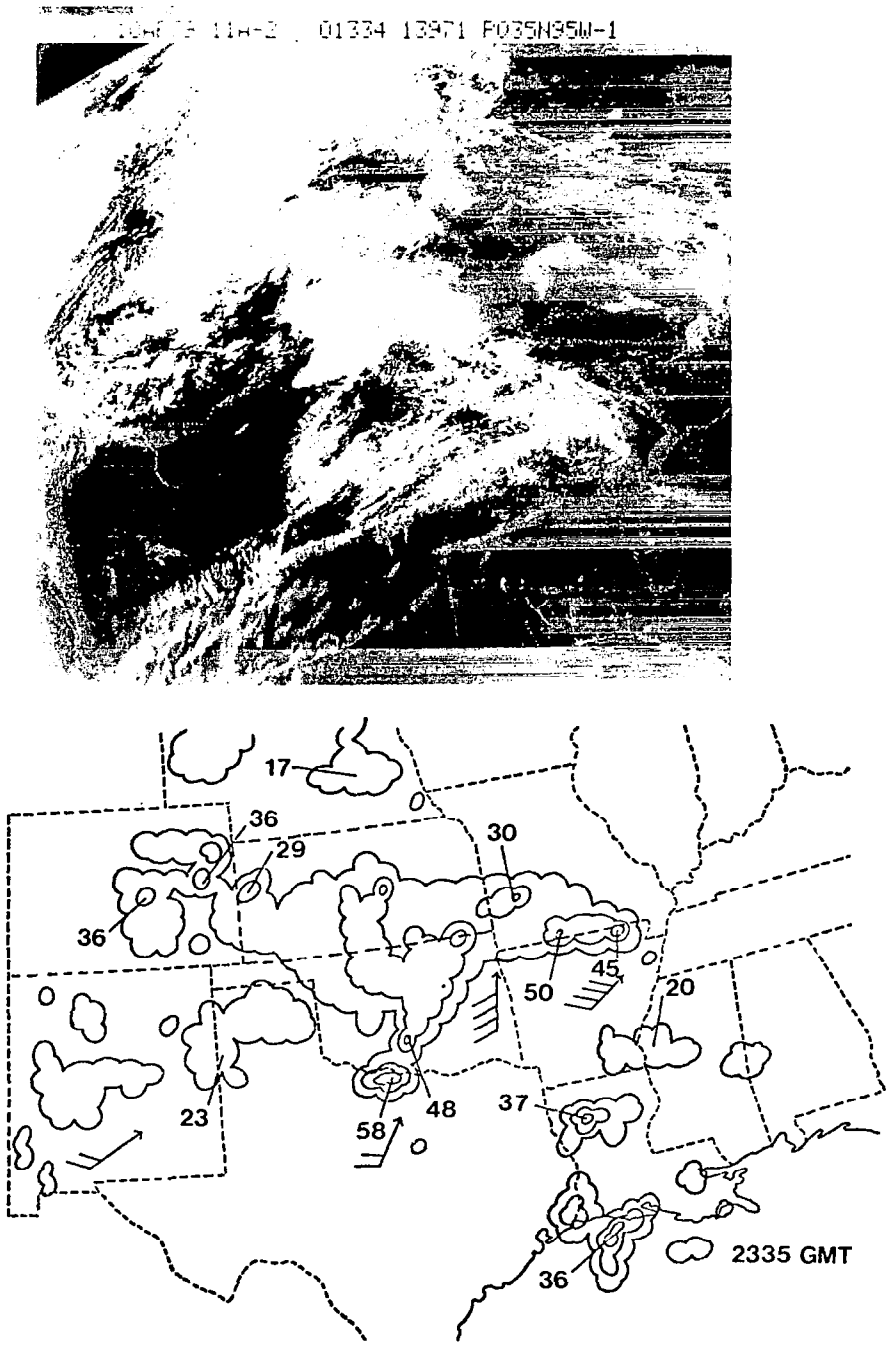

Figure 9. GOES visible satellite image at 2300 GMT and radar summary at 2335 GMT 10 April 1979. Echo tops are in thousands of feet.

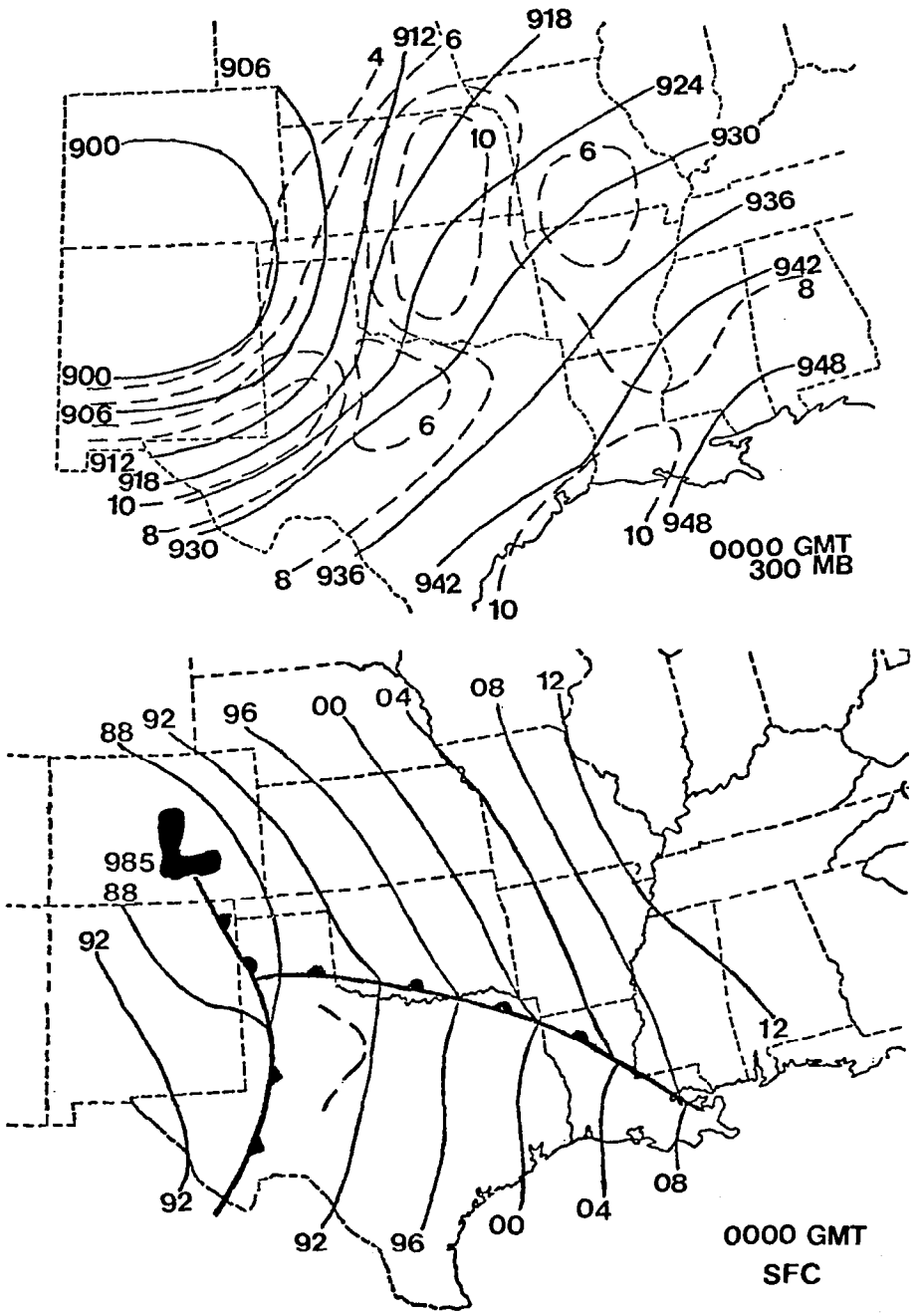

Figure 10. Surface and 300 mb charts at 0000 GMT 11 April 1979. Surface contours are in millibars. Height lines at 300 mb are in tens of meters and isotachs are in tens of knots.

and 30 m over Oklahoma City. These falls were in the left exit region of the upper-level jet over western Texas. The secondary jet streak noted at 2100 GMT over Oklahoma (Fig. 7) had expanded to include most of Kansas. Its space-time correspondence suggests a link to the convection.

The radar summary for 0235 GMT (Fig. 11) shows intense convection in three separate areas. The storms encompassing the Red River Valley at 0000 GMT (Fig. 9) moved into Oklahoma producing heavy rains but no additional tornado activity. A larger area of less intense convection covered most of Kansas and Missouri. A new area of convection formed in westcentral Texas with echo tops reaching 53,000 ft (17.2 km).

Surface conditions at 0300 GMT (Fig. 12) showed little movement of the warm front from its position 3 h earlier. The dry line in the warm sector became diffuse. A closed low (991 mb) formed at the southern end of the cold front over the Big Bend region of Texas while the major low (985 mb) remained over southeastern Colorado. The low-level jet strengthened and moved eastward into Arkansas.

At 300 mb (Fig. 12), the height perturbation now was positioned over central Oklahoma where 3 h height tendencies (not shown) indicated falls of 40 m over Oklahoma City and Durant, and 30 m over Childress. This perturbation corresponds with the area of convection over Oklahoma. No significant height perturbations in the upper levels were associated with the west Texas storms at this time. However, the isotach field at 300 mb

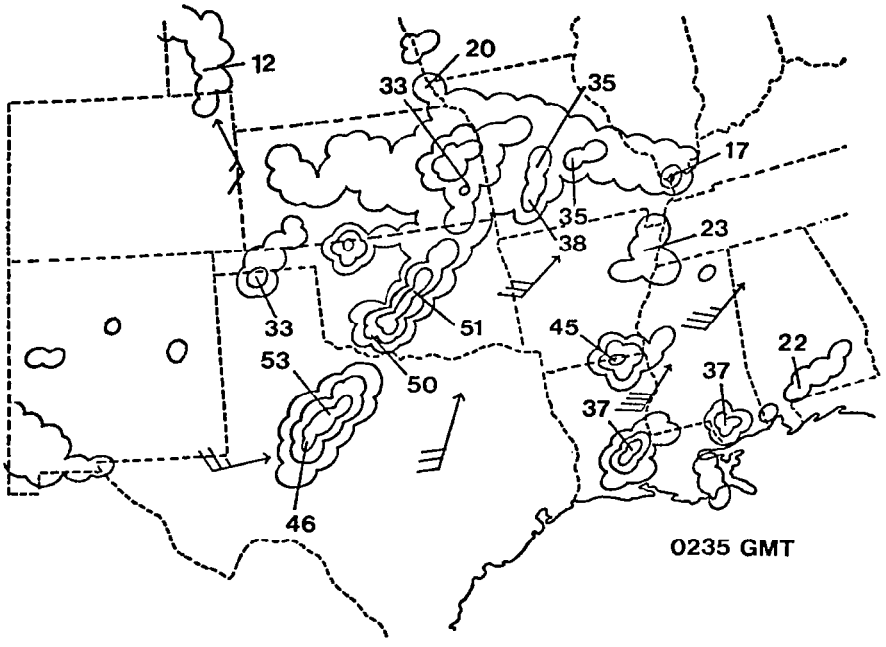

Figure 11. Radar summary for 0235 GMT 11 April 1979. Echo tops are in thousands of feet.

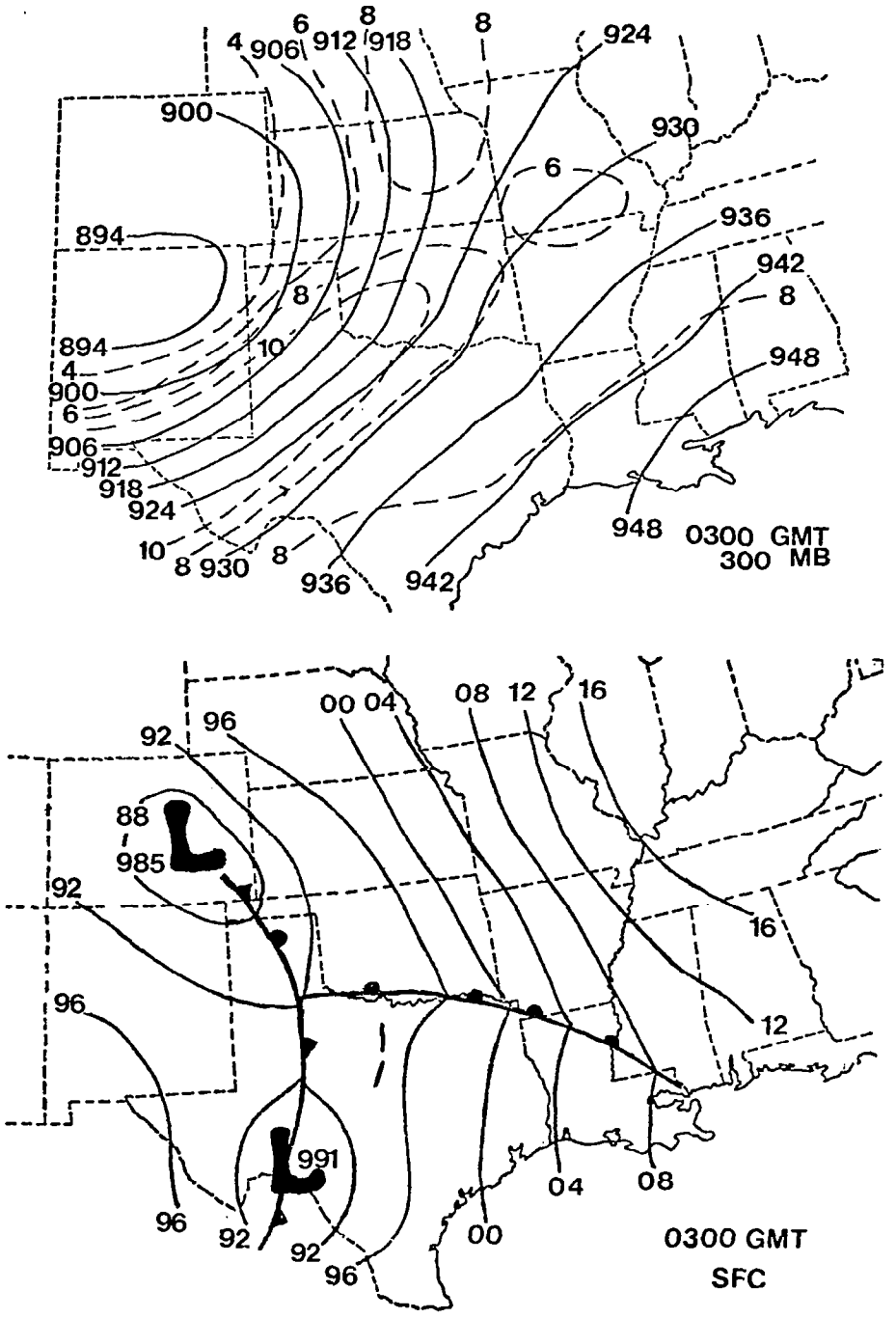

Figure 12. Surface and 300 mb charts at 0300 GMT 11 April 1979. Surface contours are in millibars. Height lines at 300 mb are in tens of meters and isotachs are in tens of knots.

indicates the advance of the major jet streak from the southwest. Winds in excess of 50 m s^{-1} extended in a narrow band from the base of the upper-level trough into Oklahoma. The secondary jet streak previously located over Oklahoma and Kansas (Fig. 10) moved northward into Kansas and Nebraska by 0300 GMT. This feature had weakened during the past 3 h and no longer corresponded to major convective regions.

d. Post-outbreak conditions

The last tornado of the RRVTO occurred near 0200 GMT 11 April. The storms producing the outbreak moved into central Oklahoma, Arkansas, and southern Missouri during the later hours of the AVE-SESAME I experiment but did not produce further severe activity. Storms which developed in western Texas near 0300 GMT produced several tornadoes that did not cause major damage or injury. This area underwent various stages of growth and decay as it moved eastward through central Texas during the night.

Synoptic conditions at the end of the AVE-SESAME I period (1200 GMT 11 April), are shown in Fig. 13. The surface low (984 mb) was positioned over southeastern Colorado with an occluded front extending just south of Oklahoma City. From this point the cold front extended southward through San Antonio, bringing cool, dry Pacific air into central Texas. The warm front extended from Oklahoma through southern Arkansas, and

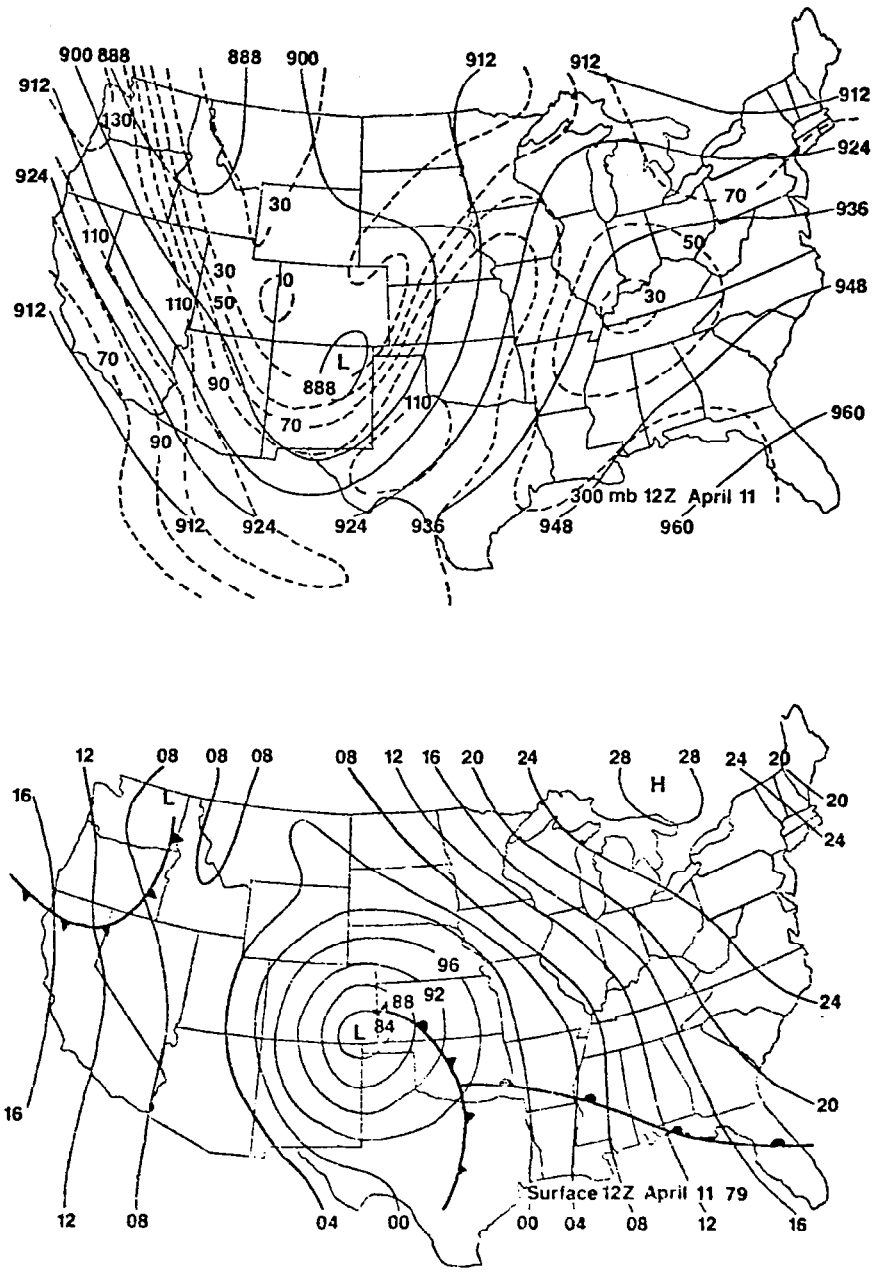

Figure 13. Synoptic conditions at 1200 GMT 11 April 1979. At the surface, pressure is in millibars (04 means 1004 mb). At 300 mb, height lines are in tens of meters and isotachs are in knots.

then along the Gulf Coast. The major upper-level trough over the mountains deepened and moved eastward throughout the period. The upper-level jet streak located at the base of the trough 24 h ago (Fig. 3) had rotated around the low and into the Midwest with winds in excess of 55 m s^{-1}. Another region of strong winds remained over the Pacific coast.

The remaining convection (Fig. 14) was concentrated in Illinois, Missouri, Arkansas, and northeastern Texas. Radar echo tops reached 48,000 ft (14.6 km) in Texas and Arkansas with more shallow convection to the north. No severe weather activity occurred with these storms.

The formation of the Wichita Falls tornado and other severe storms in the area seem related to subsynoptic-scale features evident in the AVE-SESAME I data. Some of these features have been described above; however, more discussion is given by Moore and Fuelberg (1981) and Carlson et al. (1980). The aim of the current research is to study these features and their relation to the convection by examining the kinetic energy balance during the outbreak.

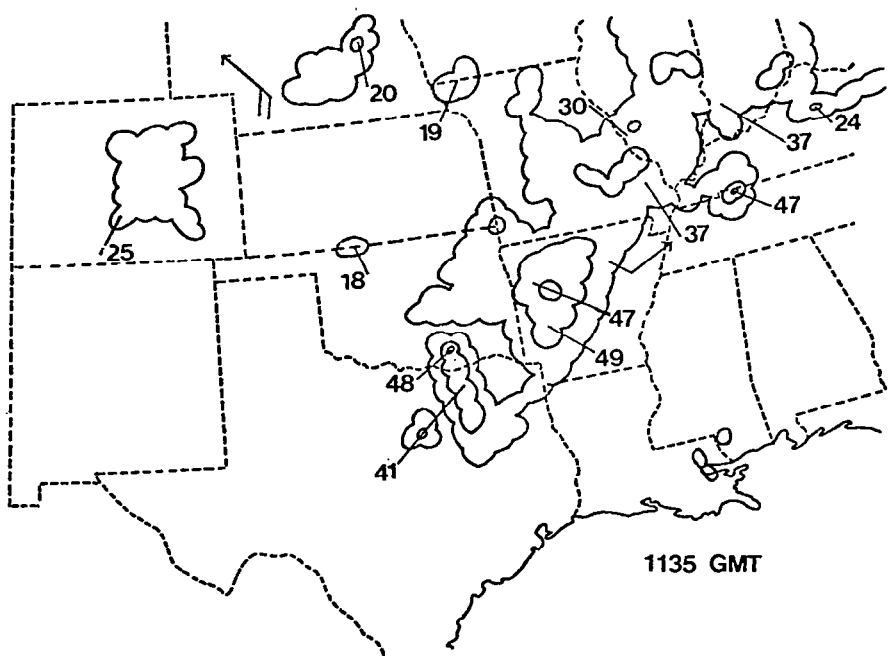

Figure 14. Radar summary at 1135 GMT 11 April 1979. Echo tops are in thousands of feet.

5. RESULTS

a. Kinematic analysis

Calculation of the kinetic energy budget necessitates the computation of divergence and vertical motion (see Section 3c). These derived parameters also describe the conditions under which convection occurs during AVE-SESAME I. In the paragraphs below, spatial fields of kinematic parameters are evaluated for time and space continuity and are compared to areas of convection in order to assess the "goodness" of the input data and computational procedures.

Values of horizontal divergence used in this study have been adjusted (see Section 3c) to produce consistency with the adjusted ω values. This procedure may increase or decrease values of divergence at a given level depending on the unadjusted ω value at 100 mb. Previous studies have indicated that fields of adjusted horizontal divergence correspond better to convection areas than do the unadjusted fields (e.g., O'Brien, 1970; Fankhauser, 1969; Chien and Smith, 1973). As an example of the adjustment procedure, Fig. 15 shows patterns of adjusted and unadjusted divergence for 300 mb at 1800 GMT 10 April. The corresponding radar summary is shown in Fig. 6. Although both fields exhibit the same general patterns, the adjusted field contains weaker upper-level divergence over those areas where convec-

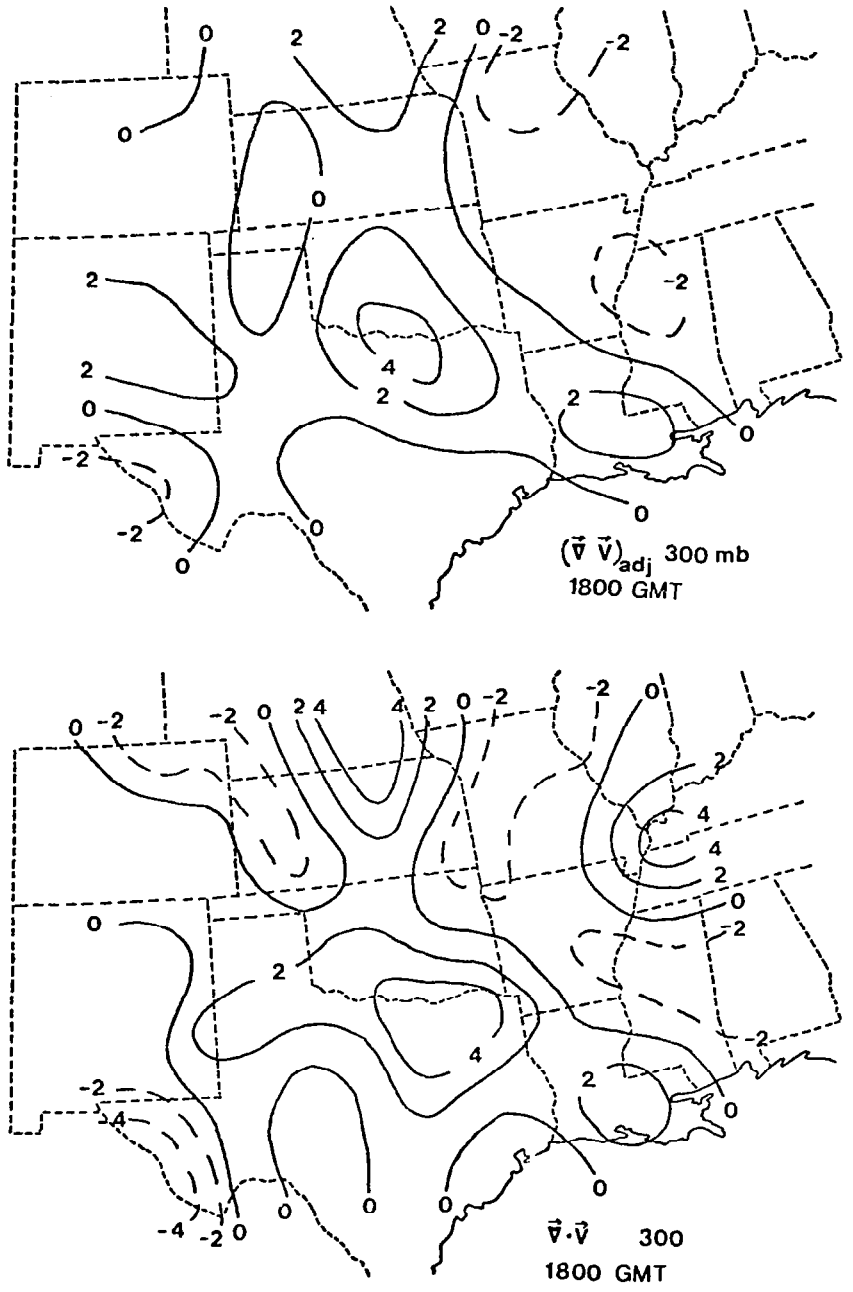

Figure 15. Adjusted and unadjusted 300 mb divergence at 1800 GMT 10 April 1979. Values in each case are x 10^{-5} s^{-1}.

tion is less intense (Kentucky, Tennessee, and Nebraska). For instance, divergence near Concordia, Kansas is reduced from 5.4×10^{-5} s^{-1} to 2.9×10^{-5} s^{-1}. Centers of divergence from either scheme are located near regions of convection. Unless otherwise noted, adjusted divergence will be used throughout this study although the word "adjusted" will be omitted.

Fields of vertical motion and advection of relative vorticity at 500 mb for 1800 GMT are shown in Fig. 16. Most of the area exhibits gentle upward motion ($\omega < 0$); however, the two major centers of strongest values over New Mexico and northcentral Texas correspond to the developing convective areas in Fig. 6. Vorticity advection supports these vertical motions since the most pronounced maximum (11.1×10^{-10} s^{-2}) corresponds to the areas of ascent in Texas and New Mexico.

Time and space continuity of the kinematic parameters is an important consideration in evaluating the success of the computational procedures. Fields of vertical motion at 500 mb and divergence at 300 mb for 2100 GMT are shown in Fig. 17. The dramatic increase in upward motion over Texas and Oklahoma (from -6.2 to -18.1 μb s^{-1}) results from increased low-level convergence (Fig. 18) and upper-level divergence (Fig. 17). The two centers of ascent at 1800 GMT (Fig. 15) apparently merged over the Red River Valley while increasing in magnitude. Upper-level divergence nearly triples during the 3 h period with values at 2100 GMT reaching 10.7×10^{-5} s^{-1}. The most intense convection at

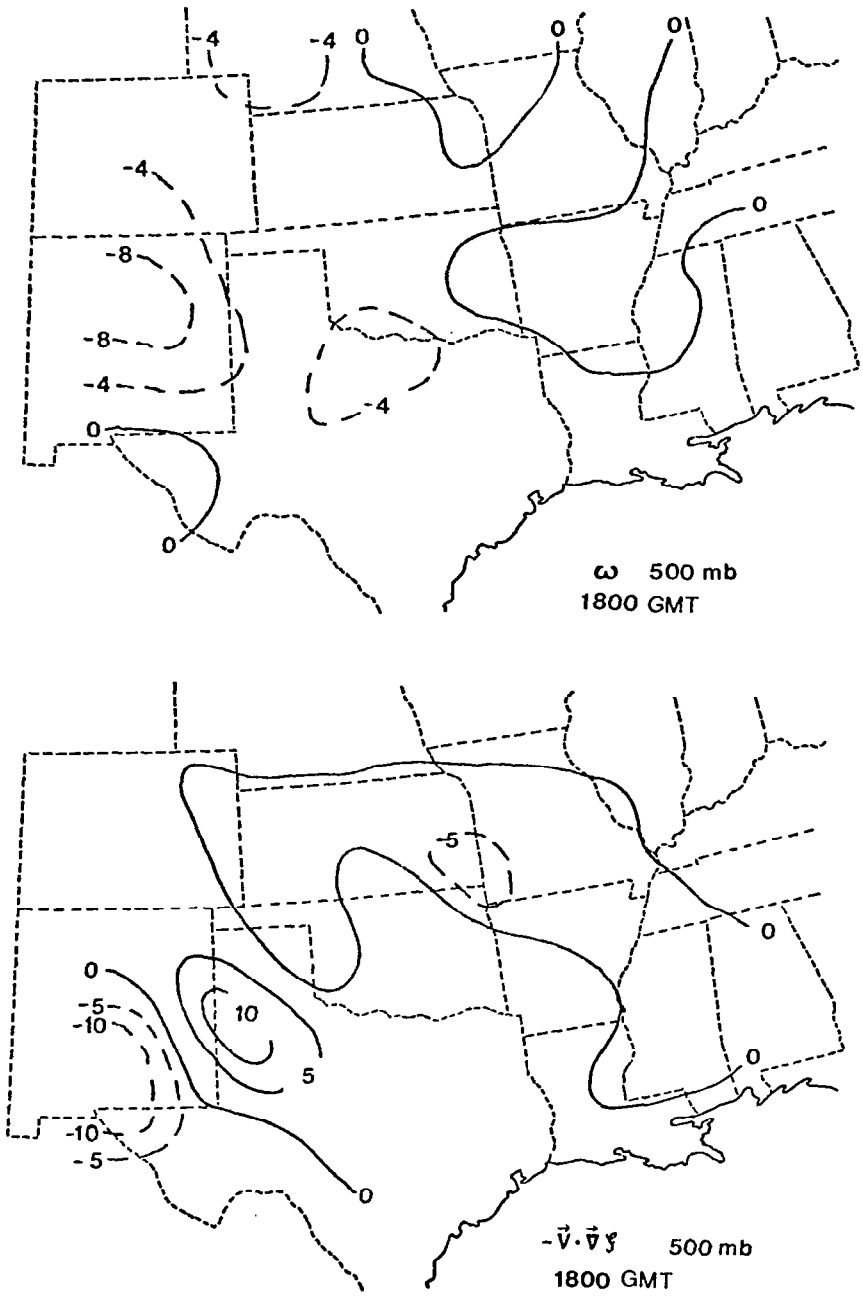

Figure 16. Vertical motion and advection of relative vorticity at 500 mb for 1800 GMT 10 April 1979. Units are $\mu b\ s^{-1}$ for vertical motion and values of advection are $\times 10^{-11}\ s^{-1}$.

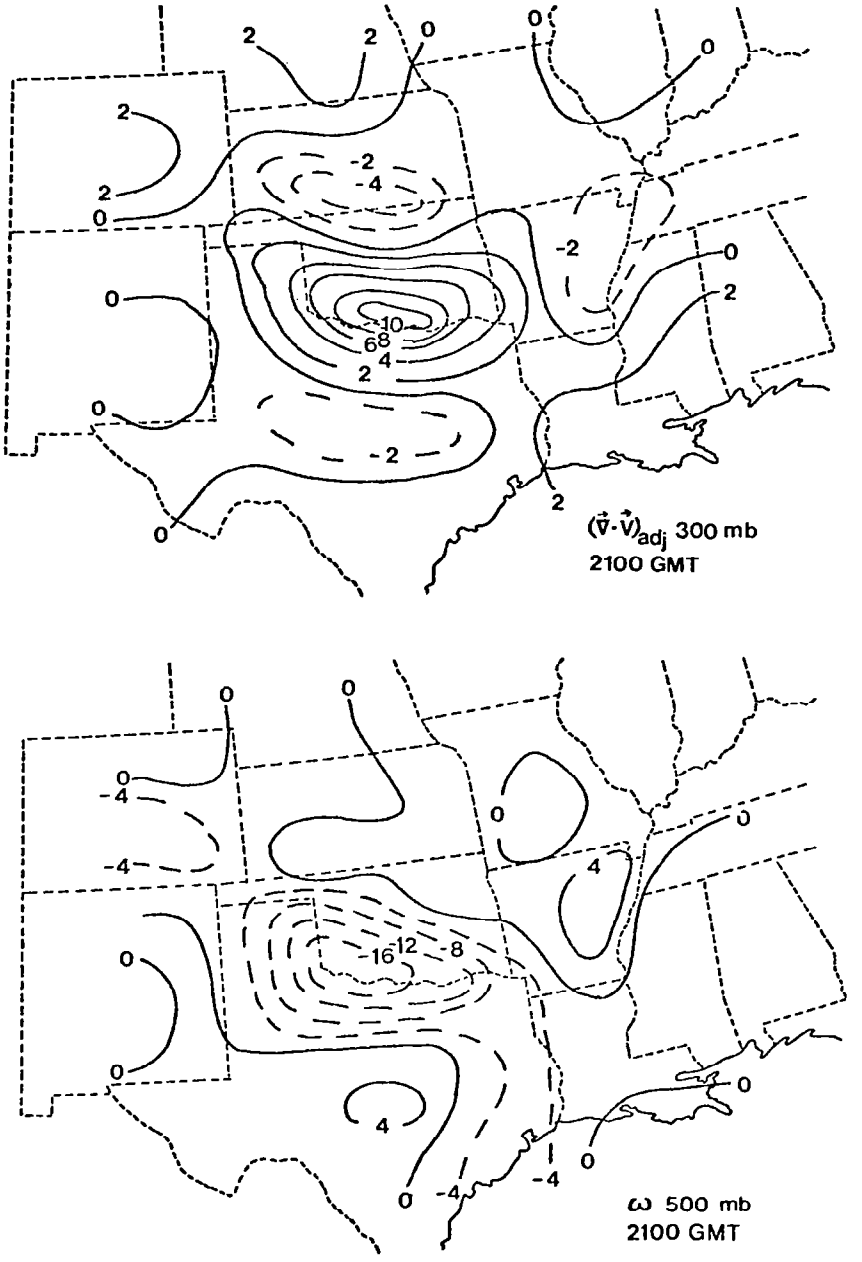

Figure 17. Vertical motion at 500 mb and adjusted divergence at 300 mb for 2100 GMT 10 April 1979. Values of divergence are x 10^{-5} s^{-1} and the units of vertical motion are μb s^{-1}.

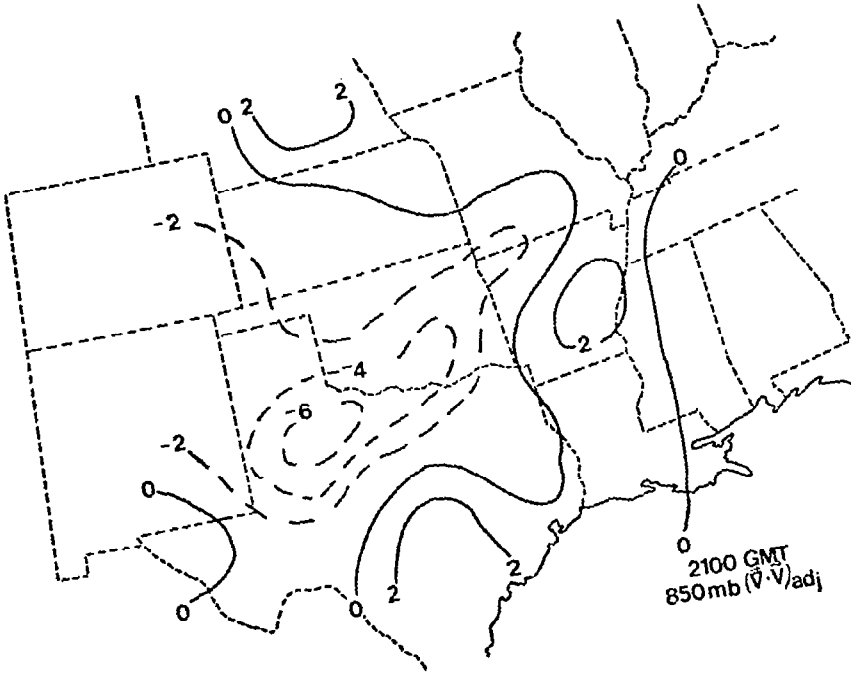

Figure 18. Adjusted divergence at 850 mb for 2100 GMT 10 April 1979. The units are x 10^{-5} s^{-1}.

2035 GMT (Fig. 8) is located southwest of the supporting centers of rising air and divergence. Kinematic fields at 0000 GMT are shown in Fig. 19. Again there is good continuity with the previous fields (Fig. 17) and also with the observed convection (Fig. 9). The area of upward motion shifts northeastward, as does the convection, obtaining a maximum value of -19.7 μb s^{-1} near Oklahoma City. Ascending motion over Missouri increases from -2.4 to -11.8 μb s^{-1} during the 3 h period as convection moves into the area. Centers of upper-level divergence over Missouri and Oklahoma are associated with the ascent and convection. Magnitudes of divergence over Oklahoma decrease during the 3 h period, but the areal coverage greatly increases. Maps for 0300 GMT (Fig. 20) show a continuation of developments over the last 6 h. The area of upward motion expands, forming a center over Kansas (-15.1 μb s^{-1}) and another over the Texas-Oklahoma border (-12.9 μb s^{-1}). Similarly, areas of upper-level divergence expand, although magnitudes are comparable to those of 3 h earlier.

In order to evaluate the effects of adding the special site data and of the more sophisticated computational procedures, synoptic-scale patterns of vertical motion at 500 mb and divergence at 300 mb (Fuelberg et al., 1980) are shown in Figs. 21-23 for 1800, 2100, and 0000 GMT. As expected there are numerous differences between the synoptic- and subsynoptic-scale fields. Vertical motions in the present

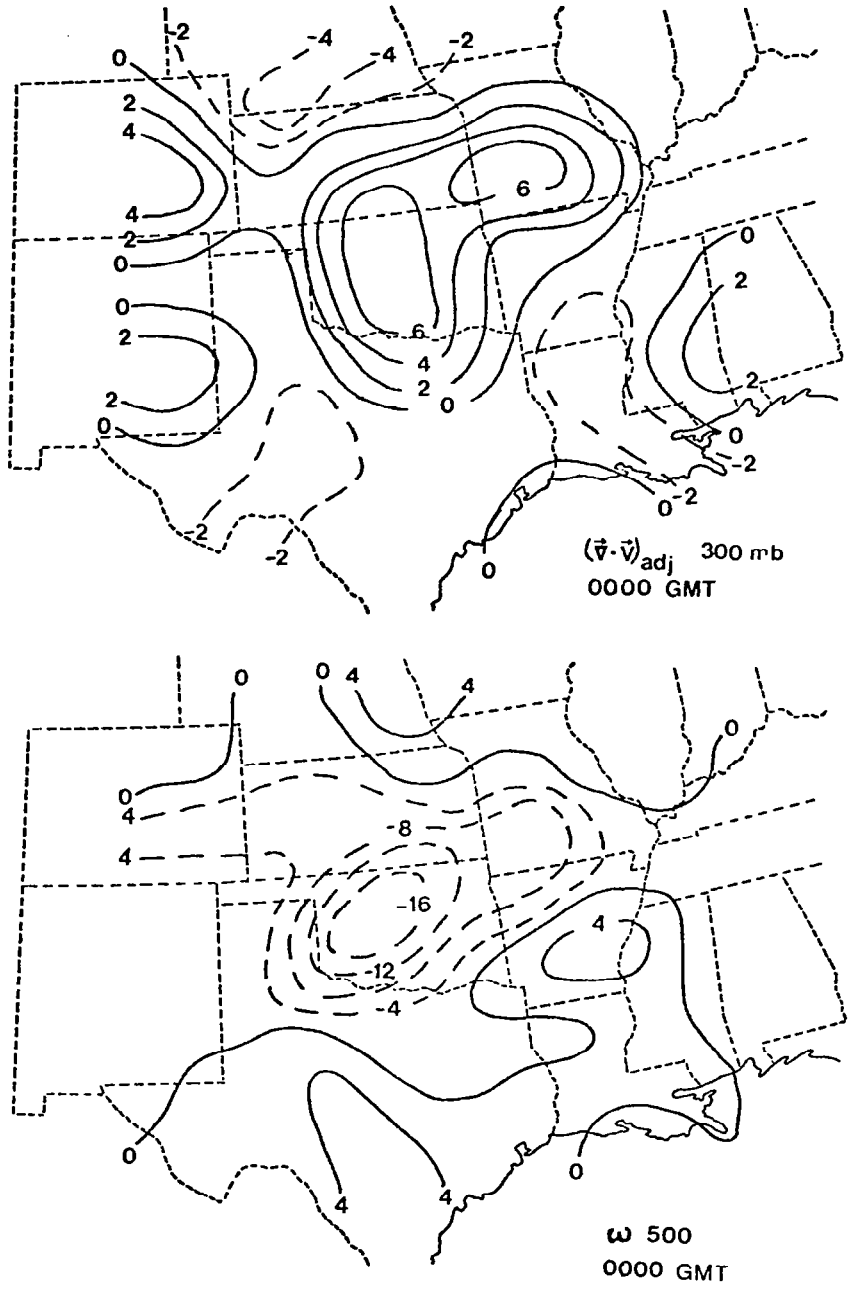

Figure 19. Adjusted divergence at 300 mb and vertical motion at 500 mb for 0000 GMT 11 April 1979. Values of divergence are x 10^{-5} s^{-1} and the units of vertical motion are μb s^{-1}.

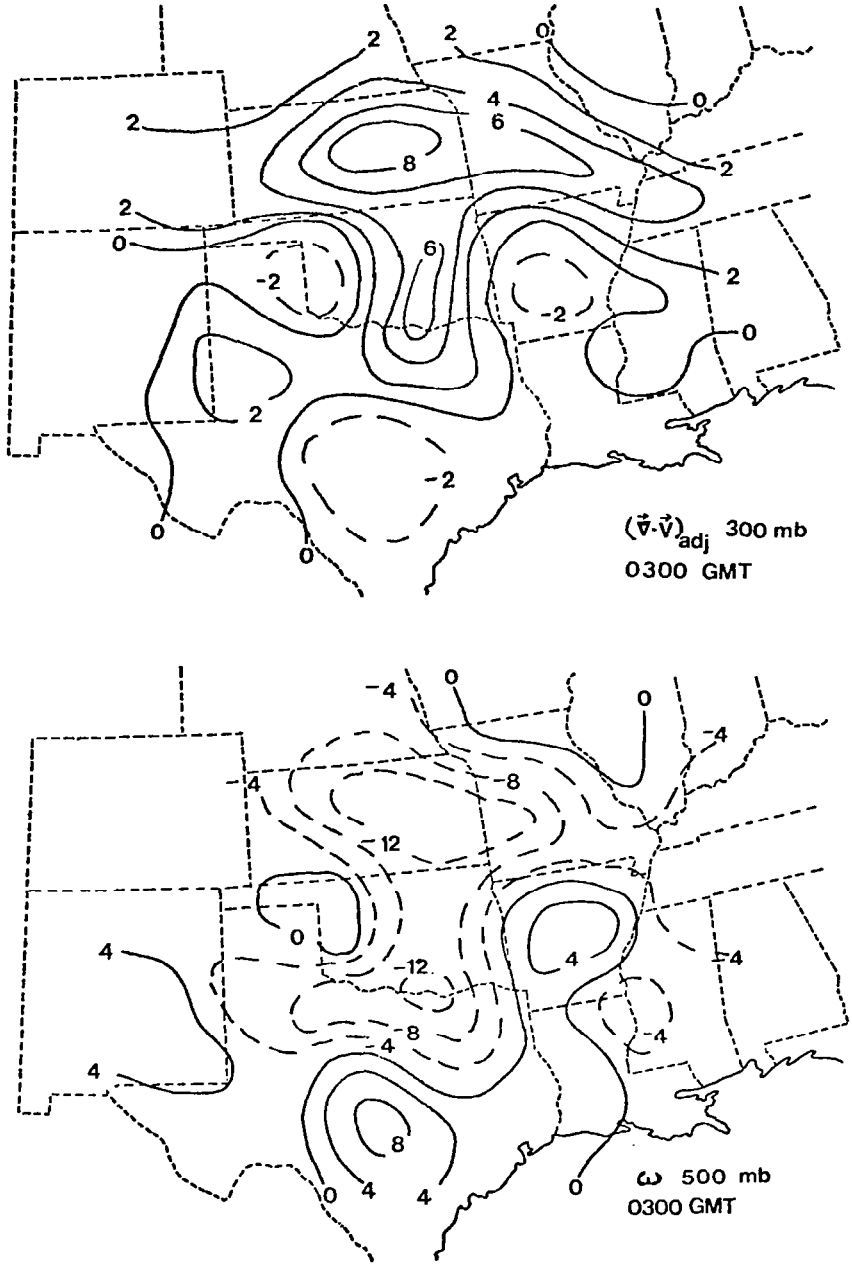

Figure 20. Adjusted divergence at 300 mb and vertical motion at 500 mb for 0300 GMT 11 April 1979. Values of divergence are x 10^{-5} s^{-1} and the units of vertical motion are μb s^{-1}.

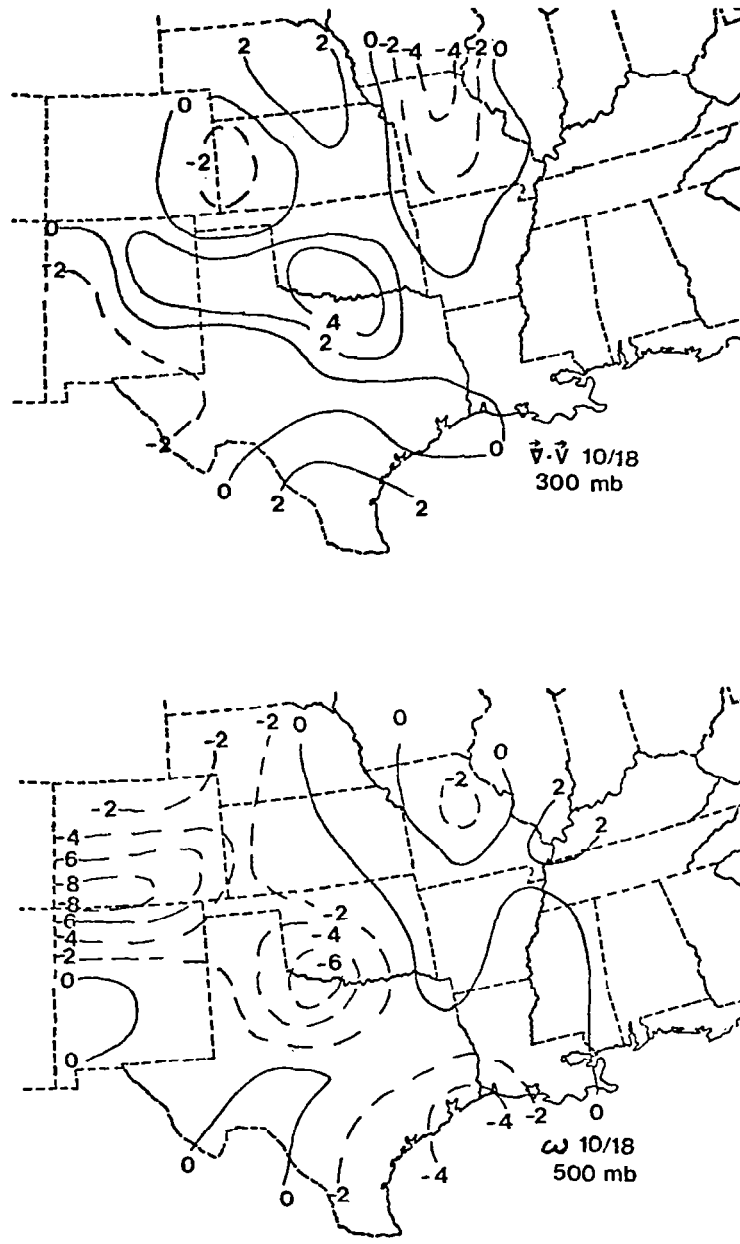

Figure 21. Synoptic-scale adjusted divergence at 300 mb and vertical motion at 500 mb for 1800 GMT 10 April 1979. Values of divergence are x 10^{-5} s^{-1} and vertical motion is $\mu b\ s^{-1}$ (Fuelberg et al., 1980).

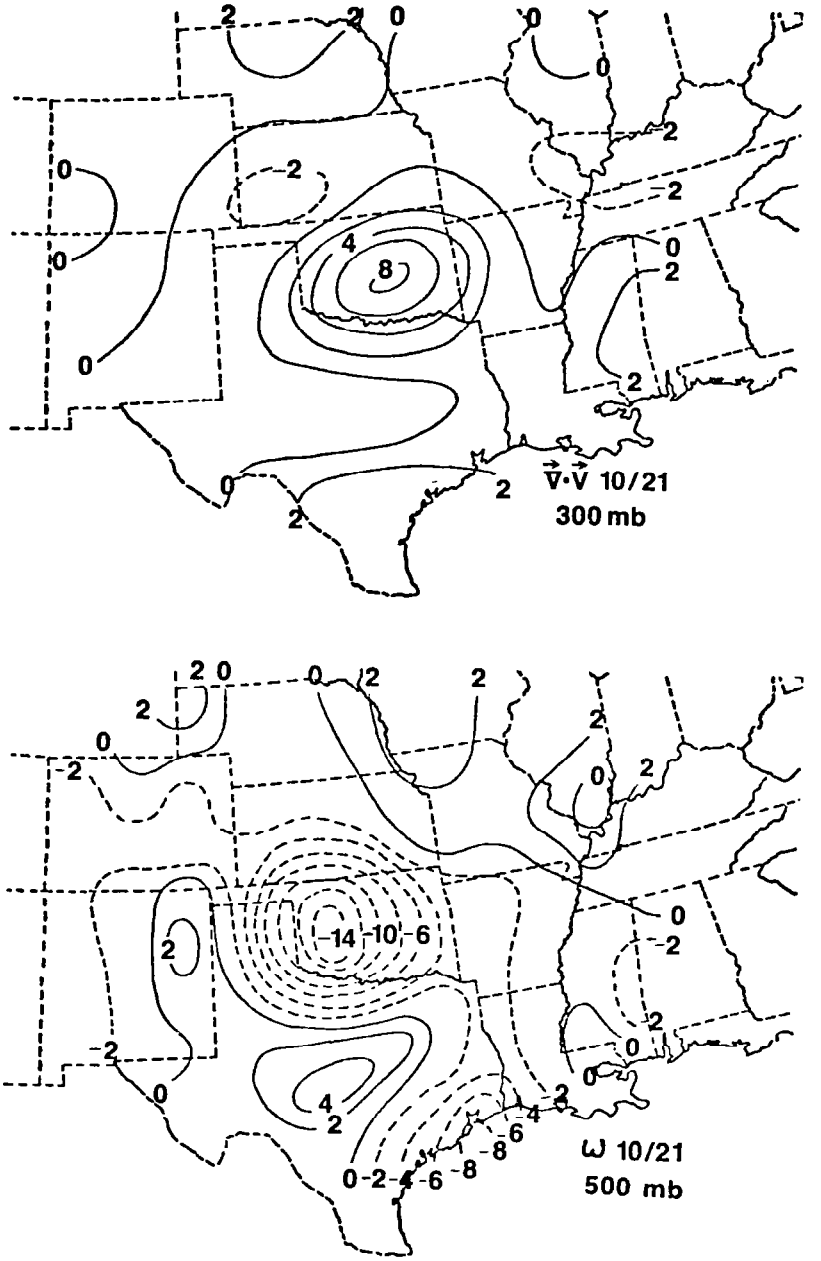

Figure 22. Synoptic-scale adjusted divergence at 300 mb and vertical motion at 500 mb for 2100 GMT 10 April 1979. Values of divergence are x 10^{-5} s^{-1} and vertical motion is μb s^{-1} (Fuelberg et al., 1980).

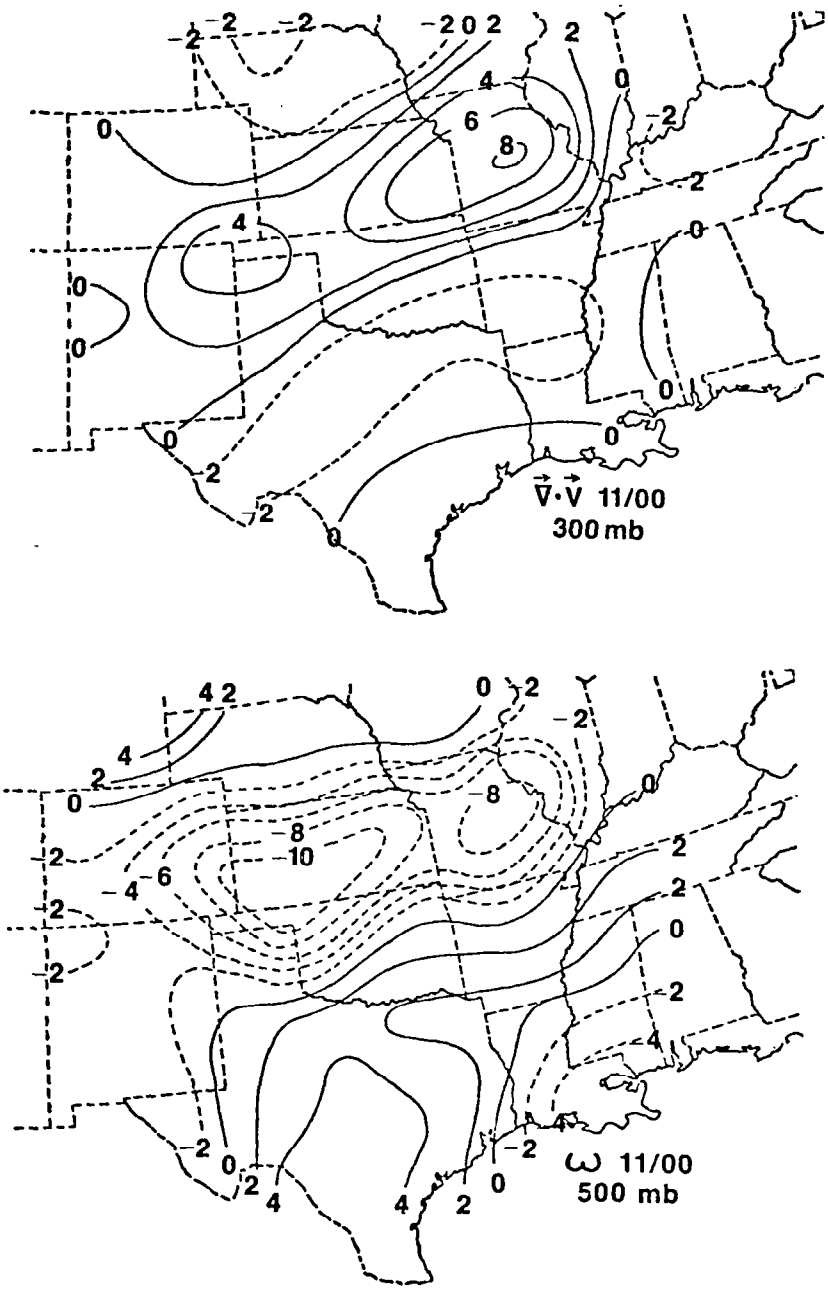

Figure 23. Synoptic-scale adjusted divergence at 300 mb and vertical motion at 500 mb for 0000 GMT 11 April 1979. Values of divergence are x 10^{-5} s^{-1} and vertical motion are μb s^{-1} (Fuelberg et al., 1980).

study (Figs. 16,17, and 19) tend to be 20-40% larger than those of Fuelberg et al. (1980). Although partly due to non-zero surface vertical motions included in the current study, the larger magnitudes primarily result from enhanced resolution of smaller scale features within the region. A similar enhancement occurs in magnitudes of upper-level divergence which tend to be 20-30% larger in the current study. Major differences in the patterns are seen at 0000 GMT when centers of maximum vertical motion and divergence have considerably different locations (Figs. 19, 23). This occurs because a significant amount of data is missing at this time, particularly in the upper levels. Current procedures linearly interpolate missing values (see Section 3) retrieving approximately 50% of the missing data. Because the synoptic-scale procedures of Fuelberg et al. (1980) did not contain the interpolation feature, they were left with data gaps over northcentral Texas and Oklahoma. The present patterns based on the combination of observed and interpolated data show better time and space continuity and better agreement with the observed convection (see Fig. 9) than those of the previous study.

The preceding results indicate that the computational procedures described in Section 3 have produced an accurate and consistent data set. In addition, results document the rapid changes in kinematic parameters that occur between 1800 and 2100 GMT, coinciding with the beginning of the RRVTO.

Armed with this information, time and space variability of the kinetic energy balance now will be described for the AVE-SESAME I period.

b. Area-time averaged energetics

The kinetic energy budget equation, (1), was evaluated at individual grid points for each of the nine observation times comprising AVE-SESAME I. In order to describe the major energy characteristics at each time, grid point values then were averaged over an interior section of the total analysis region shown in Fig. 1. This particular area was chosen for two reasons. First results along the periphery, which were derived from grid points having comparatively few nearby rawinsonde reports, should not be included. Second, the selected region corresponds closely to the area used by Fuelberg et al. (1980) in their synoptic-scale study.

A comparison of the two areas, shown in Fig. 24, reveals that both are approximately 1.6×10^6 km^2. Although the current area (solid line) is shifted northeastward by about 100 km, due to the spacing and orientation of the grid, this should have little effect on differences between the two sets of results. The nine area-averaged kinetic energy budgets then were combined to produce the area-time averaged budget given in Table 1. Synoptic-scale vertical totals from Fuelberg et al. (1980) also are shown. Meanings of the

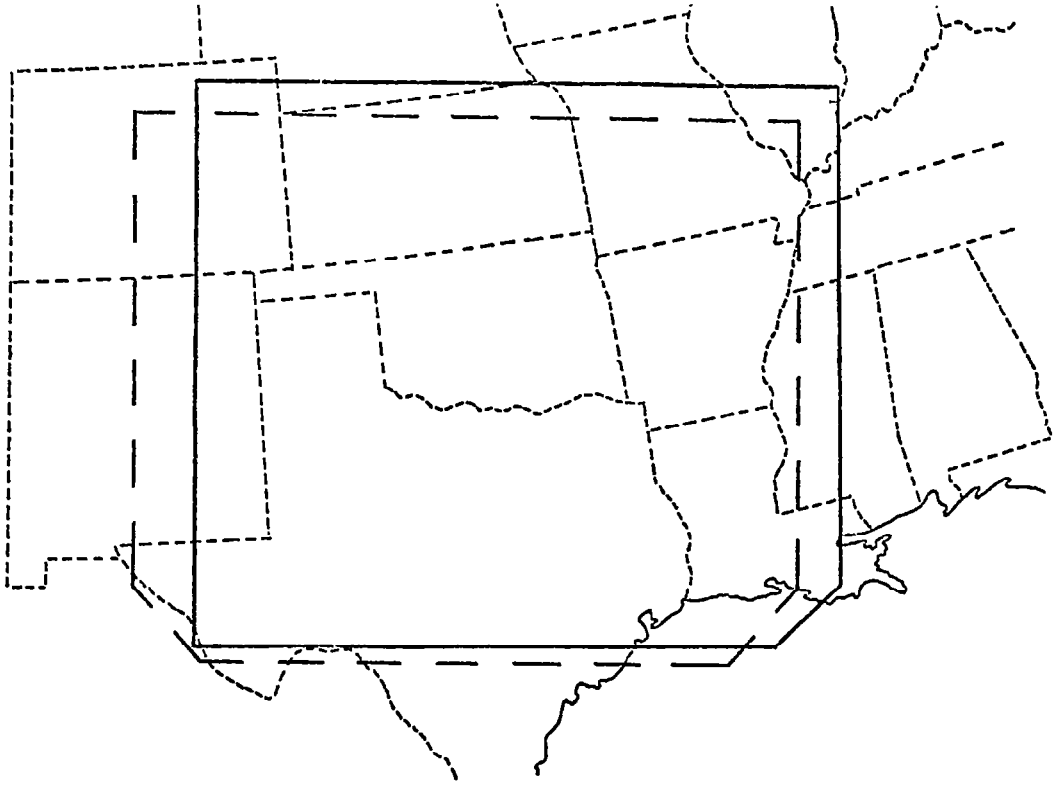

Figure 24. Energy budget averaging areas for the current and synoptic-scale studies. The current area (solid) is shifted to the northeast by about 100 km from the previous area (dashed) (Fuelberg et al., 1980).

Table 1. Area-time averaged subsynoptic-scale kinetic energy budget for AVE-SESAME I. Vertical totals for the synoptic-scale AVE-SESAME I (Fuelberg et al., 1980) are given at the bottom. All units are $W\ m^{-2}$ except for K which is $10^5\ J m^{-2}$.

Pressure Layer (mb)	K	$\partial k/\partial t$	$-\vec{V}\cdot\vec{\nabla}\phi$	$\vec{V}\cdot k\vec{V}$	$(\vec{V}\cdot k\vec{V})_{adj}$	$k(\vec{V}\cdot\vec{V})_{adj}$	$\vec{V}\cdot\vec{\nabla}k$	$\frac{\partial \omega k}{\partial p}$	disp	$(disp)_{adj}$
200-100	8.0	1.3	-6.2	1.7	-1.2	5.1	-6.3.	-5.2	3.9	1.0
300-200	8.4	2.1	-8.8	-1.4	-3.7	6.5	-10.2	-3.8	5.6	3.4
400-300	6.0	3.9	-5.8	-10.3	-11.4	1.7	-13.1	0.6	-0.1	-1.1
500-400	4.4	3.3	-1.5	-6.2	-6.7	0.8	-7.5	0.7	-0.6	-1.1
600-500	3.1	2.3	1.4	-2.1	-2.5	0.0	-2.6	1.9	0.7	0.2
700-600	2.1	1.2	2.2	-0.8	-1.1	-0.6	-0.4	2.2	0.3	0.1
800-700	1.6	1.4	3.0	-1.1	-1.2	-1.0	-0.3	1.5	-1.3	-1.4
900-800	1.3	1.1	5.7	-0.9	-1.0	-0.8	-0.2	1.2	-4.3	-4.4
Sfc-900	0.5	0.4	4.2	-0.2	-0.3	-0.2	-0.1	0.8	-3.2	-3.3
Vertical Total	35.4	17.0	-5.7	-21.5	-29.2	11.5	-40.7	0.0	1.1	-6.6
Vertical Total (Fuelberg et al., 1980)	35.3	13.3	-30.9	-38.6	-33.6	-----	-----	0.0	5.6	10.6

various energy terms were given in Section 2 with the exception of $(\vec{\nabla}\cdot k\vec{\nabla})_{adj}$, $(k\vec{\nabla}\cdot\vec{\nabla})_{adj}$, $\vec{\nabla}\cdot\vec{\nabla}k$, and $(disp)_{adj}$ which will be explained below.

Kinetic energy content of the surface to 100 mb column is 35.4×10^5 J m^{-2}, with maximum contributions from the upper troposphere near the level of the jet stream. This total is very similar to that of the synoptic-scale study indicating that comparable amounts of energy are resolved on both scales of resolution when all observations are grouped together. In each study the area experiences a local increase in energy during the 24 h period. The greater subsynoptic-scale value (17.0 W m^{-2}) is due mostly to differing contributions from the middle and upper levels. Larger local increases can occur without a corresponding difference in time averaged energy content because contents at the individual times differ even though the average for the entire period is similar. Time variability of the energetics will be described in a later section.

Local changes in kinetic energy content are due to various sources, sinks, and external transports. Destruction of kinetic energy by cross-contour flow ($-\vec{\nabla}\cdot\vec{\nabla}\phi < 0$) produces a vertical total of -5.7 W m^{-2} when subsynoptic-scale data are used. Significant generation of energy below 500 mb is outweighed by destruction in the upper atmosphere producing the overall negative value. This result is substantially different from that of the synoptic-scale study where cross-

contour flow produced a much larger sink (-30.9 W m^{-2}). Although the area-time averaged totals of the two resolutions are considerably different, this is not to say that the better resolved motions at particular locations and times are less ageostrophic. Instead, the overall effect of the higher resolution is to produce an area-time average revealing smaller destruction at the finer scale. Horizontal flux convergence ($\vec{\nabla}\cdot k\vec{V} < 0$) is the major source of kinetic energy to the region. The largest contribution to the vertical total of -21.5 W m^{-2} is found in the upper levels where jet intrusion from the southwest occurs. A secondary maximum is located in the 800-700 mb layer due to the low-level jet. The magnitude of the vertical total is less than that at the synoptic scale (-38.6 W m^{-2}). Although import of kinetic energy is smaller for the overall average when subsynoptic-scale data are employed, transport is not necessarily less important at individual locations.

The horizontal flux term can be separated into two components as shown in (3)

$$\vec{\nabla}\cdot k\vec{V} = \vec{V}\cdot\vec{\nabla}k + k\vec{\nabla}\cdot\vec{V}. \qquad (3)$$

The first term on the right represents horizontal advection of kinetic energy while the second term is horizontal divergence weighted by kinetic energy. As mentioned in Section 3c, horizontal velocity divergence can be adjusted to produce consistency with adjusted vertical motions. These adjusted values then can be used in computing the horizontal flux

term as shown below (see Fuelberg et al., 1980)

$$(\vec{\nabla}\cdot k\vec{V})_{adj} = \vec{V}\cdot\vec{\nabla}k + k(\vec{\nabla}\cdot\vec{V})_{adj} \quad . \tag{4}$$

Values of the new quantity on the left, called "adjusted horizontal flux" and the contributions from each term on the right are given in Table 1. Although the adjusted flux indicates a greater import of energy than does the unadjusted value, this external source still is smaller than when synoptic-scale data are employed. It is noteworthy that the major contribution to adjusted flux results from advection of kinetic energy rather than the divergence effect. The divergence term dominates only in the lower layers where velocity convergence is quite strong and significant advection is confined to the vicinity of the low-level jet.

Several points about the adjusted horizontal flux should be made. First, the two terms which comprise it usually have opposite signs particularly in the upper levels. At some times and/or locations the adjusted flux might be a very small difference between two larger quantities and thus be influenced by error in either term. This is not an important consideration in the vertical totals of Table 1, but should be considered for individual layers. Second, differences between the two flux terms indicate the nature of the divergence adjustment. At the finer resolution, the adjustment of velocity divergence produces an increase in horizontal flux convergence in the area-time averaged vertical total. At the synoptic scale, however, the adjustment reduces the

flux convergence. Horizontal flux convergence can decrease only if the adjustment increases the upper-level velocity divergence. In the current study, however, upper-level velocity divergence is decreased thereby producing larger values of flux convergence. This suggests that the upper-level unadjusted divergence patterns resolved by the subsynoptic-scale data must differ considerably from the unadjusted synoptic-scale fields.

Individual layer values of the vertical flux divergence term show an export of energy ($\frac{\partial \omega k}{\partial p} > 0$) in the lower and middle layers and a large vertical import in the 300-100 mb layer. This result is consistent with the widespread ascending motion during much of the AVE-SESAME I period. Vertical transport of energy is a greater source to many layers than is the contribution due to adjusted horizontal flux. Even though vertical flux divergence in the total column integrates to zero during the time and space averaging, this need not be the case at individual locations, since only vertical motion at 100 mb was prescribed to be zero.

The vertical total of dissipation (disp) (1.1 W m^{-2}) indicates a small source of energy from the subgrid scales to the resolvable (subsynoptic) scales of motion. Traditional mechanical and thermodynamical frictional effects produce a sink of energy (disp <0) in the lowest layers. Individual layer values are small in the middle troposphere but increase to become a significant source of energy (disp <0) above

300 mb. This profile is similar to that of the synoptic-scale study, except that the previous vertical total is slightly larger (5.6 W m^{-2}). An "adjusted dissipation" term, $(disp)_{adj}$, arises from using adjusted horizontal flux in (1) to compute this residual term. The vertical profile of adjusted dissipation is similar to that of the unadjusted values; however, the upper-level source from subgrid scales of motion has been reduced, making the vertical total negative (a sink of energy).

Caution must be exercised in physically interpreting the dissipation terms. Since they are computed as residuals, they contain the traditional frictional influences, upwelling effects from subgrid-scale processes, as well as any data and computational errors contained in all other terms. However, the adjusted dissipation term may be slightly more reliable because of the errors that are reduced in the adjustment process. Previous studies (e.g., Robertson and Smith, 1980; Vincent and Chang, 1975; Fuelberg and Scoggins, 1980) have used error analysis techniques to establish confidence limits in energy budget calculations. Results of error simulation using the current subsynoptic-scale data are described in Section 3d and the Appendix.

To the author's knowledge, no other studies have investigated energetics using input data with a spacing near 250 km. Therefore, a direct comparison of current results with those using similar data is not possible. Table 2 gives the area-time

Table 2. Vertically integrated area-time averaged kinetic energy budgets for various studies. All units are W m^{-2} except for K which is 10^5 J m^{-2}.

Study	Scale	K	$\partial k/\partial t$	$\vec{V}\cdot\vec{\nabla}\phi$	$\vec{V}\cdot k\vec{V}$	$(\vec{V}\cdot k\vec{V})_{adj}$	$\frac{\partial \omega k}{\partial p}$	disp	$(disp)_{adj}$
Current study RRVTO	meso-α 3 h	35.4	17.0	-5.7	-21.5	-29.5	0.0	1.1	-6.6
Fuelberg et al. (1980) RRVTO	synoptic 3 h	35.3	13.3	-30.9	-38.6	-33.6	0.0	5.6	10.6
Robertson and Smith (1980) Palm Sunday 1965	synoptic 12 h	28.7	6.7	-27.6	-25.6	------	---	8.7	----
Fuelberg and Scoggins (1978) AVE 4	synoptic 3 and 6 h	19.9	-3.7	-4.0	1.6	------	0.0	1.6	----
Tsui and Kung (1977) Convective cases	meso-β 1½ h	21.0	4.6	89.5	-11.0	------	-0.2	-96.0	----
Tsui and Kung (1977) Non-convective cases	meso-β 1½ h	9.5	0.2	-34.9	4.6	------	-0.1	39.7	----

averaged kinetic energy budget for the current study along with others using different scales of input data. All studies encompassed periods of major convective activity. Although the current results have already been compared with the concurrent synoptic-scale study of Fuelberg et al. (1980), these values also are included for easy reference. Robertson and Smith (1980) investigated synoptic-scale energetics associated with the Palm Sunday 1965 tornado outbreak which was characterized by the propagation of a short wave through a long wave trough in the western portion of the region. Generally, the energetics of the Palm Sunday outbreak are similar to those of the RRVTO. Kinetic energy content is somewhat smaller, as is the local change of kinetic energy. The latter may be due to their longer period of investigation (36 h). Cross-contour destruction of kinetic energy is similar to that of the synoptic-scale study but is considerably larger than that of the present subsynoptic-scale investigation. Values of horizontal flux convergence are similar in both cases. Like the RRVTO, the Palm Sunday outbreak is characterized by a small subgrid-scale source of energy. Fuelberg and Scoggins (1978) conducted a synoptic-scale study during a period containing two mesoscale convective complexes (AVE4) which formed during a period of basically zonal flow. Their energy budget values tend to be smaller than current results because jet intrusion into the region did not occur. Horizontal flux divergence and generation were sinks of energy with the only source arising from subgrid scales of motion.

Results from data having a meso-β scale resolution (∿170 km) now will be compared with the current study. Tsui and Kung (1977) used NSSL observations to perform an energy study of convective, non-convective, and frontal situations. Kinetic energy content and the local change of energy for their composite convective case are comparable to values of the current study; however, source and sink terms are quite different. Cross-contour flow is a major source of energy and is nearly balanced by a dissipational loss to smaller scales of motion (disp< 0). Although horizontal flux convergence is an external source of energy, its magnitude is relatively small. The energetics of their non-convective composite case are radically different from those of the composite convective case with cross-contour destruction and positive dissipation being the dominant processes.

A comparison of the energy balances associated with different scales of resolution is difficult because there are many variables which influence the energetics of each particular area. One can only speculate on the observed trends. During the convectively active AVE-SESAME I period, destruction of kinetic energy by cross-contour flow trends toward generation as the resolution of smaller scales increases. In a similar way, the convective category of Tsui and Kung, using data having 85 km spacings, shows much more generation than found during convective periods derived from synoptic-scale data. These results suggest that the near storm environment may generally be characterized by strong cross-contour generation. There also may be a trend towards negative dissipation in the convective environment as resolution focuses

on progressively smaller scales. Values of horizontal flux divergence and convergence seem to become smaller in magnitude with finer resolution. Upward transport of kinetic energy has been observed in the convective environments of all cases. Much more investigation must be performed to verify these tentative hypotheses.

c. Time variability of area averaged energetics

One of the advantages of 3 h rawinsonde data is that they allow an analysis of short term atmospheric variability. The time variability of vertical totals of area averaged kinetic energy parameters is shown in Fig. 25. The region experiences an increase in kinetic energy at all times except 0300 GMT as values climb from 26.5 x 10^5 J m^{-2} at the first observation to a final value of 41.1 x 10^5 J m^{-2}. The increases are nonlinear, as indicated by the local change term which reaches a minimum at 0300 GMT. A slight decrease in kinetic energy content occurs between 0000 and 0300 GMT, but the change term does not become negative because of the 6 h time differencing. Time variability for the synoptic-scale study (Fuelberg et al., 1980) is shown in Fig. 26. Magnitudes and trends of kinetic energy content and local change generally are similar in both studies, and both indicate two general surges of increased kinetic energy content--one during the first half of the period, and the second during the latter half.

Values of the generation term ($-\vec{V}\cdot\vec{\nabla}\phi$) also exhibit two maxima. Although the area-time averaged value indicated destruction (Table 2), generation occurs in the vertical column near 2100 GMT and 0900 GMT. To further investigate this time variability, a pressure-time cross section is shown in Fig. 27. In the upper layers between 1200 and 1800

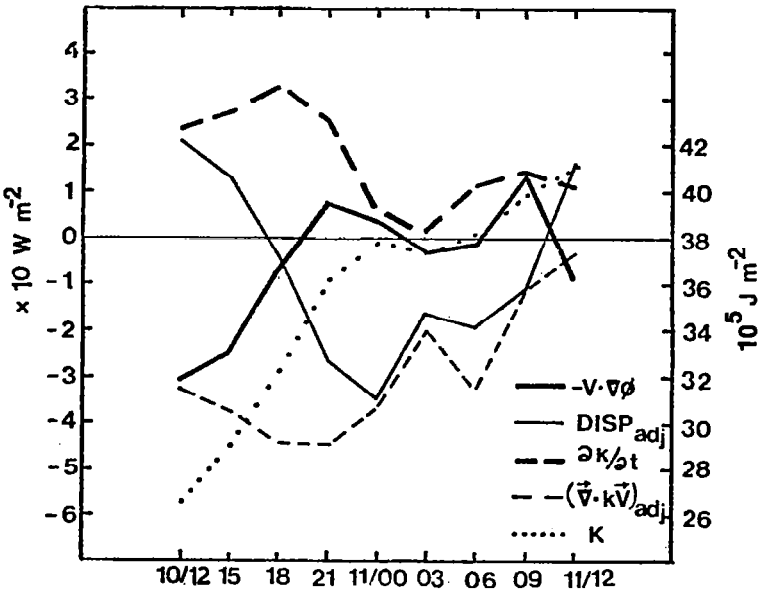

Figure 25. Time series of subsynoptic-scale energy budget terms integrated between the surface and 100 mb. Three-hour time intervals are indicated on the horizontal axis.

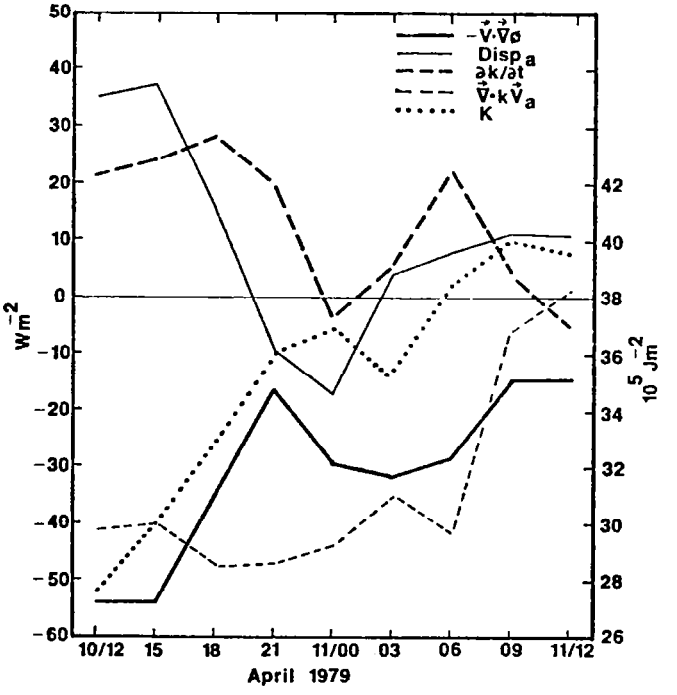

Figure 26. Time series of synoptic-scale energy budget terms integrated between the surface and 100 mb. Three-hour time intervals are indicated on the horizontal axis (Fuelberg et al., 1980).

GMT, strong cross-contour destruction accompanies the increase in winds associated with jet intrusion from the southwest. The minimum of destruction near 2100 GMT occurs as the major wind perturbation develops over Oklahoma and Kansas. Finally, the latter half of the period again is characterized by destruction as the main jet axis becomes superimposed over the area. Maximum low-level generation between 2100 and 0900 GMT is related to the formation and movement of the low-level jet stream. The tendency toward greater positive generation using subsynoptic-scale data that was noticed earlier in Table 1, again is evident by comparing Figs. 25-26. Although magnitudes indicate that more positive generation occurs with the subsynoptic-scale resolution, time variability between the two studies is quite similar.

Horizontal flux convergence of kinetic energy is the greatest source to the vertical column at all times, with a maximum adjusted value of -44.5 W m^{-2} at 2100 GMT. A secondary maximum of -32.4 W m^{-2} occurs at 0600 GMT. Time variability indicated in this term is similar to that of the synoptic-scale study with largest variations occuring in the upper levels (Fig. 28). Horizontal flux divergence develops above 250 mb after 0000 GMT as the jet streak advances from the southwest.

Although adjusted dissipation was found to be a small sink of energy in the area time-average (Table 1), Fig. 29 shows that upper-level transfer of energy from subgrid-

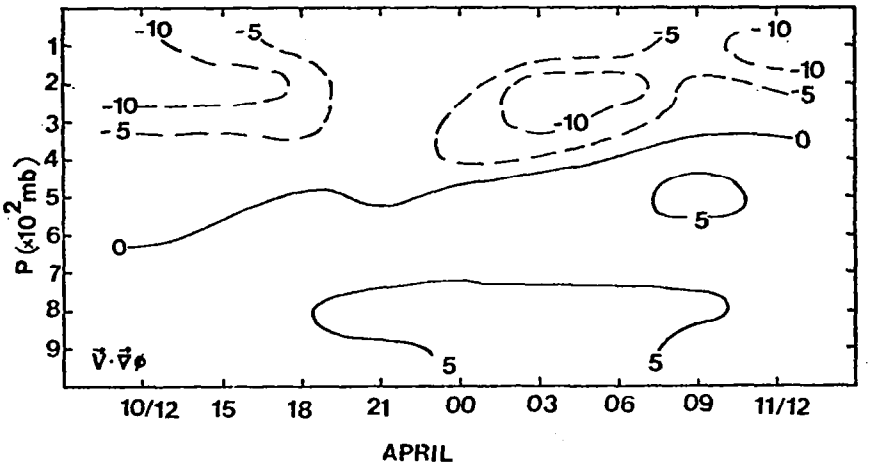

Figure 27. Pressure-time cross section of area averaged generation of kinetic energy. Units are W m^{-2}/100 mb.

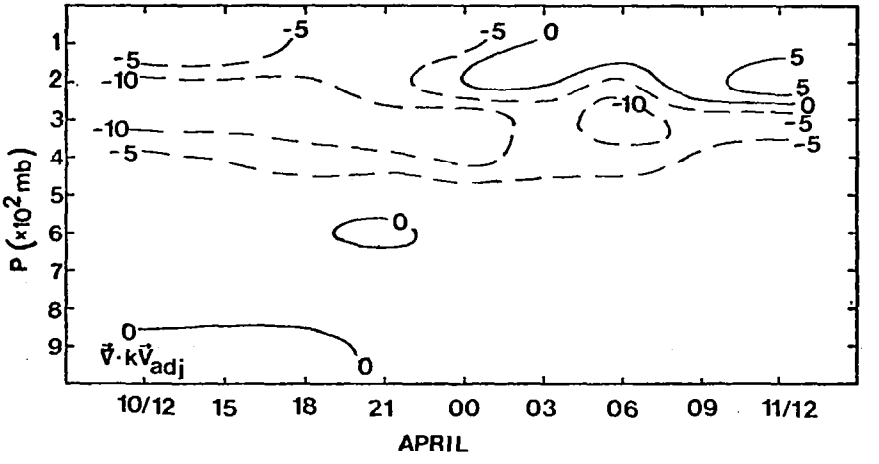

Figure 28. Pressure-time cross section of area averaged adjusted horizontal flux divergence of kinetic energy. Units are W m^{-2}/100 mb.

scales into the resolvable scales produces positive vertical totals near the beginning and end of the Experiment. The pressure-time cross sections of dissipation and generation (Fig. 27) show similarities; negative generation tends to occur with positive dissipation and vice versa. The maximum loss of kinetic energy via this term (-34.2 W m^{-2}) occurs near the height of the RRVTO (0000 GMT).

Because vertical flux divergence of kinetic energy is near zero in the vertical total, it is not shown in Fig.25. Figure 30, however, shows its pressure-time variability averaged over the area. The lower and middle troposphere are regions of vertical flux divergence (export) at all times, while the upper layers experience flux convergence from below (import). Magnitudes are small until 2100 GMT, when upward vertical motion increases dramatically (Fig. 16). Between 0300 and 0600 GMT, upward transport of kinetic energy is the largest source to the 300 to 100 mb layer.

Results of this section have indicated large time variability in the area averaged energetics. The next section will focus further on these changes by considering the energetics of particular areas of interest.

d. Limited jet streak formation

The sudden appearance of an upper-level isotach maximum over Oklahoma at 2100 GMT (Fig. 7) was associated with

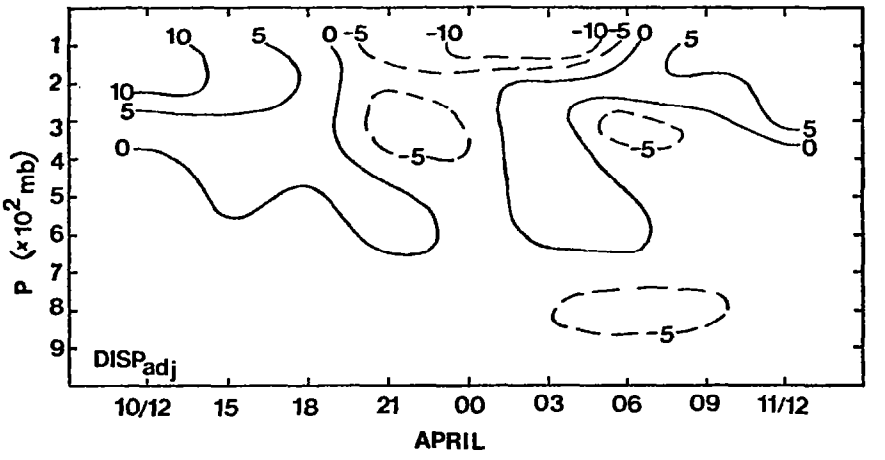

Figure 29. Pressure-time cross section of area averaged adjusted dissipation of kinetic energy. Units are W m^{-2}/100 mb.

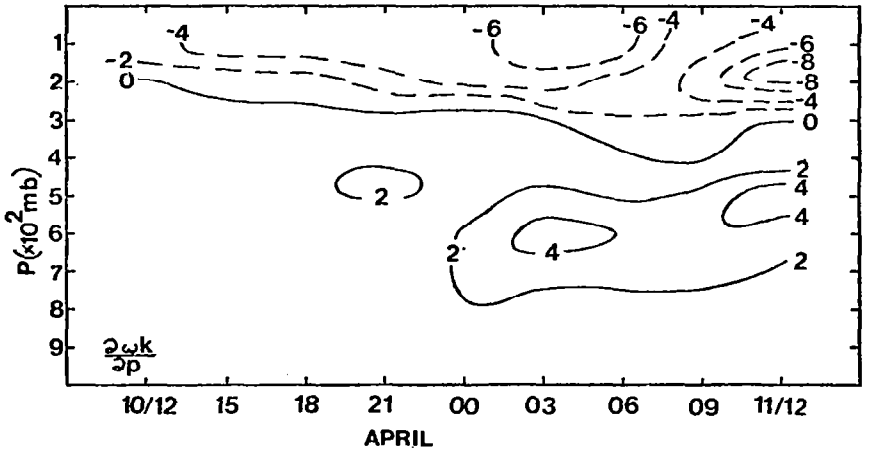

Figure 30. Pressure-time cross section of area averaged vertical flux divergence of kinetic energy. Units are W m^{-2}/100 mb.

rapid changes in kinematic parameters and a rapid development of severe convection in the area. This section investigates the energetics surrounding the formation of this important feature. The presentation evaluates several possible mechanisms for its formation and seeks to determine the most likely cause.

Simple advection of kinetic energy into the region is one process capable of producing the limited jet streak. Figures 31 and 32 show advection of kinetic energy ($\vec{V}\cdot\vec{\nabla}k$) integrated over the middle (700-400 mb) and upper (400-100 mb) atmosphere for 1800 GMT and 2100 GMT, respectively. This component dominates the horizontal flux divergence term of kinetic energy in those areas where velocity divergence is relatively weak (see (3)). At 1800 GMT advection acts as a sink of kinetic energy in the Red River Valley and southern Oklahoma at both the middle and upper layers ($\vec{V}\cdot\vec{\nabla}k > 0$). Although weak negative advection serves as a source of energy north of the Valley, cross sections reveal that it is confined to thin layers near 200 mb and below 600 mb (not shown). Largest magnitudes of advection are located over southwest Texas and New Mexico, in advance of the major jet streak. At 2100 GMT (Fig. 32), kinetic energy is advected into northern Oklahoma and Kansas in both layers; however, advection acts as an energy sink over the Red River Valley. This couplet pattern is due to the newly formed jet streak over central Oklahoma. The large area of nega-

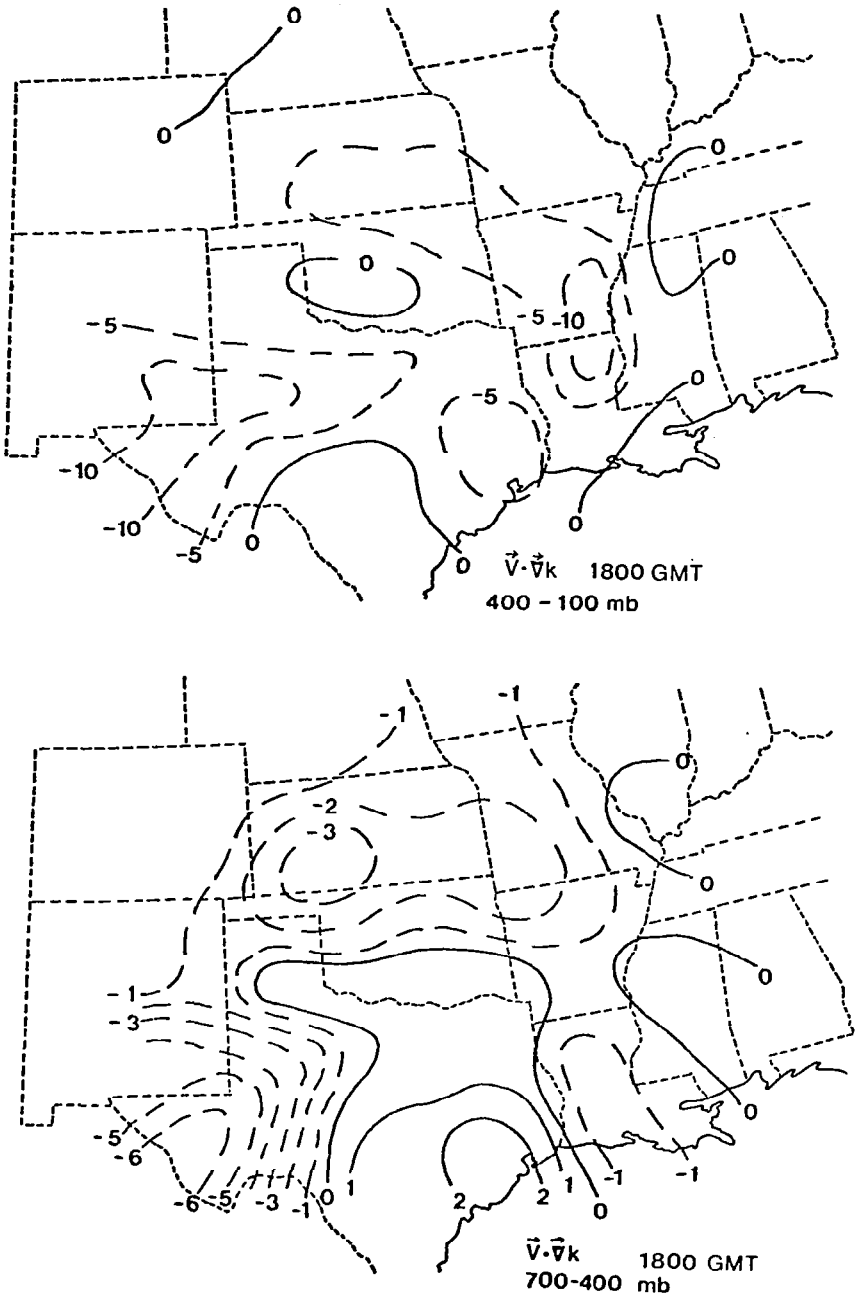

Figure 31. Horizontal fields of kinetic energy advection integrated over the 700-400 mb layer and the 400-100 mb layer for 1800 GMT 10 April 1979. Values are x 10^{1} W m^{-2}.

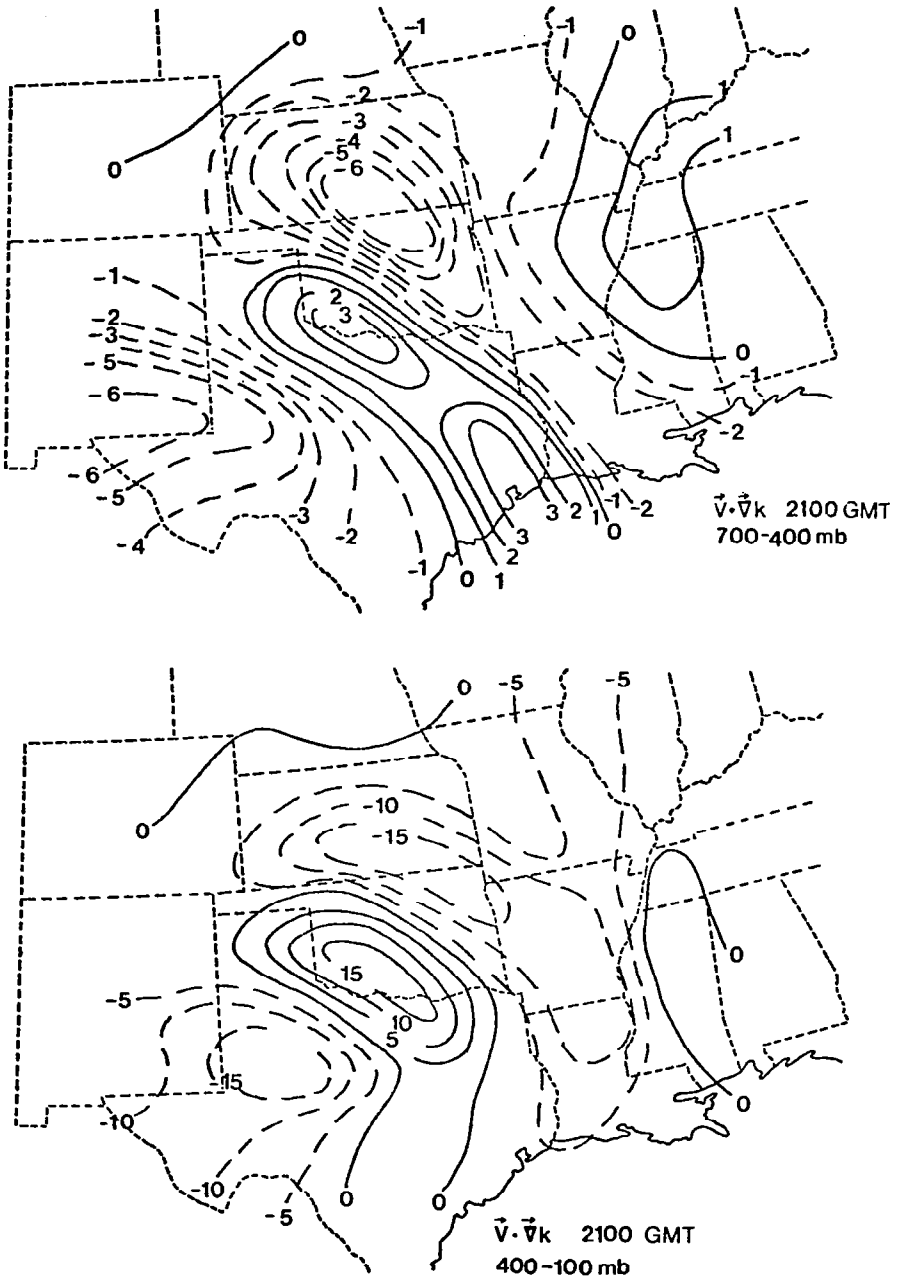

Figure 32. Horizontal fields of kinetic energy advection integrated over the 700-400 mb layer and the 400-100 mb layer for 2100 GMT 10 April 1979. Values are x 10^{1} W m^{-2}.

tive values over southwest Texas continues to indicate jet intrusion from the southwest corner of the region. Similar maps for later times suggest that significant advection into central Oklahoma from the southwest does not occur until 0600 GMT, well after formation of the smaller streak. If the streak over Oklahoma had translated into the area, a forward motion of approximately 50 m s^{-1} would have been required. This value is much greater than has been observed with previous jet streaks (Palmén and Newton, 1969).

Since advection does not appear to be a likely cause, the jet streak over Oklahoma must be due to local creation of kinetic energy. In order to investigate the possible sources of energy responsible for this feature, spatial cross sections were produced for each term of the kinetic energy budget equation along a line running north-south through the Red River Valley (Fig. 33). Selected cross sections for 2100 GMT are presented in Fig. 34. The cross section of kinetic energy content indicates the newly formed jet streak over Oklahoma and Kansas. The wind maximum contains a peak energy value of 6.15 J m^{-2}/100 mb near 300 mb and has a vertical depth of approximately 400 mb. The separate maximum of kinetic energy over southern Texas represents the northern extension of the subtropical jet stream. Its maximum value within the region is 9.12 J m^{-2}/100 mb near the 150 mb level. The cross section of the generation term indicates a strong source of kinetic energy through the entire

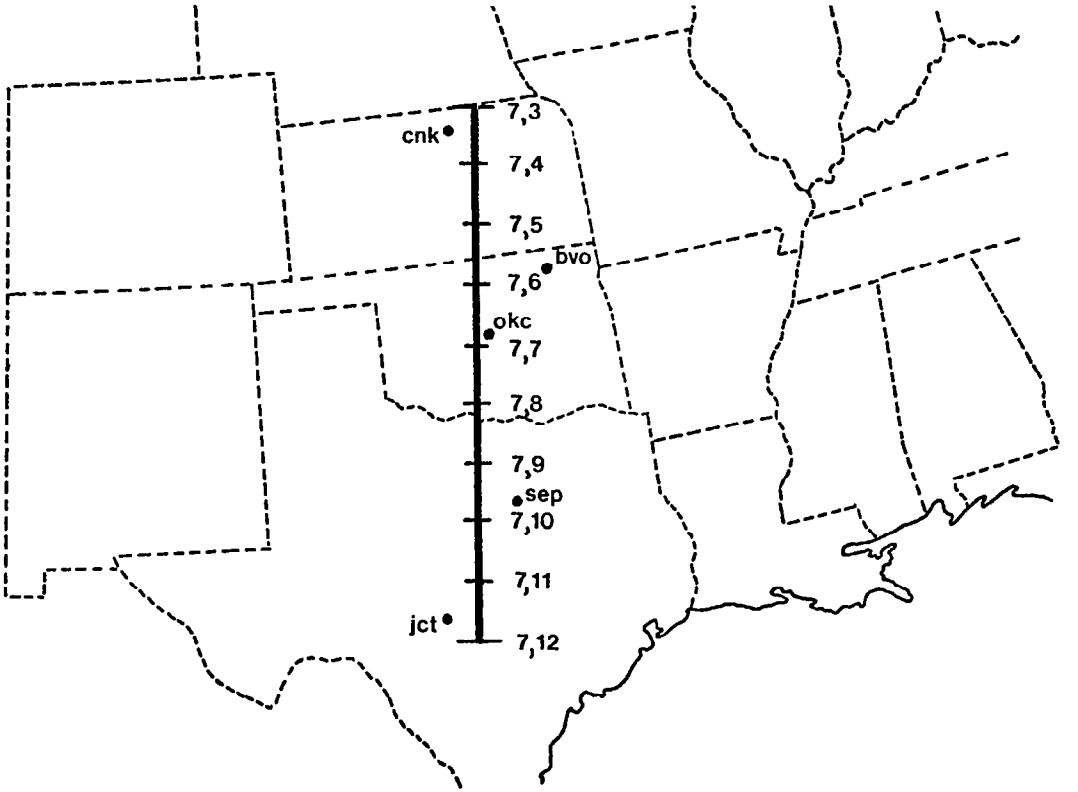

Figure 33. AVE-SESAME I area map indicating the north-south cross section line through the region. Grid points correspond to those of the analysis region shown in Fig. 1.

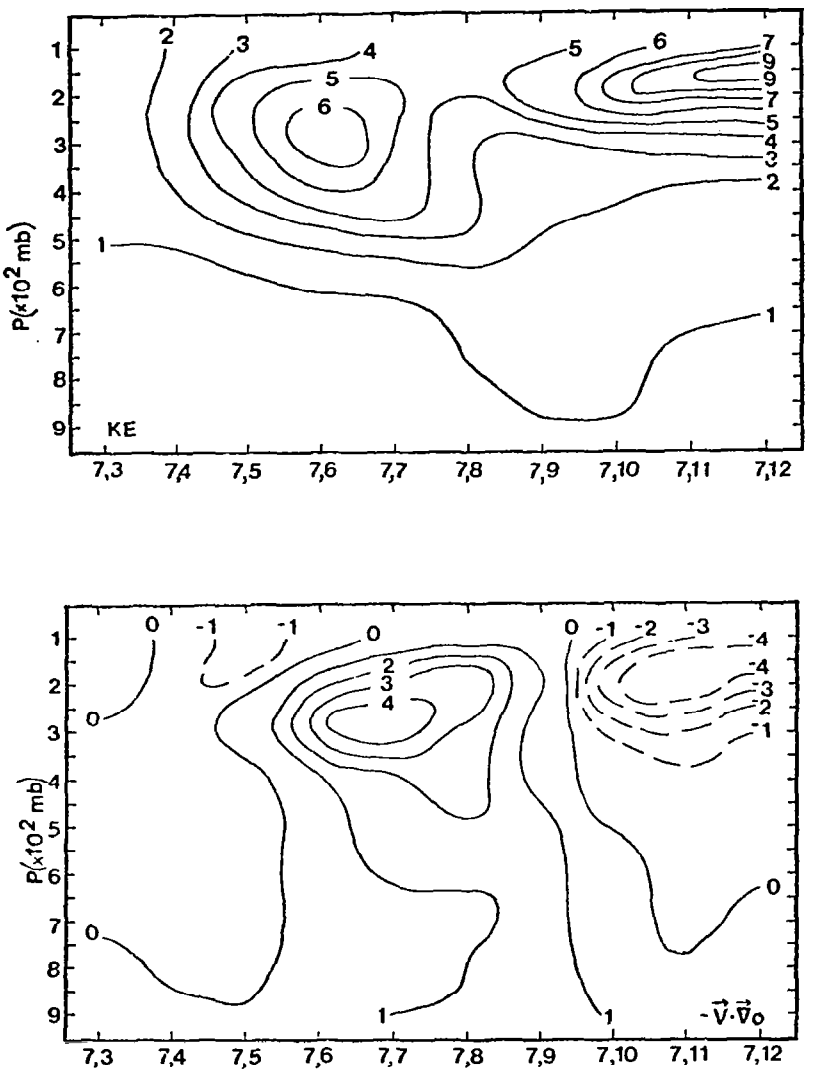

Figure 34. Cross sections for various energy budget terms at 2100 GMT 10 April 1979. Values are x 10^{1} W m^{-2}/100 mb except for kinetic energy (KE) which is x 10^{5} J m^{-2}/100 mb.

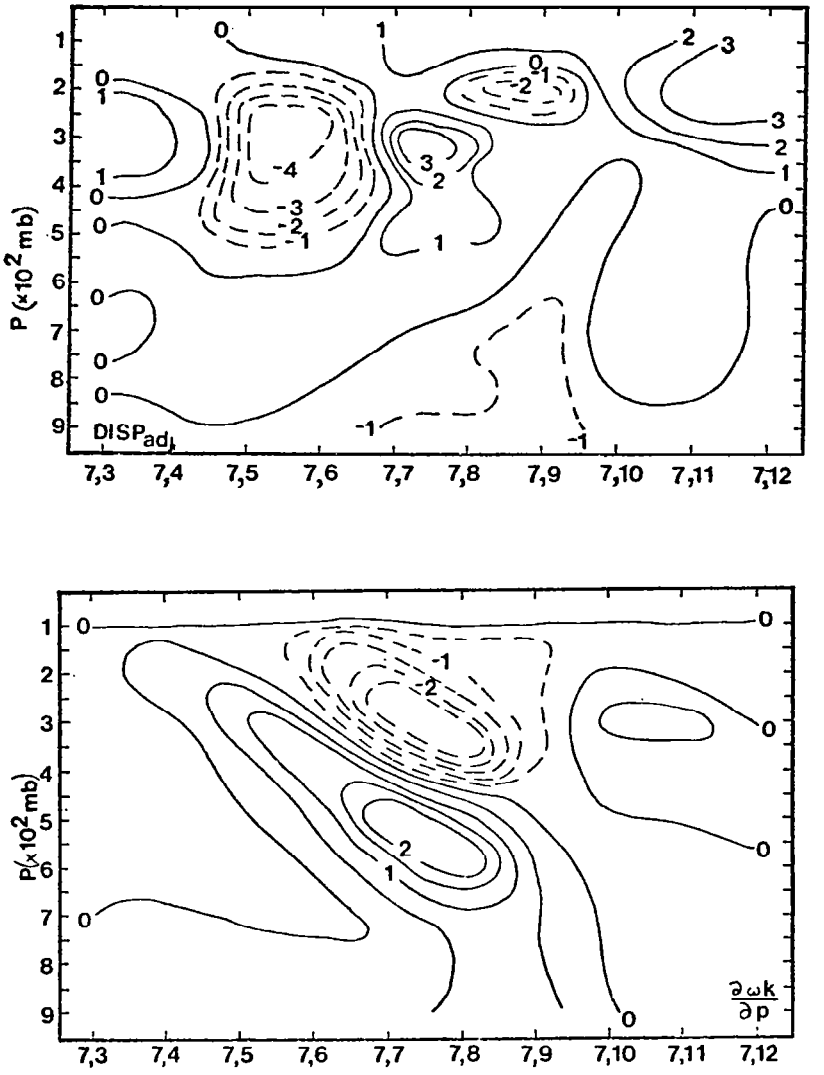

Figure 34. (continued)

vertical column from northern Oklahoma into Texas. This area of generation, having a central value of 43.9 W m^{-2}/100 mb at 300 mb, is displaced slightly southward from the kinetic energy maximum. The corresponding figure for the dissipation term shows a source of energy from subgrid scales of motion over only a small portion of the streak's area. In fact, major dissipational losses occur over a much larger region stretching from northern Oklahoma into Kansas above 500 mb. Vertical flux convergence ($\frac{\partial \omega k}{\partial p} < 0$) is a major energy source to the upper levels near the jet streak. Values greater than 25.0 W m^{-2}/100 mb occur near 300 mb. Upward motion is an important transporter of energy contained in the middle levels. Rising motions in the area can lift the energy of the middle layers by 200 mb in just 3 h.

In order to quantify the magnitudes of the various source and sink terms over Oklahoma and the Red River Valley, grid point values of the energy budget were averaged over a fixed sub-volume (box) of the total area (Fig. 35). The area so studied is approximately 1.3 x 10^5 km^2. Vertical distributions of the energy budget terms averaged over this area are presented in a pressure-time series from 1800 GMT through 0300 GMT (Fig. 36). Although the streak was contained within the sub-volume at 2100 GMT, it had begun to move northward by 0000 GMT. Integrated totals for the 500-100 mb layer are tabulated in Table 3.

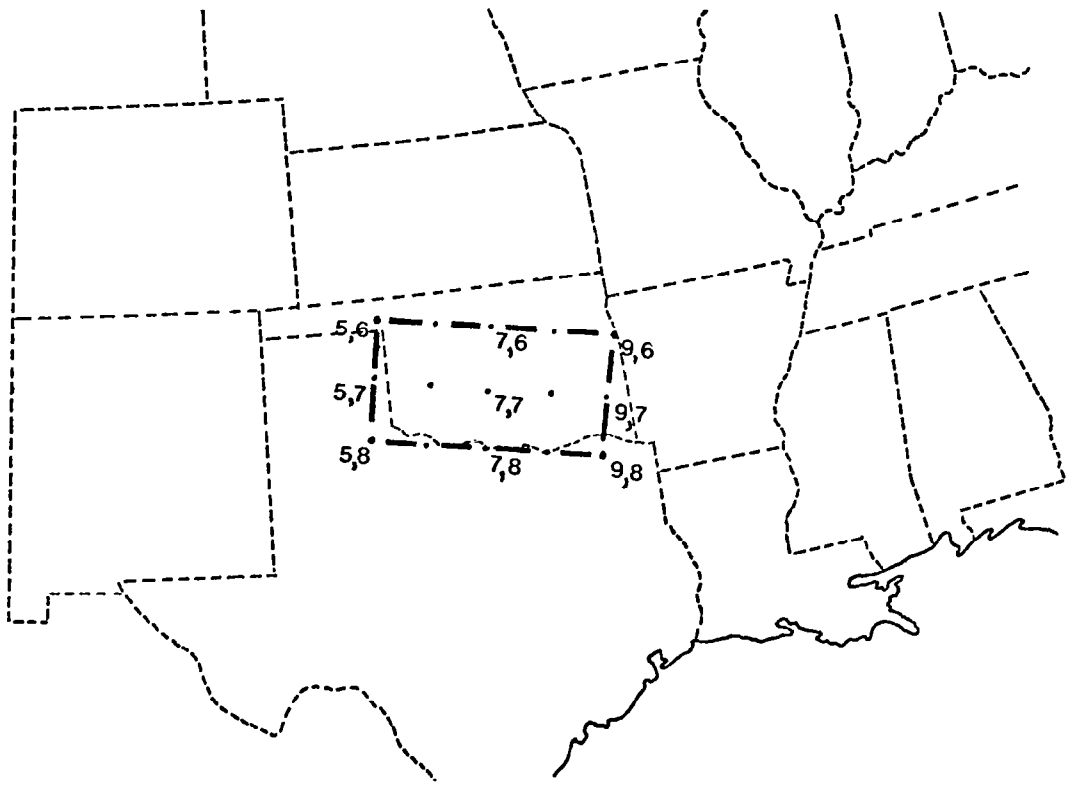

Figure 35. AVE-SESAME I area map indicating the Oklahoma sub-volume over which the energetics were averaged. Grid points correspond to those of the analysis region shown in Fig. 1.

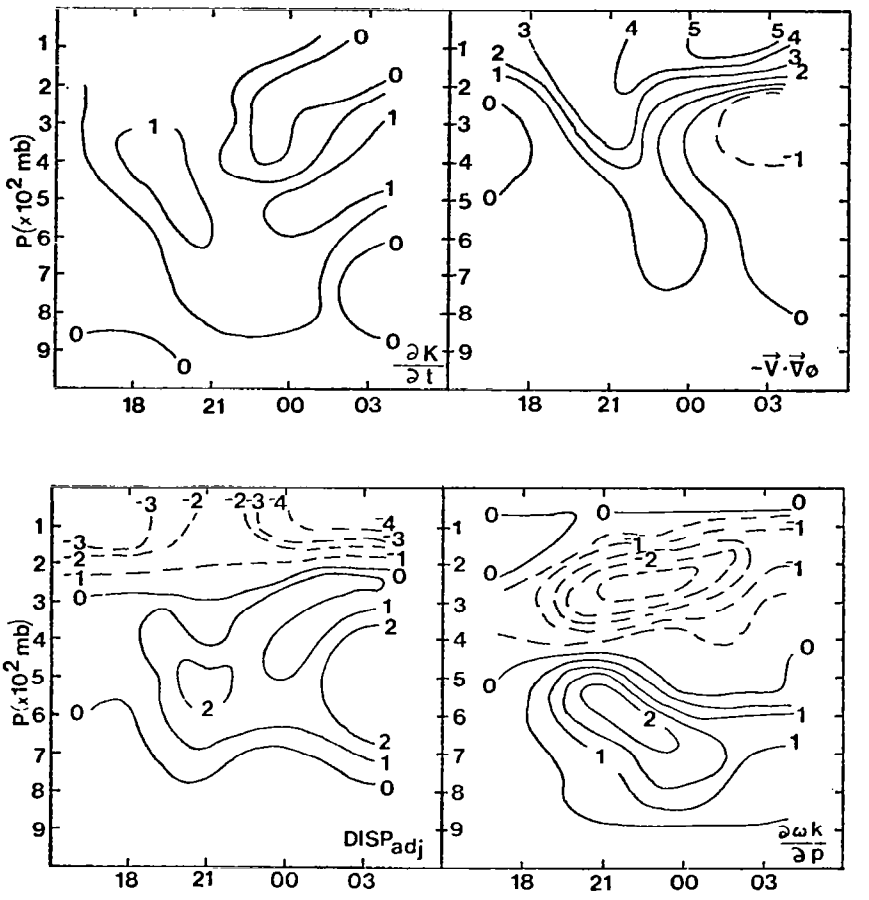

Figure 36. Pressure-time cross section of energy budget terms averaged over the Oklahoma sub-volume. Values are x 10^{1} W m^{-2}/100 mb. Times are indicated on the horizontal axis (00 means 0000 GMT).

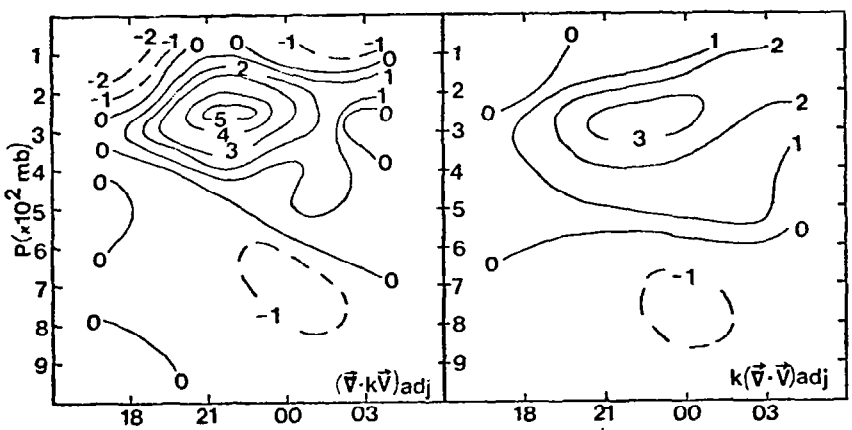

Figure 36. (continued)

Table 3. Vertically integrated 500 to 100 mb totals for various kinetic energy budget terms in a sub-volume at 1800,2100, and 0000 GMT 10-11 April 1979. All units are in W m^{-2}.

Parameter	Layer	1800 GMT	2100 GMT	0000 GMT
$\partial k/\partial t$	500-100 mb	39.4	23.2	5.0
$-\vec{V}\cdot\vec{\nabla}\phi$	500-100 mb	36.5	104.0	53.8
$(disp)_{adj}$	500-100 mb	-27.7	-13.3	-29.0
$\frac{\partial \omega k}{\partial p}$	500-100 mb	-7.2	-52.8	-47.6
$(\vec{\nabla}\cdot k\vec{V})_{adj}$	500-100 mb	-23.1	119.7	67.3

Local increases in kinetic energy occur above 650 mb at 1800 GMT, include the entire vertical column by 2100 GMT, and are confined only to the middle layers at 0000 GMT as the jet streak moves northward. Within the 500-100 mb layer, greatest increases occur at 1800 GMT when the value reaches 39.4 W m^{-2}. Production of kinetic energy by cross-contour flow is the largest source to the limited region at all times presented (Table 3). The maximum value for the 500-100 mb layer is 104.0 W m^{-2} at 2100 GMT. Greatest generation occurs in the upper levels between 0000 and 0300 GMT, but significant middle-level generation is observed from 2100 GMT through 0000 GMT. The pressure-time series for adjusted dissipation indicates a fairly strong middle-level source of energy from the unresolvable scales of motion. However, the 500-100 mb layer totals indicate a loss of energy at all times due to dissipational processes in the uppermost levels. Vertical flux convergence is the second greatest source of energy to the upper levels at 2100 GMT and 0000 GMT (Table 3). Flux divergence provides a major sink of energy for the middle and lower troposphere.

Horizontal flux convergence provides the second greatest energy source to the 500-100 mb layer at 1800 GMT, with a value of -23.1 W m^{-2} (Table 3). This term becomes a sink to the upper levels after 1800 GMT as the streak develops. The pressure-time series for the divergence component $(k\vec{\nabla}\cdot\vec{V})$ of the horizontal flux term (see Section 5b) indicates that

divergence is the greatest contributor to the magnitude and variability of the overall flux term.

Based on the information just presented, several conclusions can be made. Although horizontal flux convergence transports energy into the region over Oklahoma at 1800 GMT (Fig. 35), local generation of kinetic energy is the major source as the limited jet streak begins to form. With development of upward vertical motion over the area by 2100 GMT, vertical flux convergence becomes a major upper-level source. It and increased local generation outweigh the outflow created by the developing streak. Generation and vertical transport continue to support the jet streak through 0000 GMT as it exits the limited region.

The mechanisms responsible for local generation of kinetic energy near the jet streak are more uncertain. At least two possible factors may have contributed to the ageostrophic motion necessary for this generation. First, the height perturbation discussed in Section 4 propagates toward the Red River Valley at these times. Height falls associated with this perturbation may alter the height gradient inducing cross-contour flow. These falls, however, are located near the observed convection in the eastern portion of the Texas panhandle (see Fig. 8), and not in Oklahoma where the streak is first detected.

A second possibility involves storm-environment interactions. Previous studies have suggested that areas of

intense convection can modify their large-scale environments by enhancing low-level convergence, upper-level divergence, and upward motion, and also by producing upper-level height rises and lower-level height falls (e.g., Aubert, 1957; Danard, 1964 and 1966; Ninomiya 1971a and b; Fuelberg and Scoggins, 1978; Fritsch and Maddox, 1980). These processes could induce ageostrophic motions and generation of kinetic energy. Unfortunately, it is not a trivial task to isolate such feedback effects because some of the environmental modifications also can be the mechanisms which initially help produce the storms. It is often a "chicken-egg" type of question.

Between 1800-0000 GMT the area near Oklahoma and the Red River Valley undergoes kinematic and energy changes which are similar to those attributed to storm inducement. This suggests that the storms may be a cause for the formation of the nearby limited jet streak. An analysis of storm locations at these times (Figs. 6, 8, and 9) can be used to discuss this hypothesis. The small area of storms in northcentral Texas at 1800 GMT (Fig. 6) moves through Oklahoma near 2100 GMT (Fig. 8) and into Kansas by 0000 GMT (Fig. 9). Thunderstorms in this area are not especially intense. The more intense storms of the RRVTO are at the eastern edge of the Red River Valley at 2100 GMT and move into Oklahoma at approximately 2300 GMT. The jet streak which forms between 1800-2100 GMT is downwind of these storms. In previous studies increases

in winds were observed north of large storm areas, while changes in horizontal divergence and vertical motion, were found to be superimposed over the storms (Fritsch and Maddox, 1980; Maddox et al., 1980; Fuelberg and Scoggins, 1978). An additional consideration is that the limited streak and the severe storms form nearly simultaneously. Fuelberg and Scoggins (1978) found a lag of several hours between storm development and maximum changes in the environmental kinetic energy balance. The time lag in the current study appears to be much shorter, however.

It should be emphasized that insufficient information is known about the time and space phasings between storm formation and resulting environmental modifications. Present results suggest that the formation of the jet streak between 1800-2100 GMT cannot be attributed totally to feedback mechanisms from the developing storms. It is reasonable to conclude, however, that feedback mechanisms were important in the intensification and maintainance of the feature. Further research will be necessary to determine what other factors, if any, are related to initial jet formation. Likewise, questions about the time and space phasings between the jet and the storms still must be answered.

e. Energetics of convective areas

The purpose of this section is to describe and contrast the energetics and flow characteristics of convective areas with those of areas not experiencing storms. Manually Digitized Radar (MDR) data (National Weather Service, 1979) were used to objectively determine the intensity and position of the radar-observed precipitation during the AVE-SESAME I period. The MDR data were obtained from radar summary charts that are routinely transmitted over the facsimile circuit. Values were assigned to each grid point (Fig. 1) at each rawinsonde observation time by taking the maximum value within ½ grid distance (∿65 km) of the point. An average energy budget then was computed for points having no precipitation (MDR 0) and another for points having moderate to intense convection (MDR 3-6). A similar procedure was used to obtain averages of certain kinematic parameters. This is not a traditional spatial average since grid points comprising a particular MDR category are not necessarily adjacent. The procedure is similar to that used by Fuelberg et al. (1980), Fuelberg and Scoggins (1978), and Wilson (1976).

Figure 37 shows vertical profiles of MDR-averaged kinematic quantities for the storm (MDR 3-6) and non-storm (MDR 0) environments. Compared to the non-storm surroundings, the storm environment is characterized by enhanced low-level velocity convergence and upper-level divergence, increased

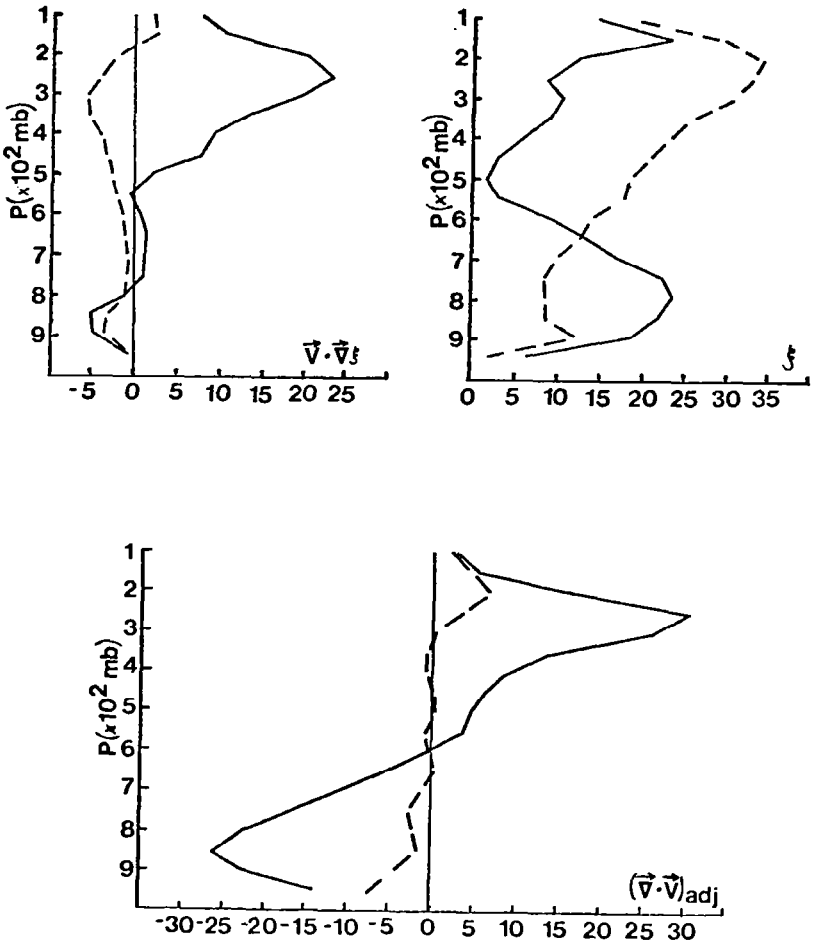

Figure 37. Vertical profiles of Manually Digitized Radar (MDR) averaged kinematic quantities. The solid line indicates moderate to intense storm areas (MDR 3-6) while the dashed line indicates the non-storm areas (MDR 0). Values of divergence are x 10^{-6} s^{-1}, vorticity x 10^{-5} s^{-1}, and advection of relative vorticity x 10^{-10} s^{-2}.

low-level positive relative vorticity and reduced upper-level positive vorticity, and strong positive vorticity advection in the upper levels. These profiles are similar to those for the synoptic-scale study (not shown) except in two respects. First, the non-storm region of the present study experiences negative vorticity advection in the upper levels while only reduced positive advection occurred in the previous study. Second, magnitudes of divergence in the storm average of the present study are much greater than at the synoptic-scale investigation. This result is consistent with findings presented in Section 5a and reflects the better resolution of small-scale features in the current study.

Vertical profiles of MDR-averaged kinetic energy budget terms are presented in Fig. 38. Totals for the complete vertical column are presented in Table 4. Profiles for the various terms indicate distinctive differences between the storm and non-storm environments. Upper-level kinetic energy content is larger in the non-storm areas while the storm environment exhibits enhanced low- and middle-level energy. This and previous results suggest that, on the average, storms developed downwind from the main upper-level jet core in areas where divergence and vertical motion are more conducive to intense storm development. Also, increased low-level flow apparently provided the necessary mass and moisture convergence necessary for the intense storms. The vertical totals of

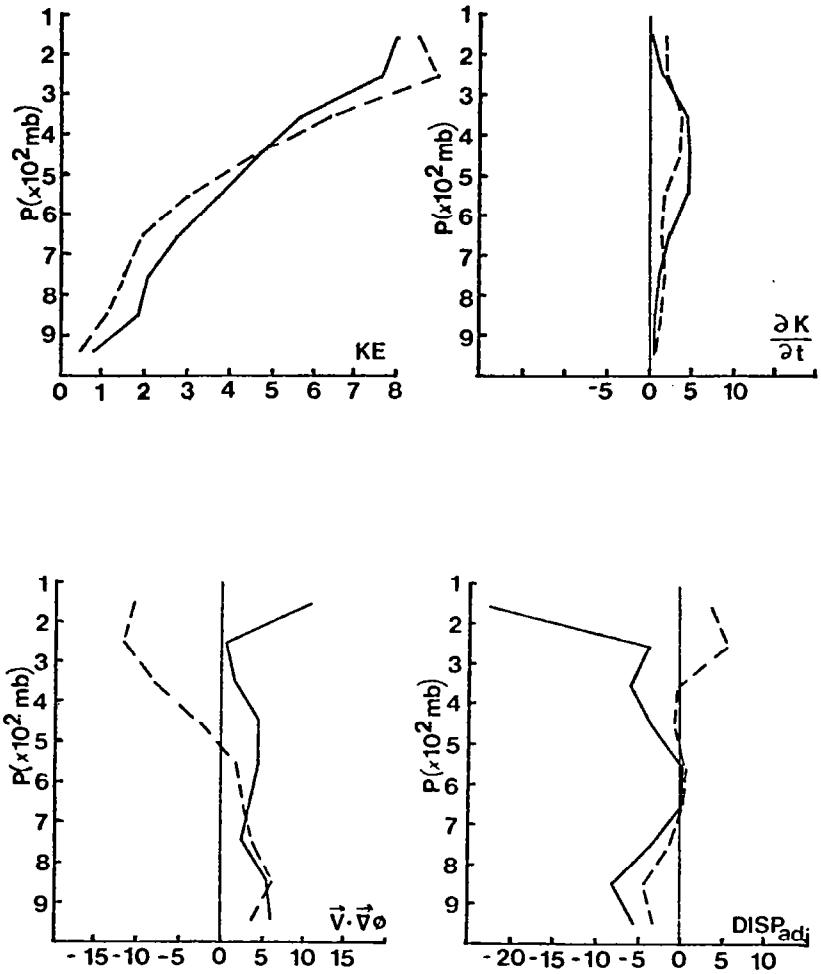

Figure 38. Vertical profiles of Manually Digitized Radar (MDR) averaged kinetic energy budget terms. The solid line indicates moderate to intense storm areas (MDR 3-6) while the dashed line indicates the non-storm areas (MDR 0). Units are W m^{-2}/100 mb except for kinetic energy (KE) which is x 10^5 J m^{-2}/100 mb.

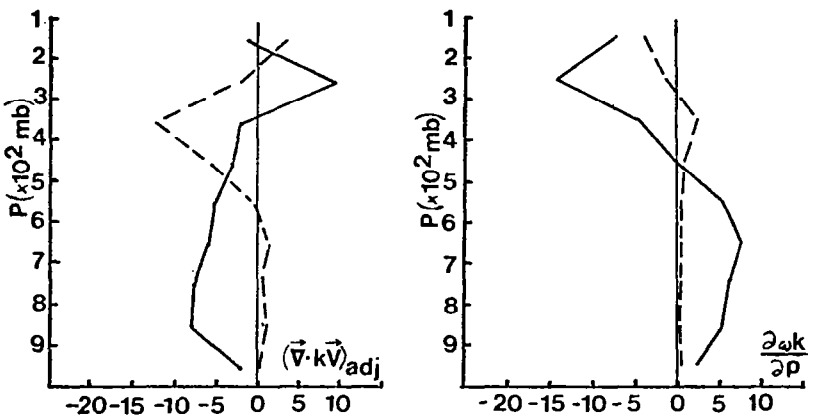

Figure 38. (continued)

Table 4. Vertically integrated Manually Digitized Radar (MDR) averaged subsynoptic-scale kinetic energy budget. Values are in Wm^{-2} except for K which is Jm^{-2}.

MDR Values	K	$\partial k/\partial t$	$-\vec{\nabla}\cdot\vec{\nabla}\phi$	$\vec{\nabla}\cdot k\vec{V}$	$(\vec{\nabla}\cdot k\vec{V})_{adj}$	$k(\vec{\nabla}\cdot\vec{V})_{adj}$	$\vec{V}\cdot\vec{\nabla}k$	$\frac{\partial \omega k}{\partial p}$	disp	$(disp)_{adj}$
MDR 3-6 Moderate-Intense Storms	37.1	18.8	39.5	-31.6	-30.4	32.2	-62.5	-0.1	-52.4	-51.2
MDR 0 Non-Storm Area	36.7	17.5	-15.8	-14.1	-27.5	5.2	-32.6	0.0	19.3	5.9

kinetic energy content are 37.1 J m^{-2} and 36.7 J m^{-2} for the storm and non-storm environments, respectively (Table 4). Vertical totals for the local change of kinetic energy also are very similar; however, the storm-area profile indicates a larger local change in the middle levels than in the non-storm environment.

Generation by cross-contour flow is a source of kinetic energy at all levels of the storm environment while destruction is prominent in the upper levels of the non-storm area. These upper-level contrasts make the vertical totals strikingly different, with values of 39.5 W m^{-2} and -15.8 W m^{-2} for the storm and non-storm area, respectively. Horizontal flux convergence is a source of energy at all levels in the storm environment except the 300-200 mb layer where it provides a substantial sink. This outflow of energy is due to the dominance of the divergence term of the horizontal flux (see Section 5c). In the non-storm environment, flux convergence is a large source of energy in the middle and upper troposphere as a result of large advection ($\vec{V}\cdot\vec{\nabla}k < 0$) and small divergence. Vertical totals show that both areas are large importers of kinetic energy, but the relative contributions of advection and divergence are considerably different. Profiles of vertical flux divergence indicate that energy is transported upward in both the storm and non-storm environments; however, in the storm environment, the process

is a much larger source of energy to the upper levels. Dissipation is a very large sink of energy to the storm environment as indicated by the vertical total of -52.4 W m^{-2}. This grid- to subgrid-scale transfer is maximized in the 200-100 mb layer with a secondary maximum near the surface. Slight positive dissipation is noted in the 700-500 mb layer. In the non-storm environment, upper-level transfers of energy from the subgrid scales to resolvable scales of motion (positive dissipation) contrast with dissipational losses of the storm environment.

Differences in energetics between the storm and non-storm environments presented here are similar to those found by Fuelberg et al. (1980) in their synoptic-scale study. Certain trends are seen in values of generation and dissipation when results of subsynoptic-, synoptic-, and meso-β scale studies are compared. Fuelberg et al. (1980) reported values of 15.5 W m^{-2} and -23.1 W m^{-2} for the generation and dissipation terms of the synoptic-scale storm environment during AVE-SESAME I.[1] Corresponding values for the composite of convective cases using meso-β scale data (Tsui and Kung, 1977) (Table 2) indicate larger generation of kinetic energy (89.5 W m^{-2}) and larger dissipational losses (-96.0 W m^{-2}).

---

[1]Values presented here differ from those originally reported by the authors and result from a more comprehensive set of MDR data.

Results from the current subsynoptic-scale study lie in between these values (Table 4). As noted in Section 5c, this suggests that increased positive generation and negative dissipation are increasingly characteristic of the storm environment as resolution focuses on smaller scale features. More investigations at the subsynoptic scale are needed to verify such relations between the different scales of motion and the effects that storms have on their environmental kinetic energy balance.

6. SUMMARY AND CONCLUSIONS

The subsynoptic-scale kinetic energy balance during the Red River Valley tornado outbreak has been studied in order to diagnose storm-environment interactions that take place during severe storm occurrences. Subsynoptic-scale data (station spacing of ∿250 km) from the AVE-SESAME I period provided a resolution of the storm environment which has not been previously achieved. Results of kinematic analyses indicate that special data handling techniques used in the study produced a consistent, unbiased data set which served as input for the kinetic energy budget calculations.

Area-time averaged energetics indicated that horizontal flux convergence was the major source of kinetic energy to the region. Destruction of kinetic energy by cross-contour flow was a small sink while vertical transport provided a major source to the 300-100 mb layer. Dissipation was the smallest of all energy parameters in the vertical total of the area-time averaged budget. Vertical profiles of source and sink terms indicated primary maxima in the upper levels that were associated with jet stream activity. Secondary maxima of some terms in the middle and lower levels seemed related to special features such as frictional processes and the low-level jet stream.

No other studies at this scale (meso-α) were available

for comparison purposes; however, results were compared with those from previous synoptic- and meso-β scale investigations encompassing storm outbreaks. Results suggested a tendency for the atmosphere in the storm environment to become more conducive to cross-contour production of kinetic energy as data resolution went from synoptic- to meso-β scales. Transfers of energy from resolvable to subgrid scales of motion (dissipational losses) appeared more dominant as finer-scale resolution was obtained. Similarly, horizontal flux convergence and divergence became relatively smaller in magnitude. Further investigations, especially at the meso-α and meso-β scales, are necessary to verify these hypotheses.

Time variability of the current subsynoptic-scale (meso-α) energy budget indicated significant fluctuations throughout the experiment. Two surges of increased kinetic energy content associated with jet intrusion from the southwest were evident. The primary and secondary maxima occurred at 0900 GMT 11 April and 2100 GMT 10 April, respectively. Destruction of kinetic energy by cross-contour flow and upwelling of energy from subgrid scales of motion (dissipational source) were associated with these increases of energy content.

The kinetic energy balance over Oklahoma during the formation of a limited jet streak over the area received special attention. Local production of energy by cross-contour flow between 1800-0000 GMT was found to be the dom-

inant source of energy for jet development. Vertical transport was responsible for concentrating energy in the upper levels. An analysis of storm locations near the time of jet formation indicated that the intense convection producing the Red River Valley tornadoes may have contributed to local generation by modifying the surrounding environment. Almost simultaneous storm and jet streak development suggested that other factors also were responsible for the wind perturbation. Even if initial streak formation was not totally due to the storms, the convection probably was responsible for the intensification and maintenance of the feature for at least six hours. Further investigations about time and space phasings between storm development and the appearance of the jet streak are needed.

The kinematics and energetics associated with areas of moderate to intense storms were found to differ greatly from those of areas without storms. In contrast to the non-storm environment, storm areas contained enhanced low-level convergence and upper-level divergence, and increased low-level positive vorticity and reduced upper-level positive vorticity. Strong generation of energy by cross-contour flow and dissipational losses to subgrid scales of motion were evident in the storm areas; however, non-storm areas exhibited destruction by cross-contour flow and a source of energy from the unresolvable scales of motion. Horizontal outflow in the 300-200 mb layer of the storm area contrasted with upper-level horizontal flux

convergence in the non-storm environment. These findings, when compared with synoptic- and meso-β scale results, again suggested that convective areas become more dominated by cross-contour sources and dissipational sinks as data resolution focuses on finer scale features.

APPENDIX

Sensitivity Analysis

Sensitivity of the energy budget parameters to errors contained in the input rawinsonde data was evaluated quantitatively. Although the data possess both systematic and random errors, only the effects of random errors were considered because no effective procedures for considering the systematic type are available. Also, the effects of computational inadequacies such as truncation error were not considered.

The sensitivity study consisted of recomputing the energy budgets after random perturbations simulating rawinsonde errors had been added to the 25 mb values of wind and height at individual stations. Budget values derived from the perturbed data were compared with those from the original data. Although the original data were used as the standard for comparison, they were not error free. The current procedure is similar to that used by Robertson and Smith (1980), Vincent and Chang (1975), and Fuelberg and Scoggins (1980).

Computer-generated random perturbations were normally distributed about zero with standard deviations varying as a function of pressure (Table 5). Values for levels not shown in the Table can be obtained by linear interpolation. These random error estimates are similar to those originally proposed by Kurihara (1961). Because of the care taken in processing and checking the AVE-SESAME data, the random

Table 5. Standard deviations of normally distributed perturbations.

Pressure level (mb)	Wind direction (deg)	Wind speed ($m\ s^{-1}$)	Height (m)
100	12.0	5.0	44.0
200	10.3	5.0	35.0
300	8.6	4.5	24.0
500	5.3	3.0	13.0
700	4.0	2.0	11.0
900	2.0	1.0	5.5

perturbations were restricted to two standard deviations from zero which included about 95% of the possible values. The 0000 GMT 11 April observation was chosen for study since it was near the time of maximum convective activity. Ten runs of the 0000 GMT data, each with a different set of perturbations at the individual 25 mb levels, were made. Because the data fluctuations were allowed to vary and accumulate collectively, results of the study probably approach the limits to be expected from random errors (Vincent and Chang, 1975). The Barnes analysis scheme together with the explicit filtering schemes treat perturbations as waves and therefore remove portions of the deliberately introduced errors. By comparing the perturbed gridded fields of height data with the original gridded fields at 0000 GMT 11 April, it was found that about 30% of the original error at the stations was removed during the objective analysis. Approximately 50% of the introduced station errors in wind direction and speed were removed. Wind data were subjected to vertical filtering in addition to the operations performed on height (see Section 3b). This ability of computational procedures to reduce errors in the data is desirable.

Mean absolute differences and mean correlation coefficients between the original area averaged energy budget at 0000 GMT and the ten budgets derived from the perturbed data are given in Table 6 for the entire area of interest (Fig. 24) and in Table 7 for the limited area centered over Oklahoma (Fig. 35).

Table 6. Area averaged subsynoptic-scale kinetic energy budget for 0000 GMT 11 April 1979. Values in parentheses are mean absolute differences between the original and ten perturbed budgets. Values in brackets are mean correlation coefficients. The budget area (Fig. 24) consists of the entire area of interest. All units of energy parameters are W m^{-2} except for K which is 10^5 J m^{-2}.

Pressure Layer (mb)	K	$\partial k/\partial t$	$-\vec{V}\cdot\vec{\nabla}\phi$	$\vec{\nabla}\cdot k\vec{V}$	$(\vec{\nabla}\cdot kV)_{adj}$	$k(\vec{\nabla}\cdot\vec{V})_{adj}$	$\vec{V}\cdot\vec{\nabla}k$	$\frac{\partial\omega\ k}{\partial p}$	disp	$(disp)_{adj}$
400-100	25.0 {0.99} (0.4)	-4.6 {0.91} (1.9)	-14.4 {0.91} (6.2)	-10.0 {0.93} (5.0)	-18.8 {0.94} (3.3)	17.2 {0.91} (1.8)	-36.0 {0.95} (2.3)	-8.7 {0.96} (1.2)	-8.6 {0.86} (6.6)	-17.7 {0.87} (6.5)
700-400	9.4 {0.99} (0.0)	4.3 {0.97} (0.6)	0.6 {0.97} (1.4)	-14.9 {0.99} (1.1)	-14.8 {0.98} (1.2)	0.5 {0.97} (0.6)	-15.3 {0.99} (0.8)	3.6 {0.95} (1.0)	-7.5 {0.95} (2.0)	-7.5 {0.95} (2.0)
sfc-700	3.4 {0.99} (0.0)	6.5 {0.99} (0.2)	17.8 {0.98} (0.4)	-2.5 {0.99} (0.1)	-2.9 {0.99} (0.1)	-3.0 {0.99} (0.1)	0.2 {0.99} (0.1)	5.2 {0.99} (0.2)	-8.6 {0.96} (0.5)	-9.0 {0.97} (0.4)
Vertical total	37.8 {0.99} (0.4)	6.2 {0.94} (1.7)	3.9 {0.95} (7.2)	-27.3 {0.95} (4.7)	-36.5 {0.95} (2.8)	14.6 {0.90} (1.7)	-51.1 {0.97} (2.3)	0.1 {0.99} (0.0)	-25.5 {0.91} (7.7)	-34.2 {0.91} (7.7)

Table 7. Area averaged subsynoptic-scale kinetic energy budget for 0000 GMT 11 April 1979. Values in parentheses are mean absolute differences between the original and ten perturbed budgets. Values in brackets are mean correlation coefficients. The budget area (Fig. 35) lies over Oklahoma and has an area of 1.3×10^5 km^2. All units of energy parameters are W m^{-2} except for K which is 10^5 J m^{-2}.

Pressure Layer (mb)	K	$\partial k/\partial t$	$-\vec{V}\cdot\vec{\nabla}\phi$	$\vec{\nabla}\cdot k\vec{V}$	$(\vec{\nabla}k\vec{V})_{adj}$	$k(\vec{\nabla}\cdot\vec{V})_{adj}$	$\vec{V}\cdot\vec{\nabla}k$	$\frac{\partial\omega\ k}{\partial p}$	disp	$(disp)_{adj}$
400-100	26.9 {0.98} (0.8)	0.0 {0.93} (4.7)	48.5 {0.82} (27.7)	88.9 {0.96} (19.1)	67.1 {0.98} (16.3)	63.3 {0.98} (7.3)	3.7 {0.99} (10.2)	-47.3 {0.98} (3.3)	-7.0 {0.91} (33.0)	-28.8 {0.90} (31.4)
700-400	14.8 {0.99} (0.3)	23.1 {0.96} (2.0)	25.7 {0.94} (6.3)	18.8 {0.99} (2.7)	14.1 {0.99} (3.2)	14.6 {0.97} (2.2)	-0.5 {0.99} (2.4)	13.7 {0.99} (2.9)	30.0 {0.95} (6.3)	25.3 {0.94} (6.6)
sfc-700	6.3 {0.99} (0.1)	11.4 {0.98} (0.4)	27.5 {0.99} (1.9)	-26.7 {0.99} (1.1)	-29.9 {0.99} (1.4)	-22.3 {0.99} (0.7)	-7.7 {0.99} (0.8)	33.5 {0.99} (1.3)	-9.3 {0.98} (2.6)	-12.5 {0.98} (2.4)
Vertical total	48.0 {0.99} (1.0)	34.5 {0.96} (5.7)	101.7 {0.94} (28.8)	81.0 {0.98} (18.9)	51.3 {0.99} (14.0)	55.7 {0.97} (4.9)	-4.4 {0.99} (10.4)	-0.1 {0.99} (0.1)	13.6 {0.94} (33.2)	-16.1 {0.94} (30.7)

Results indicate that the dissipation term is the most sensitive to random errors in the input data. On the other hand, terms expressing kinetic energy content and vertical flux divergence are the most reliable. Sensitivity of all terms increases with altitude because the rawinsonde data were assumed to become less accurate at the higher levels. At any level, one can be more confident of terms with large magnitudes than those with near zero values. Mean absolute differences for the smaller area (Table 7) are larger than those for the entire area (Table 6), but original values also are larger. Therefore, ratios of mean difference to original value for the two areas are similar.

To examine the sensitivity of individual grid point values, linear correlation coefficients were computed between the original and ten perturbed budgets for both the complete and limited areas (Tables 6-7). Mean values between the surface and 700 mb are never less than 0.96 for either area. In the 400-100 mb layer, the generation term has the lowest mean correlation for the entire area (0.86) while dissipation exhibits the lowest mean value for the limited region (0.82). The lowest correlation of any single perturbed run for the entire region is 0.79 for dissipation in the 400-100 mb layer. The square of the correlation coefficient, which represents the variance of the original quantity that is explained by the perturbed run, then has a minimum value of 0.62.

Pattern similarity between energy fields derived from perturbed data with those from original data is shown in Figs. 39-41. For each parameter, the perturbed field having the lowest correlation of the ten runs is shown together with the original field. The perturbed field for dissipation (Fig. 39) has the lowest correlation of any parameter of any run (0.79). The patterns for these worst cases generally show good agreement in terms of maximum/minimum centers and overall orientation; however, the magnitudes of some central values are altered more significantly.

Overall results suggest that inherent random errors in rawinsonde data generally should not affect the interpretation of calculations of this study. In addition, good time and space continuities of spatial fields provide additional confidence.

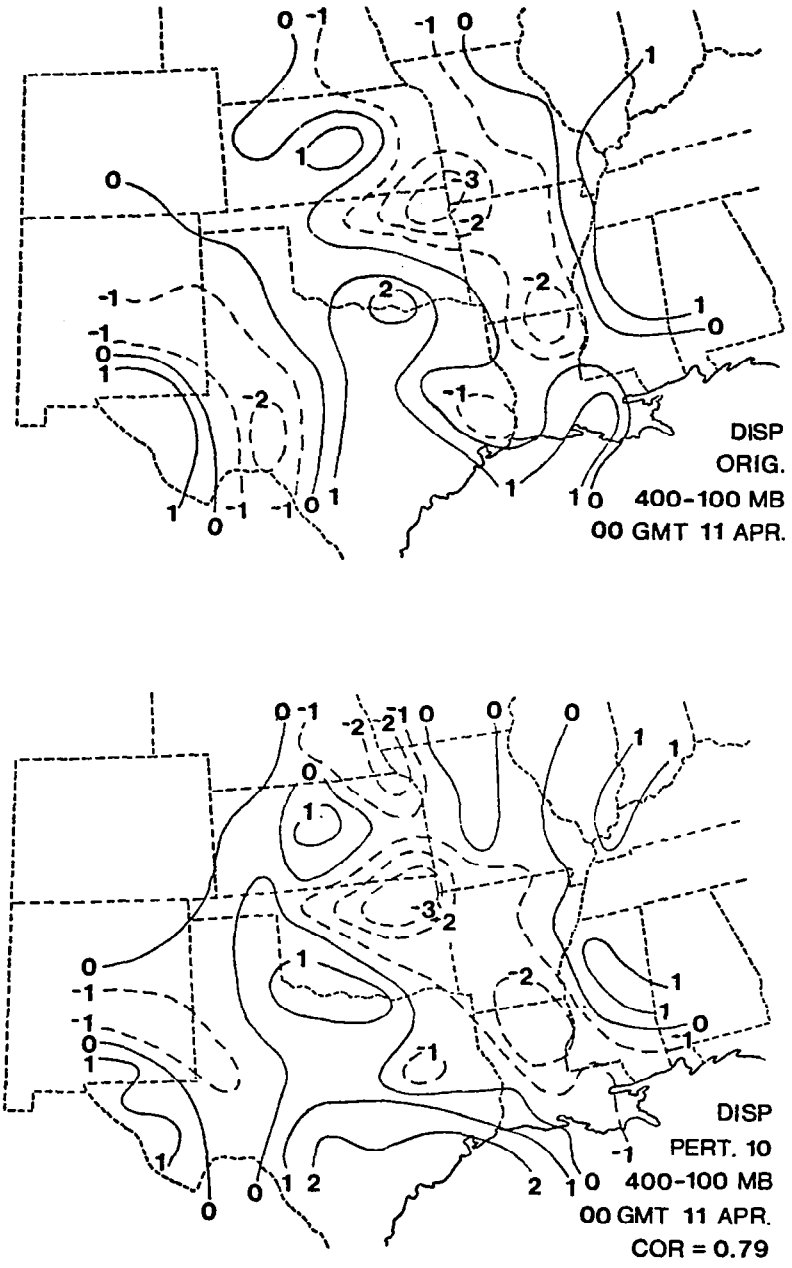

Figure 39. Integrated values of dissipation for the 400-100 mb layer of the original and perturbation run 10 of 0000 GMT 11 April. Units are 10^2 W m^{-2}.

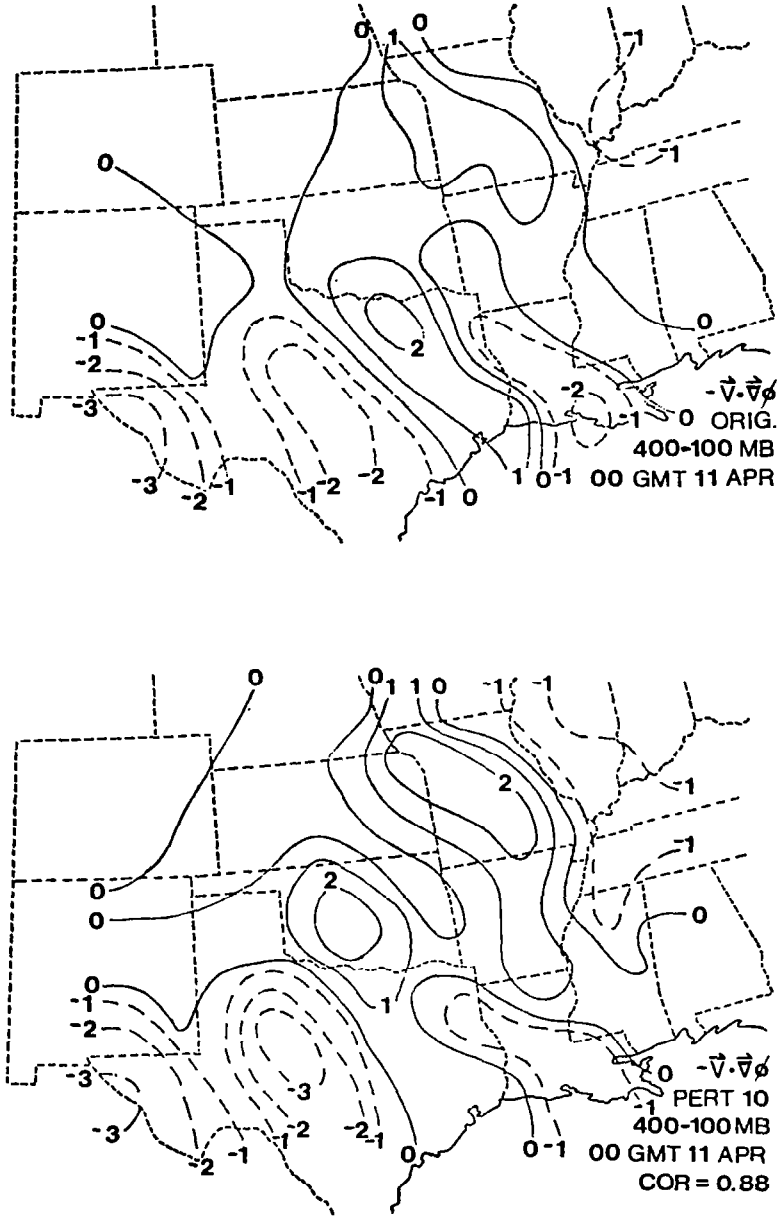

Figure 40. Integrated values of cross-contour generation for the 400-100 mb layer of the original and perturbation run 10 of 0000 GMT 11 April. Units are 10^2 W m^{-2}.

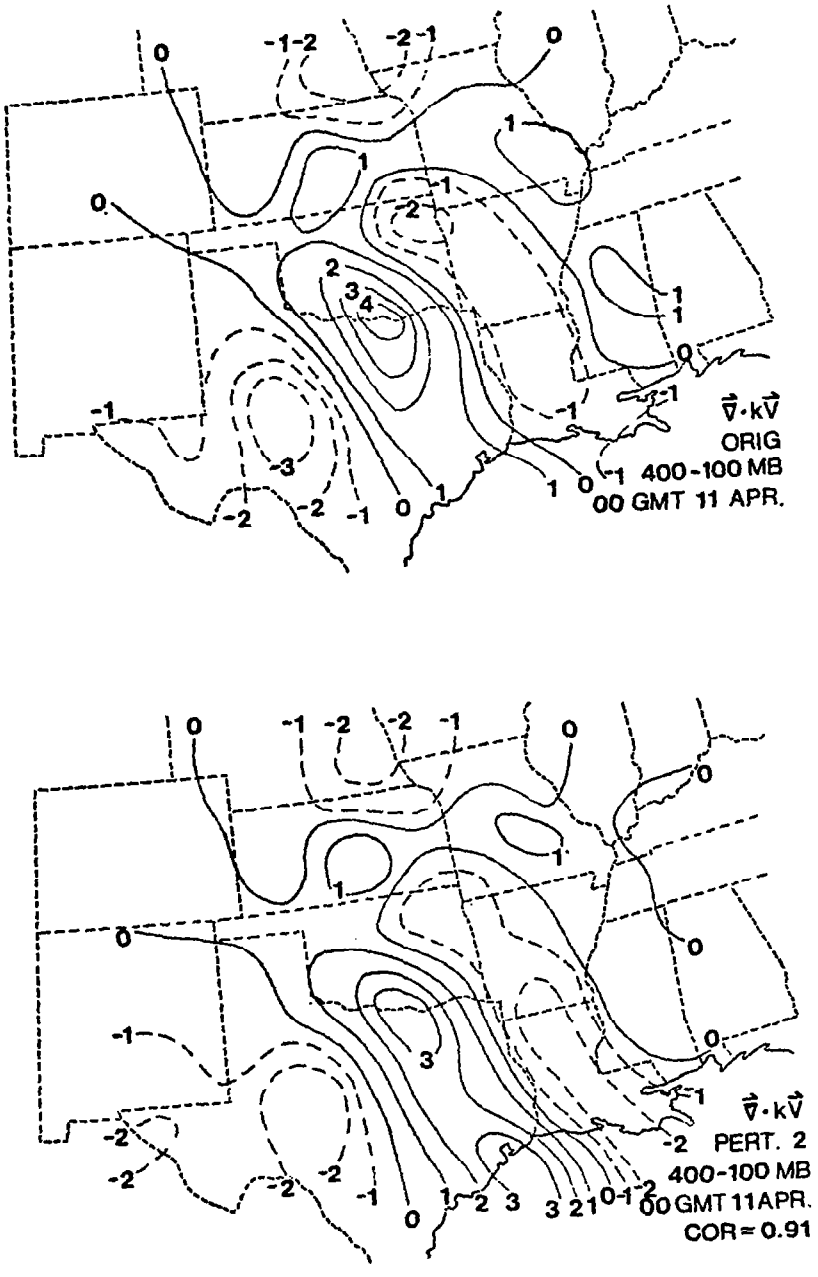

Figure 41. Integrated values of horizontal flux divergence for the 400-100 mb layer of the original and perturbation run 2 of 0000 GMT 11 April. Units are 10^2 W m^{-2}.

BIBLIOGRAPHY

Alberty, R. L., D. W. Burgess, C. E. Hane, and J. F. Weaver, 1979: SESAME 1979 Operations Summary. Environmental Research Laboratory, Boulder, Colorado. 253 pp.

Aubert, E. J., 1957: On the release of latent heat as a factor in large-scale atmospheric motions. J. Meteor., 14, 527-542.

Barnes, S. L., 1964: A technique for maximizing detail in numerical map analysis. J. Appl. Meteor., 3, 396-409.

_____, 1979: SESAME 1979 field processed rawinsonde data from supplementary sites: April 10-June 8. Environmental Research Laboratory, Boulder, Colorado. 252 pp.

Carlson, T. N., R. A. Anthes, M. Schwartz, S. G. Benjamin, and D. G. Baldwin, 1980: Analysis and prediction of severe storms environment. Bull. Amer. Meteor. Soc., 61, 1018-1032.

Chien, T., and P. J. Smith, 1973: On the estimate of kinematic parameters in the atmosphere from radiosonde wind data. Mon. Wea. Rev., 101, 252-261.

Danard, M. B., 1964: On the influence of latent heat on cyclone development. J. Appl. Meteor., 3, 27-37.

_____, 1966: On the contribution of released latent heat to changes in available potential energy. J. Appl. Meteor., 5, 81-84.

Fankhauser, J. C., 1969: Convective processes resolved by mesoscale rawinsonde network. J. Appl. Meteor., 8, 778-798.

_____, 1971: Thunderstorm-environment interactions determined from aircraft and radar observations. Mon. Wea. Rev., 99, 171-197.

Fritsch, J. M., and R. A. Maddox, 1980: Analysis of upper-tropospheric wind perturbations associated with mid-latitude mesoscale convective complexes. Preprints Eighth Conf. on Weather Forecasting and Analysis, Denver, 339-349.

Fuelberg, H. E., E. M. Berecek, D. M. Ebel, and G. J. Jedlovec, 1980: Kinetic energy budgets in areas of intense convection. NASA Contractor Report 3336, George C. Marshall Space Flight Center, Al., 173 pp.

_____, and J. R. Scoggins, 1980: Kinetic energy budget during strong jet stream activity over the eastern United States. Mon. Wea. Rev., 108, 69-77.

_____, and _____, 1978: Kinetic energy budgets during the life cycle of intense convective activity. Mon. Wea. Rev., 106, 637-653.

_____, 1974: Reduction and error analysis of the AVE II pilot experiment data. NASA CR-120496, Marshall Space Flight Center, Al., 131 pp.

Gerhard, M. L., H.E. Fuelberg, S. F. Williams, and R. E. Turner, 1979: AVE-SESAME I: 25-mb sounding data. NASA TM-78256, Marshall Space Flight Center, Al., 364 pp.

Hill, K., G. S. Wilson, and R. E. Turner, 1979: NASA's participation in the AVE-SESAME '79 program. Bull. Amer. Meteor. Soc., 60, 1323-1329.

Holton, J. R., 1972: An Introduction to Dynamic Meteorology. Academic Press, New York, 319 pp.

Kung, E. C., 1977: Large-scale energy transformations in the intense winter monsoon over the Kuroshio Region. J. Meteor. Soc. Japan, 55, no. 5, 498-510.

_____, and T. L. Tsui, 1975: Subsynoptic-scale kinetic energy balance in the storm area. J. Atmos. Sci., 32, 729-740.

Kurihara, Y., 1961: Accuracy of winds aloft data and estimation of errors in numerical analysis of atmospheric motions. J. Meteor. Soc. Japan, 39, 331-345.

Maddox, R. A., 1980: A satellite based study of midlatitude, mesoscale convective complexes. Preprints Eighth Conf. on Weather Forecasting and Analysis. Denver, 329-338.

_____, D. J. Perkey, and J. M. Fritsch, 1980: The evolution of upper-tropospheric features during the development of a midlatitude, mesoscale convective complex. Preprints Eighth Conf. on Weather Forecasting and Analysis. Denver, 233-239.

McInnis, D. H., and E.C. Kung, 1972: A study of subsynoptic-scale energy transformations. Mon. Wea. Rev., 100, 126-132.

Moller, A. R., 1980: Mesoscale surface analysis of the 10 April 1979 tornadoes in Texas and Oklahoma. Preprints Eighth Conf. on Weather Forecasting and Analysis, Denver, Amer. Meteor. Soc., 36-43.

Moore, J. T., and H. E. Fuelberg, 1981: A subsynoptic scale analysis of the first AVE-SESAME '79 period. Submitted to Bull. Amer. Meteor. Soc.

National Weather Service, 1979: Digital radar code users guide. Silver Springs, Md., 26 pp.

Ninomiva. K.. 1971a: Dynamical analysis of outflow from tornado producing thunderstorms as revealed by ATS III pictures. J. Appl. Meteor., 10, 275-294.

_____, 1971b: Mesoscale modification of synoptic situations from thunderstorms as revealed by ATS III and aerological data. J. Appl. Meteor., 10, 1103-1121.

NOAA, 1980: Red River Valley tornadoes of April 10, 1979. National Disaster Survey Report 80-1, Rockville, Md. 60 pp.

O'Brien, J. J., 1970: Alternate solution to the classical vertical velocity problem. J. Appl. Meteor., 9, 193-203.

Palmén, E. and C. W. Newton, 1969: Atmospheric Circulation Systems. Academic Press, New York, 603 pp.

Rao, G. V., and A. W. Hassebrock, 1972: Mesoscale latent heat release and its influence on midtropospheric warming. J. Appl. Meteor., 11, 1271-1283.

Robertson, F. R., and P. J. Smith, 1980: The kinetic energy budgets of two severe storm producing extratropical cyclones. Mon. Wea. Rev., 108, 127-143.

Sechrist, F. S., and T. M. Whittaker, 1979: Evidence of jet streak vertical ciculations. Mon. Wea. Rev., 107, 1014-1021.

Shuman, F. G., 1957: Numerical methods in weather prediction: II. Smoothing and filtering. Mon. Wea. Rev., 85, 357-361.

Smith, P. J., and S. P. Adhikary, 1974: The dissipation of kinetic energy in large scale atmospheric circulations. Rev. Geophys. Space. Phys., 12, 281-284.

_____, 1973: The kinetic energy budget over North America during a period of major cyclone development. Tellus, 25, 411-423.

_____, 1969: On the contribution of a limited region to the global energy budget. Tellus, 21, 202-207.

Tsui, T. L., and E. C. Kung, 1977: Subsynoptic-scale energy transformations in various severe storm situations. J. Atmos. Sci., 34, 98-110.

Uccellini, L. W., and D. R. Johnson, 1979: The coupling of upper and lower tropospheric jet streaks and implications for

the development of severe convective storms. Mon. Wea. Rev., 107, 682-703.

Vincent, D. G., and T. W. Schlatter, 1979: Evidence of deep convection as a source of synoptic-scale kinetic energy. Tellus, 31, 493-504.

_____, and L. N. Chang, 1975: Kinetic energy budgets of moving systems. Case studies for an extratropical cyclone and hurricane Celia,1970. Tellus, 27, 215-233.

Ward, J. H., and P. J. Smith, 1976: A kinetic energy budget over North America during a period of short synoptic wave development. Mon. Wea. Rev., 104, 836-848.

Wilson, G. S., 1976: Large-scale vertical motion calculations in the AVE IV experiment. Geophys. Res. Lett., 3, 735-740.

1. REPORT NO.	2. GOVERNMENT ACCESSION NO.	3. RECIPIENT'S CATALOG NO.
NASA CR-3456		

4. TITLE AND SUBTITLE	5. REPORT DATE
A Subsynoptic-Scale Kinetic Energy Study of the Red River Valley Tornado Outbreak (AVE-SESAME I)	August 1981
	6. PERFORMING ORGANIZATION CODE
7. AUTHOR(S)	8. PERFORMING ORGANIZATION REPORT #
Gary J. Jedlovec and Henry E. Fuelberg	
9. PERFORMING ORGANIZATION NAME AND ADDRESS	10. WORK UNIT NO.
Department of Earth and Atmospheric Sciences Saint Louis University Saint Louis, Missouri 63103	M-355
	11. CONTRACT OR GRANT NO.
	NAS8-33370
	13. TYPE OF REPORT & PERIOD COVERED
12. SPONSORING AGENCY NAME AND ADDRESS	Contractor Report
National Aeronautics and Space Administration Washington, D.C. 20546	14. SPONSORING AGENCY CODE

15. SUPPLEMENTARY NOTES

Marshall Technical Monitor: Kelly Hill
Interim Report

16. ABSTRACT

The subsynoptic-scale kinetic energy balance during the Red River Valley tornado outbreak is presented in order to diagnose storm-environment interactions. Rawinsonde data from the first AVE-SESAME period, having a station spacing of approximately 250 km, provide meso-α scale resolution of the storm environment. Several data handling techniques are used which normally are not performed on synoptic-scale data; these include time interpolation to adjust for nonsimultaneous sonde release and to partially generate missing data, and adjustments for balloon drift downwind.

Area-time averagedenergetics indicate that horizontal flux convergence provides the major energy source to the region, while cross-contour flow provides the greatest sink. Maximum energy variability is found in the upper levels in association with jet stream activity. Area averaged energetics at individual observation times show that the energy balance near times of maximum storm activity differs considerably from that of the remaining periods.

The local kinetic energy balance over Oklahoma during the formation of a limited jet streak receives special attention. Cross-contour production of energy is the dominant local source for jet development. Intense convection producing the Red River Valley tornadoes may have contributed to this local development by modifying the surrounding environment.

The energetics associated with areas of convective storms is found to differ greatly from that of areas without storms. Current results using subsynoptic-scale data are compared with those from a concurrent study using only NWS rawinsonde data. A random error analysis is presented to assess confidence limits in the energy parameters.

17. KEY WORDS	18. DISTRIBUTION STATEMENT
Synoptic scale data Jet stream activity Rawinsonde data Convective storms	Unclassified - Unlimited STAR Category 47

19. SECURITY CLASSIF. (of this report)	20. SECURITY CLASSIF. (of this page)	21. NO. OF PAGES	22. PRICE
Unclassified	Unclassified	126	A07

MSFC - Form 3292 (Rev. December 1972)

For sale by National Technical Information Service, Springfield, Virginia 22161

NASA-Langley, 1981